Implications of neuronal excitability and morphology for spike-based information transmission

D I S S E R T A T I O N

zur Erlangung des akademischen Grades

doctor rerum naturalium
(Dr. rer. nat.)
im Fach Biologie (Theoretische Biologie)

eingereicht an der
Lebenswissenschaftlichen Fakultät
Humboldt-Universität zu Berlin

von

Janina Hesse
M.Sc.

Präsidentin der Humboldt-Universität zu Berlin:
Prof. Dr.-Ing. Dr. Sabine Kunst

Dekan der Lebenswissenschaftlichen Fakultät:
Prof. Dr. Bernhard Grimm

Gutachter/innen:
1. Prof. Dr. Susanne Schreiber
2. Prof. Dr. Fred Wolf
3. Prof. Dr. Jan Benda

Eingereicht am 11. Mai 2017
Tag der mündlichen Prüfung: 12. Juli 2017

In Erinnerung an Magdalena Heislitz.

Abstract

Signal processing in nervous systems is shaped by the connectome as well as the cellular properties of nerve cells. In this thesis, two cellular properties are investigated with respect to the functional adaptations they provide: It is shown that neuronal morphology can improve signal transmission under energetic constraints, and that even small changes in biophysical parameters can switch spike generation, and thus information encoding. In the first project of the thesis, mathematical modeling and data are deployed to suggest energy-efficient signaling as a major evolutionary pressure behind morphological adaptations of cell body location: In order to save energy, the electrical signal transmission from dendrite to axon can be enhanced if a relatively *small* cell body is located between dendrite and axon, while a relatively *large* cell body should be externalized. In the second project, it is shown that biophysical parameters, such as temperature, membrane leak or capacitance, can transform neuronal excitability (*i.e.*, the spike onset bifurcation) and, with that, spike-based information processing. This thesis identifies the so-called saddle-node-loop bifurcation as the transition with particularly drastic functional implications. Besides altering neuronal filters and stimulus locking, the saddle-node-loop bifurcation leads to an increase in network synchronization, which may potentially be relevant for the initiation of seizures in response to increased temperature, such as during fever cramps.

Zusammenfassung

Signalverarbeitung im Nervensystem hängt sowohl von der Netzwerkstruktur, als auch den zellulären Eigenschaften der Nervenzellen ab. In dieser Abhandlung werden zwei zelluläre Eigenschaften im Hinblick auf ihre funktionellen Anpassungsmöglichkeiten untersucht: Es wird gezeigt, dass neuronale Morphologie die Signalweiterleitung unter Berücksichtigung energetischer Beschränkungen verstärken kann, und dass selbst kleine Änderungen in biophysikalischen Parametern die Aktivierungsbifurkation in Nervenzellen, und damit deren Informationskodierung, wechseln können. Im ersten Teil dieser Abhandlung wird, unter Verwendung von mathematischen Modellen und Daten, die Hypothese aufgestellt, dass Energie-effiziente Signalweiterleitung als starker Evolutionsdruck für unterschiedliche Zellkörperlagen bei Nervenzellen wirkt. Um Energie zu sparen, kann die Signalweiterleitung vom Dendrit zum Axon verstärkt werden, indem relativ *kleine* Zellkörper zwischen Dendrit und Axon eingebaut werden, während relativ *große* Zellkörper besser ausgelagert werden. Im zweiten Teil wird gezeigt, dass biophysikalische Parameter, wie Temperatur, Membranwiderstand oder Kapazität, den Feuermechanismus des Neurons ändern, und damit gleichfalls Aktionspotential-basierte Informationsverarbeitung. Diese Arbeit identifiziert die sogenannte "saddle-node-loop" (Sattel-Knoten-Schlaufe) Bifurkation als den Übergang, der besonders drastische funktionale Auswirkungen hat. Neben der Änderung neuronaler Filtereigenschaften sowie der Ankopplung an Stimuli, führt die "saddle-node-loop" Bifurkation zu einer Erhöhung der Netzwerk-Synchronisation, was möglicherweise für das Auslösen von Anfällen durch Temperatur, wie bei Fieberkrämpfen, interessant sein könnte.

Contents

Part I.

Introduction

1. Overview

One of the hallmarks of modern times is arguably an increase in interactions on many levels of daily life. Examples include the enhanced information flow in society due to new media, the increased number in social relations, and globalization of both economy and politics. Such *complex systems* are marked by a set of individual players, whose interactions result in sometimes perplexing dynamics as compared to the individual. In real-world systems, the emerging dynamics depends on both the connectivity and the properties of the players. For example, global economy can be influenced either on the level of the connections (via tolls or free trade agreements) or on the level of individual players (via support by subsidies). In a similar way, the spreading of an infectious disease in a network of individuals can be stopped on both levels, by quarantine, cutting the connections of infected individuals, or by vaccination, changing the properties of individuals (reducing the susceptibility of a subpopulation). Also in the nervous system, the global network dynamics depends both on the connections (the synapses) and on the players (the neurons). While the impact of synaptic connections on network dynamics has been considered elsewhere [125], this thesis mainly investigates single neurons, and shows how cellular properties affect signal transmission and spike-based information transmission, which will influence network performance. It is shown how the morphology can optimize energy-efficient signal transmission, and how spike-based coding is influenced by passive parameters such as membrane capacitance and temperature. Both projects provide examples for the intricate relationship between cellular properties and neuronal processing.

1.1. Information processing in the nervous system

On the level of individual neurons, signaling involves the conversion of (synaptic) inputs to spikes as output. The first project of the thesis focuses on the transmission of dendritic signals to the axon, where the spike is typically generated. A theoretical analysis supported by data shows that the associated energetic cost is minimized by different neuronal morphologies, which may explain differential cell body locations observed in mammalian and insect neurons. The second project of the thesis considers spike generation from a dynamical system's perspective, and identifies a switch between different spike generation mechanisms that strongly influences the neuron's contribution to network synchronization and information transmission. It is shown that the switch occurs in many neuron models and is induced by various cellular parameters such as membrane capacitance and leak conductance. With this, its environment provides an interesting, accessible regime for highly flexible spike-based coding.

1.2. Signaling in different morphologies

The first project of this thesis is motivated by the observation that neuronal morphologies of insects and mammals often differ in the location of the cell body (the *soma*). While the typical mammalian neuron locates the soma between dendrite and axon, insect neurons often externalize the soma at the end of an additional neurite, compare Fig. 2.1. The first publication of this thesis shows that both morphologies contribute to energy-efficient signaling [67]. Multi-compartmental modeling with different soma locations and analytical solutions are used to investigate signal transmission from dendrite to axon. This kind of signal transmission is essential for neuronal signaling, because in most neurons, the dendrites provide a prominent location for synaptic input, while the output is generated in the axon. The dendritic input hence needs to be transferred to the axon, or more precisely, to the beginning of the axon (the *axon initial segment*), where the spike is typically initiated. While a central soma, as in mammals, requires that the signal is transmitted trough the soma, an externalized soma, as in insects, allows the signal to be directly transmitted between dendrite and axon. The first publication of Part II shows that the morphology with stronger, more energy-efficient signal transmission depends on several basic model parameters, including the dimensions of soma and dendrites.

1.3. Spike generation and spike-based coding

While the spatial transmission of neuronal inputs to the axon is considered in the first project, the second project focuses on the generation of the spike once the input has reached the axon. The transformation of the input into spikes requires the generation of spikes, which involves a transition (*bifurcation*) in the voltage dynamics from rest to repetitive spiking. The second project investigates how spike generation at different bifurcations influences signal processing. While parameter changes affect signal processing only *quantitatively* as long as the same bifurcation reigns neuronal dynamics, *qualitative* changes occur when the bifurcation type itself becomes different. As shown in this thesis, particular drastic changes result from a switch in spike generation from a *saddle-node on invariant cycle* bifurcation to a *saddle homoclinic orbit* bifurcation. This happens at the *saddle-node-loop bifurcation*, the analysis of which forms the core of the second publication [69][1]. In particular, it is shown how this transition changes the sensitivity of the spike train to weak perturbations. The analysis is based on a phase reduction, which allows to capture major features of neuronal processing by a single measure, the *phase-response curve*. Once the relation between spike generation and phase-response curve is established, important implications for neuronal function can be inferred. For example, the neuron's ability to synchronize can be highly enhanced by an approach of the saddle-node-loop bifurcation. The functional implications of the saddle-node-loop bifurcation are only relevant for neuronal processing if the bifurcation can indeed be reached in a biological neuron. That this is often the case is shown in the second publication. Not only is the saddle-node-loop bifurcation accessible by various system parameters such as membrane capacitance, leak conductance or

[1] Shared first authorship with Jan-Hendrik Schleimer.

temperature, it also occurs generically in two-dimensional conductance-based neuron models (under mild assumptions). This, together with the increased synchronization around the saddle-node-loop bifurcation, make this transition potentially relevant for medical conditions marked by enhanced synchronization (Chapter 10).

1.4. Energetic costs of signal processing

The implementation of information processing in biological tissue requires energy for the maintenance of the cell and, above all, the signaling itself. As the energetic costs will be considered in both project, energy consuming aspects of neuronal signal processing are introduced in the following.

For an organism with nervous system, fast and reliable signaling is essential for the survival in a world with restricted resources and able competitors (meaning that the signaling has to be sufficiently fast and reliable to compete). The advantages resulting from a nervous system come, however, at a cost: The brain is one of the organs with the highest energy consumption, estimated to account for up to 20% of the total energy used by the organism [111]. As signal processing is particularly costly, with large amounts of energy spent for synaptic transmission as well as spiking [64], solutions with low energetic costs are thought to be evolutionary favored [98, 114, 150]. This poses a constraint on signal processing, encouraging solutions with a minimal, or at least relatively low energetic cost. This perspective is taken up by the first project, which proposes signal transmission at a low energetic cost as a major driving force for the divergent development of the soma location in neurons.

For neurons, the voltage across the cell membrane is used as encoding medium for information processing. Three elements of the encoding can be distinguished. *(i)* In absence of input, the membrane voltage is typically constant around -60 mV (the *resting potential*). *(ii)* Inputs are typically received at synaptic connections, where the opening of ion channels in response to neurotransmitters result in small voltage excursions (*post-synaptic potentials*). *(iii)* In response to sufficient input, a voltage elevation in the axon triggers the generation of a full-blown spike (also called *action potential*).

Coding, based on resting potential, synaptic potentials and spikes, requires a tight control of the membrane voltage. This consumes a large proportion of the energy available to the nervous tissue (the estimates amount to 50% to 80% in Hasenstaub et al. [64], and 20% to 60% in Sengupta et al. [150]). A considerable amount of the energy is consumed by ion pumps that actively reestablish the ion-concentration gradient between in- and outside of the cell. Different ion concentrations on both sides of the membrane result in an electric potential difference, the membrane voltage. The membrane voltage is controlled by the permeability of the membrane to ions. Ion channels, trans-membrane proteins that can open or close, dynamically regulate the flow of ions through the membrane, and with that the voltage. Ion channels open, for example, in response to neurotransmitters (such ion channels are used at chemical synapses) or in response to an increase in the membrane voltage (as used for spike generation). Open ion channels enable ions to move down the concentration gradient. This ion flow changes the membrane potential, but it also decreases the ion-concentration gradient over the cell membrane. The concentration gradient is reestablished by the ion pumps under the consumption of a fixed amount of energy

per transported ion.

Different parts of a neuron consume different amounts of energy, each allowing for specific ways to save energy. Energetically costly are, in particular, the spike initiation site and synapses, due to their high density of ion channels. The enhanced ion channel density results in a potentially large ionic current, and energy has to be deployed subsequently in order to reverse this flow. At the spike initiation site, ion channels typically open in response to an increase in the axonal voltage (which results from the accumulation of synaptic inputs all over the neuron). Energy can be saved by a decrease of the ionic current during the action potential, for example by an increased temporal separation of the counteracting sodium and potassium currents [21, 148]. At post-synaptic terminals, ion channels open in response to synaptic transmission. In addition to the energy spent there, synaptic transmission also requires energy on the pre-synaptic side, for example, to pack the neurotransmitters in vesicles [154]. Synaptic coupling has been estimated to be the major sink of energy in the brain. In mammals, synaptic transmission accounts for about half of the energy required by the brain [4, 62, 148]. Energy can be saved by reducing synaptic coupling, as fewer or smaller post-synaptic potentials result in lower ion flow. The mean amplitude of the synaptic coupling, sometimes called the *coupling strength*, is in the following used as approximation for synaptic energy consumption.

Energetically less costly than synaptic and neuronal signaling, but still relevant for the discussion of the soma location, is the synthesis of ion channels and other proteins, which happens to a large part in the soma. Ion channels are, for example, replaced every three days, as reviewed by Devor [30]. This implies that ion channels first need to be synthesized, and then transported to their location, both of which consumes energy [18, 71]. An open question is how costly the synthesis is compared to the transport of ion channels. This is particular interesting in light of recent reports on protein synthesis in axons and dendrites, as reviewed by Spencer et al. [153], which saves on the costs related to transportation from the soma to the distal parts of the neuron. The energetic costs of protein transportation will be relevant for the discussion of neuronal morphologies.

The following sections will introduce background information for the two publications of Part II that form the core of this cumulative thesis. Both publications are put into a broader context in Part III.

2. Signal transmission in uni- and multipolar neurons

The first project of this thesis investigates the transmission of signals, from the dendritic tree to the axon, in two different morphologies, unipolar versus multipolar neurons. Neurons with dendrites and axons show two potential locations for the cell body (also called *soma*). The soma can either be located between axon and dendrite (bi- or multipolar neuron), or it can be externalized at the end of an additional neurite, the *stem neurite* (Fig. 2.1). The first publication of this thesis shows that both morphologies contribute to energy-efficient signaling. This chapter provides background information on the soma location, in particular from an evolutionary perspective (Sec. 2.2), and reviews alternative explanations for different soma locations (Sec. 2.3), both of which are reconsidered in the discussion (Chapter 7).

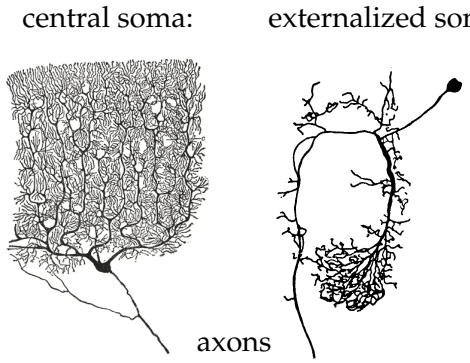

Figure 2.1.: Neurons with central or externalized soma. The neuron with central soma on the left (multipolar neuron) is from cat cerebellar cortex by Santiago Ramón y Cajal, the neuron with externalized soma on the right (unipolar neuron) is from locust metathoracic ganglion by Andreas Stumpner.

2.1. The soma location

For the typical mammalian neuron, the soma is located between dendrites and axon. This morphology is called *bipolar* or *multipolar*, depending on whether a single or multiple proximal dendrites arise from the soma. Unipolar neurons (sometimes also called *monopolar* neurons), in contrast, locate the soma out of the path of signal transmission. A single neurite, which is called *primary neurite* or *stem neurite*, leaves the soma. Several tens to hundreds of micrometer proximal from the soma, the stem neurite commonly broadens and branches into an axon and the dendritic tree. The connection point between stem neurite and other processes is often called *T-junction*.

In old publications, the term *pseudo-unipolar* cell is sometimes used in alternative to the term *unipolar* cell to describe, for example, dorsal root ganglion cells in the spinal cord of mammals. These cells have an externalized soma, but differ from other unipolar cells, because the stem does not connect to the beginning of the axon, but arises from its middle part; the branches on both sides of the T-junction are wrapped in myelin. Recent literature does no longer make this distinction, and nor does this thesis. To facilitate readability, the term *unipolar* neurons is used to refer to neurons with an externalized soma, *i.e.*, unipolar or pseudo-unipolar cells, and the term *multipolar* neuron is used to refer to neurons with a central soma, *i.e.*, bipolar or multipolar cells. In this terminology, bipolar cells are multipolar cells that have, next to the axon, only a single dendrite arising from the soma.

For many cells of the central nervous system in insects and mammals, dendritic and axonal trees are distinguished. The separation of neuronal processes into input-receiving dendrites and output-transmitting axon is assumed for the analysis in the first project, where signal transmission from dendrite to axon is investigated. This implies a directionality of signaling which is known as *functional polarization*. Different aspects of functional polarization are discussed in Sec. 7.1. Note that functional polarization is not related to the purely morphological terms *unipolar* and *multipolar*.

While the processes of a neuron are mainly engaged with signal processing, the soma, in addition, plays an essential part in the maintenance of the neuron. Most of the metabolic and protein-synthesizing machinery is found in and around the soma [169][1]. Hence, the location of the soma can be expected to influence both neuronal maintenance and signal processing, as discussed in Chapter 7.

2.2. Evolutionary account of the soma location

The investigation of signal transmission in neurons with central and externalized soma was inspired by their distribution throughout the animal kingdom. In particular, neurons with central soma are commonly found in the central nervous system of mammals, while neurons with externalized soma are commonly found in the central nervous system of insects. This section summarizes the evolutionary development of unipolar and multipolar cells, which will be further discussed in Sec. 7.4. The overview begins with bipolar neurons, and then considers the derived morphologies of unipolar and multipolar cells more in detail, both on a cellular level, as well as in their network arrangement. The evolutionary perspective on the first project provides the framework within which I develop my arguments.

For simplicity, I will use *higher* and *lower* animals to denote species that are evolutionary later, respectively earlier derived, where the meaning of *later* and *earlier* should be understood in the context of the trait under consideration. In order to facilitate readability for the non-biologist, I also take the liberty to use the old-fashioned, but still common, terms of vertebrates and invertebrates. A more appropriate separation of the animal kingdom for the evolution of the soma location would be the use of super-phyla: Multipolar neurons are predominant in the central nervous system of all

[1] Ulfhake and Cullheim [169] refers to Peters *et al.*, *Fine Structure of the Nervous System: Neurons and Their Supporting Cells* from 1976.

deuterostomia including besides the vertebrates, for example, the closest cousins of the vertebrates, the *echinodermata* (sea urchin, starfish, sea cucumber, ...). Unipolar neurons, in contrast, are predominant in the central nervous system of most higher *protostomia*, such as *hexapoda* (insects), *crustacea* or *cephalopoda*. The soma location of various species can be found in the first publication, Supplemental Information.

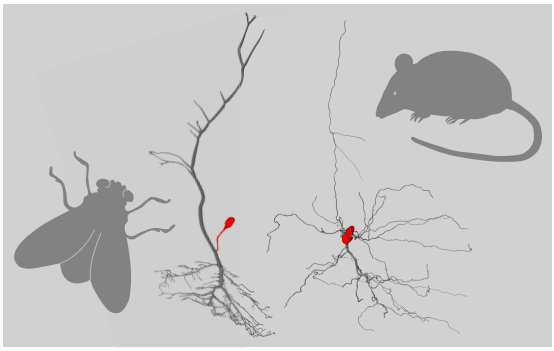

Figure 2.2.: Neurons with externalized soma are common in insects, those with central soma in mammals.

2.2.1. Evolutionary origin

The evolutionary oldest morphology with dedicated axon and dendrite is probably the bipolar neuron. Most phyla with a nervous system evolved during the Cambrian explosion 570 to 530 million years ago [70]. Probably the first neurons were receptor cells that directly affected muscle tissue. The bipolar morphology lends itself to the transmission of signals from sensory receptors at the dendritic end, to a neuro-muscular junction at the axonal end. Indeed, the bipolar shape of motor neurons is much conserved over many phyla. In contrast to motor neurons, sensory neurons are commonly bipolar or unipolar[2]. Yet, the bipolar shape is more common and probably the original shape of primary sensory cells [61]. Bipolar neurons are also abundant in the nervous system of lower invertebrates such as *C. elegans*, where a clear separation between periphery and central nervous system is often difficult. Together, these data suggest that the bipolar shape is one of the evolutionary oldest neuronal morphologies.

2.2.2. Complex signal processing

The development of interneurons, which relay information between sensory and motor neurons, allowed for more complex signal processing. The multipolar morphology with additional dendrites is a rather simple ramification of the bipolar shape, and probably evolutionary older than the unipolar morphology. Indeed, most lower invertebrates predominantly show multipolar neurons [157]. In more complex central nervous systems, such as those of insects or mammals, neurons have undergone a divergent

[2]Bipolar sensory neurons are common in invertebrates (exceptions are found, *e.g.*, in the tentacles of the *actinia* (sea anemones) and *pulmonata* (snails and slugs)) [61], as well as in lower vertebrates such as fish and in the cochlear and vestibular ganglia of higher vertebrates such as mammals. Unipolar sensory neurons predominate in all other sensory ganglia of higher vertebrates [119].

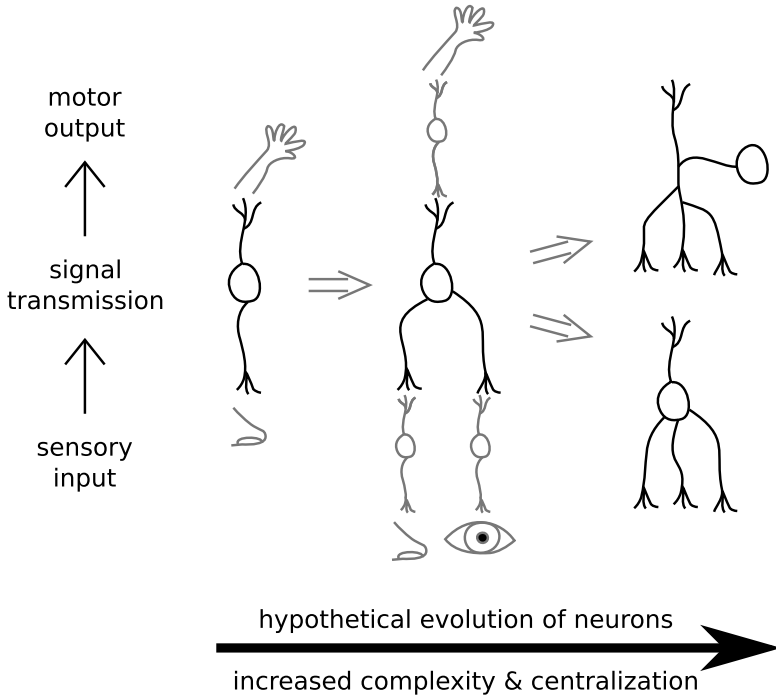

Figure 2.3.: Hypothetical evolution of neuronal morphology from bipolar cells that directly link sensation and behavior, over simple interneurons (suitable for multi-sensory integration) to more complex unipolar and multipolar cells typical for the central nervous system of higher animals.

evolution of the soma location [154, 157]. Evolutionarily, the morphology with a central soma is probably the original, as suggested by the predominance of the multipolar shape in *platyhelminthes* (flatworms) and *echinodermata*. A flatworm is probably similar to the ancestor of the vertebrates before invertebrates and vertebrates split[3], and *echinodermata* are our closest cousins along the branch of the *deuterostomia*, compare the first publication, Supplemental Information.

A continuous development away from multipolar cells to unipolar cells is suggested by the increasing proportion of neurons with externalized soma from *turbellaria* over *annelida* and some *mollusca* until in the central nervous system of arthropods nearly all neurons have an externalized soma [61]. Unipolar cells have developed several times during evolution. For example, dorsal root ganglion cells are bipolar in fish, but unipolar in birds and mammals [107], and hence clearly separate from the evolution of unipolar neurons in invertebrates[4].

2.2.3. Centralization of the nervous system

In addition to a potential increase in complexity, the divergent evolution of unipolar and multipolar cells co-occurs with an increased centralization of the nervous system.

[3]Besides the multipolar shape, their neurons have dendritic spines, a single axon, and relatively little activity, while invertebrates show a tenfold higher spontaneous activity than *planaria* and vertebrates [139, 140].

[4]Neurons with externalized soma are, for example, also common in the optic tectum of fish [171].

Classically, the development of unipolar neurons in higher invertebrates is associated with centralization of their nervous system in ganglia. In ganglia, neuronal processes lie in the central neuropil, while the somata are located on the surface in a separate soma layer (the cortex layer), see Fig. 2.4. Not only the predominance of unipolar neurons, also the separation between central neuropil and cortex layer increase from *turbellaria* over *annelida* and some *mollusca*, and is, eventually, fully developed in arthropods [61].

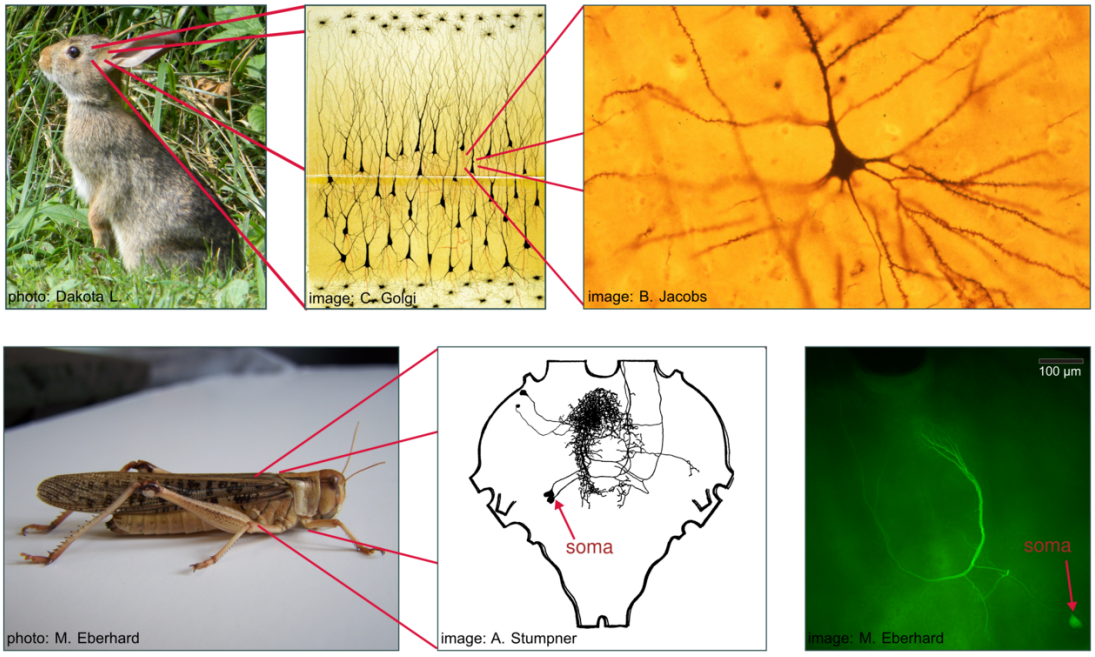

Figure 2.4.: Neuronal arrangement. Top: In the rabbit (left), the nervous system is mostly organized in layered structures with somata and processes in direct proximity to each other (middle). The individual neurons are mostly multipolar (right). Bottom: In the locust (left), the nervous system is mostly organized in ganglia with the processes in a central neuropil, and the somata in a separate, superficial soma layer (middle). The individual neurons are mostly unipolar (right).

In contrast to the common claim that the separation between somata and neurites is related to the unipolar morphology, such a separation can also be observed in vertebrates with multipolar cells. The evolutionary oldest organization of the tectum in vertebrates is a laminar structure of alternating layers of somata and neuropil [33], and more examples can be found in Rivera-Alba et al. [133]. Furthermore, the separation of somata and neurites seems to have little consequence for function, as separated and non-separated somata and neurites can be observed in homologue structures: Homologue brain regions in mammals and *sauropsida* can show different histological organizations, the neocortex in mammals is for example layered, while the dorsal ventricular ridge in *sauropsida* forms *nucleoids* (ganglion-like structures) [33]. I take these observations as a hint that an explanation of unipolar and multipolar neurons is more likely to be found on the level of single neurons than on the level of the network arrangement, in line with the hypothesis from the first publication that soma location may optimize signal transmission in single cells.

2.2.4. Cellular similarities between unipolar and multipolar neurons

Besides their morphology, unipolar and multipolar neurons seem to be surprisingly similar. The cellular organization of neurons is, irrespective of their soma location, remarkably conserved throughout evolution. For example with regard to ion channels and signal transmission at chemical synapses, neurons function similarly across phyla [138]. It seems that evolution has not so much changed the cell biology of neurons, but rather their number and arrangement [154].

The cellular similarity between unipolar and multipolar neurons becomes particularly evident during neuronal development. Neurons of both morphologies go through similar phases, with the only apparent difference that the dendritic tree of unipolar neurons develops from the axon and not from the soma [135]. In fact, a small proportion of usually unipolar neurons from higher invertebrates naturally develop dendrites arising from the soma [87, 135]. On the other hand, dendrites growing off the axon have also been observed in healthy mammals [161]. The distinction between unipolar and multipolar neurons becomes especially fuzzy when grown outside of their natural environment: Insect neurons, which are unipolar *in vivo*, become multipolar when grown *in vitro* [85, 88, 94]. On the other hand, multipolar cells also develop dendrites branching from the axon [85].

The developmental flexibility of soma location in neurons shows that unipolar and multipolar neurons are indeed very similar. In particular, the flexibility of the soma location *in vitro* shows, so I would argue, that an evolutionary switch between unipolar and multipolar morphologies is conceivable (and has indeed happened several times throughout evolution, for example the above mentioned dorsal root ganglion cells in the mammalian spinal cord, which developed independently from the insect unipolar shape). The reason for the clear dominance of one or the other morphology in insects and mammals is hence of functional nature, and does not arise from an evolutionary "dead end".

2.3. Soma location under spatial constraints

The literature provides mainly two explanations for the externalization of the soma in unipolar neurons: Minimization of wiring length or tissue volume, and better access to superficial neuronal somata. These explanations use mostly spatial arguments, in contrast to the efficient energy argument put forward in the first publication (via efficient signaling). Evolution is, in most cases, multifactorial, and probably all alternatives have contributed to the divergent evolution of the soma location. While their explicatory power is analyzed more in detail in Chapter 7, a short overview over alternative explanations for different soma locations is presented in the following.

2.3.1. Volume minimization

Tissue volume and wiring length is thought to be minimized by externalized somata, because neurites and synapses can be packed more tightly when the somata are dis-

located to the surface[5] [157]. Also the somata can be packed tighter when separated from the rest, because supporting glia can be restricted to the soma layer. That minimal wiring is indeed an evolutionary constraint is suggested by studies that reproduce the spatial arrangement of Drosophila neurons in simulations when optimizing minimal wiring cost under simultaneous volume exclusion (*i.e.*, neurons are not allowed to overlap in space) [132].

2.3.2. Supply of nutrition to the soma

Superficially located somata provide a good point of access for many substances, such as nutrients or neuromodulators, especially when an open circulatory system is used. The mammalian brain is interlaces with a dense net of blood vessels that allow for a targeted supply of nutrients and other substances to somata and neurites independent of their location (closed cardiovascular system). In contrast, in the open circulatory system of insects, nutrients are not confined by vessels but are simply dissolved in the hemolymph that surrounds all organs, and the supply of nutrients to neurons relies mostly on diffusion. Especially in insects, the location of the somata at the surface is thought to allow for a better access to the nutrients of the hemolymph [61, 157].

This argument does not hold generically. Unipolar neurons are common in cephalopods (*e.g.*, octopus) with a closed cardiovascular systems [113], and even with a open cardiovascular system, blood vessels form a dense net inside the neuropil of lobster [86]. Moreover, both in higher invertebrates and vertebrates, neurons are separated from the blood or hemolymph by glia cells, who supply energy to the neurons based on neuronal activity, as reviewed by Freeman and Doherty [43]. Specialized glia cells are also found in the neuropil, where they wrap neuronal processes, and help to maintain the axons by supply of trophic support [43]. In general, glia cells are much more abundant in vertebrates compared to invertebrates. While the ratio of the number of glia cells to the number of neurons is only one sixth in *C. elegans* [20], and about one in insects [23], it is typically around three in mammals [127], and in the human cortex even four [20]. Maybe it is the development of glia cells with an efficient transportation system that allowed neurons to become independent from the proximity of nutrient carrying fluids, such as blood or hemolymph.

Somata located on the surface of a ganglion may have the advantage that nutrients have a shorter path through the supporting glia cells. This may be more relevant for insects and other higher invertebrates than for lower invertebrates, because the centralization of the nervous systems in higher invertebrates increases the local energy demand. However, this advantage is diminished by the larger distance between soma and neurites. Any substance taken up or synthesized by the soma has to travel down the stem neurite before reaching dendritic tree and axon, often with the help of energy-consuming active transportation mechanisms [18, 71].

One additional advantage of a spatially separated soma layer and neuropil may be the independent adjustment of the ion concentration of the extracellular medium [157],

[5] Tight packing may be especially important when many afferents converge on relatively few neurons: If many axonal processes have to connect to few dendritic trees, the separation of neuronal somata prevents the neurites from encircling the somata, and may hence allow for a tighter packing (illustration in Fig. 7.4) [100].

or intracellularly, as further discussed in Sec. 7.2.2. In the neuropil, for example, a larger difference between ion concentrations in- and outside of the cell leads to a larger driving force on the ionic currents and could hence facilitate spiking.

2.4. Energy-efficient signal transmission

Most of the alternative explanation from the last section derive the unipolar shape as a secondary adaptation in response to ganglia formation. In addition to these spatial considerations, already Santiago Ramón y Cajal suspected that externalization of the soma also increases the conduction speed of the neuron, whereas multipolar neurons are better adapted for supporting large dendritic trees with many connections [128]. This intuition is confirmed in the first publication with the help of simulations (simple multi-compartmental models) and with biological data. The models suggest that an externalization of the soma can decrease the stimulation amplitude required to activate the neuron. This decreases the amount of synaptic activation and thereby the synaptic energy consumption. As minimization of energy consumption appears to be one of the main driving forces in evolution [150], the divergent evolution of central and externalized somata may hence be explained by energetic arguments.

In the first publication, strong signal transmission from dendrite (input region) to axon (output region) is considered as energetically favorable. The relation between signal transmission and energy consumption can be considered from two alternative perspectives. From the first perspective, a fixed dendritic input is assumed, and optimal signal transmission then minimize the amount of ion channels required to initiate a response, *i.e.*, a spike. The more ion channels are required, the more energy is spend on signal transmission. However, the relation between amount of ion channels and energy is non-trivial, as the actual ion flow (and hence the energy) depends the properties and the location of the ion channels (*e.g.*, dendritic, somatic or axonal).

The relationship between energy and signal transmission is better visible in the following, second perspective. This perspective concentrates on the amplitude of the input, and assumes that a spike is triggered when a certain voltage threshold is reached in the axon. Energy can be reduced by a minimization of the amplitude of the dendritic input required to reach threshold, because less dendritic input demands for less energetically costly synapses. In the first publication, the required input is minimized by optimization of the signal transmission between dendrite and axon. The scaling of synaptic numbers with input strength suggests a simple (potentially linear) relation between synaptic energy consumption and desired dendritic input (compare Sec. 1.4). This underlies the energy arguments used in the first publication. Neurons are considered as energetically favorable when the signal transmission between dendrite and axon is high.

In the models used in the first publication, a weighted ratio of the soma size and the process dimension decides on whether an externalization of the soma optimizes energy efficiency. This result allows to structure experimental observations on the soma location over many animals in an unprecedented way, and, as shown in the first publication, the experimental data qualitatively supports the trend suggested by the theoretical analysis.

2.5. Recapitulation

This chapter has reviewed the evolution of unipolar and multipolar neurons as parallel developments starting from neurons with a multipolar morphology, but potentially with a weaker functional polarization as typical for mammalian cells. In contrast to multipolar cells, unipolar neurons are often organized in ganglia, with the somata on the surface of a central neuropil. This arrangement has led other researchers to explain the morphology of unipolar neurons by their ganglionic arrangement, and the associated spatial advantages. The results of the first project suggest an alternative explanation based on energy efficient signal transmission.

3. Signal processing in mean-driven neurons

While the first project mainly considers signal *transmission* (along the neuron from dendrite to axon), the second project focuses on signal *transformation* (from input to a spike train as output). Signal processing depends intrinsically on the dynamical properties of the neurons, which are determined both by active properties, such as voltage-gated ion channels, and passive properties, such as leak conductance or membrane capacitance. While many aspects of neurons are evolutionary conserved, in particular the diversity of ion channels has increased throughout evolution [113]. The intricate interplay of a neuron's ion channels decides on the transformation of input signals into a spike train, the relation of which is captured by the *response properties* of the neuron. The response properties do not only depend on *active* conductances, but also on *passive* properties such as membrane capacitance or leak conductance. The second project of the thesis demonstrates that passive parameters can induce transitions in neuronal dynamics. At these bifurcation points, particular drastic changes in the response properties are to be expected because bifurcations are generally marked by *qualitative* changes in the underlying dynamics.

This chapter provides background on neuronal dynamics that is important for an understanding of the second part of the thesis. It introduces conductance-based neuron models, which allow for a rich set of dynamics (Sec. 3.2). Attractors in the dynamics are fixed points as well as limit cycles (Sec. 3.3), both of which are essential for the analysis of neuronal processing in the second publication. In order to assess spike-based coding, the analysis assumes a mean-driven neuron with constant firing rate, subjected to small perturbations. In this case, the neuron model corresponds to a weakly perturbed oscillator, which allows for a phase reduction (Sec. 3.4). The advantage of a phase reduction is that major features of the dynamics are captured by a single measure, the phase-response curve. Once the phase-response curve is identified, as done in the second publication, various implications for spike-based coding follow. The theory how the second publication derives synchronization properties from the phase-response curve is summarized in Sec. 3.4.1, while other functional implications are considered later (Sec. 8.3). From a functional perspective, the dynamical regime around a saddle-node-loop bifurcation allows for a minimal change in neuronal parameters to induce a transition in spike onset dynamics. The resulting switch in the neuron's synchronization capacity has potential relevance for health and disease.

3.1. Spike onset dynamics

The second project considers spike-based coding in a mean-driven neuron, *i.e.* a neuron with a mean input large enough to induce repetitive firing. The transition from rest to

tonic spiking occurs at a bifurcation, which is decisive for certain coding properties. Bifurcations that can induce spiking are shortly reviewed below.

At rest, the membrane voltage is, without input, typically constant around -60 mV. This *resting membrane potential* suggests the existence of a fixed point in the dynamics, the *resting state*. In contrast to the resting state, repetitive spiking observed with sufficient input indicates limit cycle dynamics. The transition from rest to spiking (in the deterministic model[1]) requires (i) the destabilization of the resting state, and (ii) the creation of a limit cycle. In neuronal models, the resting state can lose stability either at a saddle-node bifurcation, or at a Hopf bifurcation [79]. In contrast to these bifurcations of the fixed point, the creation of the limit cycle typically involves one of four possible codimension-one bifurcations [79]. All relevant bifurcations will be shortly described in Sec. 3.3.

The transition from rest to spiking allows neurons to encode information. The associated bifurcation occurs with the input as bifurcation parameter. With a single bifurcation parameter, this is an example for a codimension-one bifurcation[2]. The transition between different codimension-one bifurcations happens at codimension-two bifurcations. Because the codimension-one bifurcation leading from rest to spiking is decisive for spike-based coding, and because this bifurcation changes qualitatively at the associated codimension-two bifurcation, exceptionally drastic changes in spike-based coding can be expected at such a bifurcation. The second project of this thesis identifies the saddle-node-loop bifurcation as highly relevant codimension-two bifurcation in neuronal dynamics: A large group of neuron models can be tuned to a saddle-node-loop bifurcation, and the numerical analysis shows particularly strong changes in spike-based coding at this bifurcation (Sec. 8.3). The saddle-node-loop bifurcation is reached with the separation of time-scales as additional parameter besides input, affected, *e.g.*, by temperature or membrane capacitance (see Sec. 3.5.1). At the saddle-node-loop bifurcation [141], two codimension-one bifurcations meet and induce a switch in neuronal dynamics when the bifurcation is passed. At this point, the limit cycle onset bifurcation switches from a saddle-node on invariant cycle to a saddle-homoclinic orbit bifurcation (or vice versa). The switch in the limit cycle onset bifurcation changes the response properties of the neuron, with fundamental consequences for signal processing, see Sec. 8.3, that may provide an attractive regime for neuronal dynamics.

From a methodological perspective, the second publication is based upon the observation that a neuron's functional characteristics, such as firing rate at spike onset, or the ability to synchronize in a network, can be derived from a dynamical system's perspective [79]. Commonly, neuronal function is investigated in models with a spike onset at a saddle-node on invariant cycle or Hopf bifurcation [35, 60]. The abundance of these two bifurcations in neuroscience is probably due to the empirical classification of neurons based on their firing rate-input curve introduced by Hodgkin: saddle-node on invariant cycle bifurcations mimic *class-I* (sometimes also *type-I*) neurons with arbitrary slow firing and Hopf bifurcations mimic *class-II* (*type-II*) neurons with a nonzero lower

[1] In an excitable system, spikes can also be triggered by sufficiently large noise deviations despite the stability of the resting state.

[2] The number of bifurcation parameters required to reach the bifurcation point corresponds to the *codimension* of a bifurcation [97]

bound on the firing rate [37, 74, 131]. The functional implications of saddle-node on invariant cycle and subcritical Hopf bifurcations have been discussed in distinct models [130, 131, 144]. Distinct models were required in these studies, because, as shown in the second publication, the stable limit at a saddle-node on invariant cycle bifurcation cannot be transformed into the stable limit cycle at a subcritical Hopf bifurcation with an infinitesimal change in system parameters. In contrast, the limit cycle onset bifurcations occurring at a saddle-node on invariant cycle and a saddle-homoclinic orbit bifurcation meet in an saddle-node-loop bifurcation, where an infinitesimal change in model parameters can indeed switch between a spike onset at a saddle-node on invariant cycle or a saddle-homoclinic orbit bifurcation. This is interesting because the switch in spike onset implies a switch in coding properties. As the switch happens in response to only a small parameter change, saddle-node-loop bifurcations constitute a particularly interesting regime for a neuronal ensemble that aims to achieve maximal functional diversity at minimal heterogeneity in system parameters. Assuming that any change in neuronal parameters is associated with some form of cost function, a small parameter variation around the saddle-node-loop bifurcation allows for substantial changes in signal processing at minimal cost (an example for such a cost is the energy required to increase the number of ion channels in the membrane).

The analysis of the saddle-node-loop bifurcation poses a particular challenge: Fixed point bifurcations are often *local* bifurcations with dynamics confined to a small area that allows for a linear approximation of the dynamics (*e.g.*, saddle-node bifurcations). In contrast, saddle-node on invariant cycle, saddle-node-loop and saddle-homoclinic orbit bifurcations are *global* bifurcations where a limit cycle emerges with a nonzero amplitude. The challenge of global dynamics is solved in the second publication by considering not the whole limit cycle, but just the part that is particularly slow, and hence dominates the dynamics.

Bridging the scales from single cells to network dynamics, this study draws from a broad methodological background. In the following, I will introduce the essential tools required to follow my discussion[3].

3.2. Conductance-based neuron model

In both publications from part II, neuronal spiking is modeled using *conductance-based neuron models* that describe the dynamics of the membrane voltage, and the ion channel gating, by ordinary differential equations.

The dynamics of the membrane voltage are given by a current balance of input, capacitive and ion currents, $I_{\text{in}} = I_{\text{cap}} + I_{\text{ion}}$. The electrical resistance of the membrane (and of the embedded ion channels) is often given by its inverse, the *conductance* (leak conductance g_{L} and maximal gating conductances g_{ion}). The ion current depends on the opening and closing of ion channels, which, in its simplest form used here, depend exclusively on the membrane voltage. The voltage changes the probability of ion channel opening and closing, and the fraction of open ion channels at fixed voltage, *e.g.*, $n_\infty(v)$ for the potassium current, is modeled by a sigmoid curve for each gating variable. The resulting conductance-based neuron model has the following structure,

[3] For a complete presentation, please refer to the references in the following.

$$\begin{aligned} \dot{v} &= 1/C_{\mathrm{m}}\left(I_{\mathrm{in}} - I_{\mathrm{ion}}(v,u)\right), \\ \dot{m} &= 1/\tau_{\mathrm{m}}\left(m_\infty - m\right), \\ \dot{n} &= 1/\tau_{\mathrm{n}}\left(n_\infty - n\right), \\ &..., \end{aligned} \tag{3.1}$$

where v is the membrane voltage, $u = (m, n, ...)$ is the vector of all gating variables of the ion channels included in the model, and $I_{\mathrm{ion}}(v,u) = \sum_i g_i \prod_k u_k^{p_k}(v - v_i)$ is the ionic current of ion channel i, with maximal conductance g_i and reversal potential v_i, gated by a subset of u (where the k^{th} entry of u, u_k, is possibly taken to the power of p_k). For a detailed discussion of conductance-based neurons models please refer to Ermentrout and Terman [38] or any other book on the basics of theoretical neurosciences.

3.3. Neuronal dynamics

This thesis considers neuronal dynamics described by Eq. 3.1 that show fixed point and limit cycle dynamics in analogy to resting membrane potential and spiking observed in real neurons. For low input I_{in} (*subthreshold* input), the voltage will relax to some constant voltage value. For sufficiently high input (*suprathreshold* input), the fixed point that underlies the stable membrane potential loses stability and is replaced by a stable limit cycle. In principle, it is possible to include more complicated dynamics, such as spike adaptation[4], but this level of detail is not essential for the following analysis.

The sudden and qualitative change in neuronal dynamics at the transition from rest to spiking happens at a bifurcation. Because a single parameter is sufficient to induce the bifurcation (the amplitude of the input current), this type of bifurcation is called a codimension-one bifurcation. The following paragraphs shortly introduce the notions relevant for the subsequent discussion. For more detail, please refer to Kuznetsov [97] for a mathematical discussion of bifurcations, or to Izhikevich [79] for their relevance in neuron models.

3.3.1. Fixed points

The mathematically simplest dynamics observable in neuron models is fixed point dynamics (*e.g.*, the resting state). From a biophysical perspective, the constant membrane voltage in response to a subthreshold, constant input is set by a balance of the ions flowing in and out of the cell[5]. From a dynamical system's perspective, the observable voltage corresponds to a fixed point that appears at the intersection of the system's *nullclines* (defined by $\dot{x} = 0$ for every dynamical variable x). Fig. 3.1 shows a two-dimensional example with voltage and potassium gating as dynamical variables. A

[4] Spike adaptation is indeed observed in the experiments described in Sec. 9.3.

[5] For each ion species, the difference between membrane potential and reversal potential sets the driving force for the ion flow. Around the resting membrane potential, the potential between the reversal potential of potassium (around -90 mV) and of sodium (around +50 mV) allows to balance these main contributors of the ion flow. For higher membrane potentials, the voltage-dependent gating of the ion channels must be taken into account.

fixed point attracts trajectories in its environment if it is linearly stable. The stability can be evaluated based on a linear approximation of the dynamics around the fixed point. The linear approximation is given by the *Jacobian*, which is given for the dynamical system (3.1) as

$$J(v,u) = \begin{bmatrix} \partial_v \dot{v} & \partial_m \dot{v} & \partial_n \dot{v} & ... \\ \partial_v \dot{m} & \partial_m \dot{m} & \partial_n \dot{m} & ... \\ \partial_v \dot{n} & \partial_m \dot{n} & \partial_n \dot{n} & ... \\ ... & & & \end{bmatrix}. \tag{3.2}$$

The stability can be read from the eigenvalues of the Jacobian evaluated at the fixed point. Stable dynamics are associated with a negative real part of all eigenvalues. Fixed points with negative and positive eigenvalues are called *saddle* and with exclusively negative or positive eigenvalues *nodes* (or *focus* for complex eigenvalues).

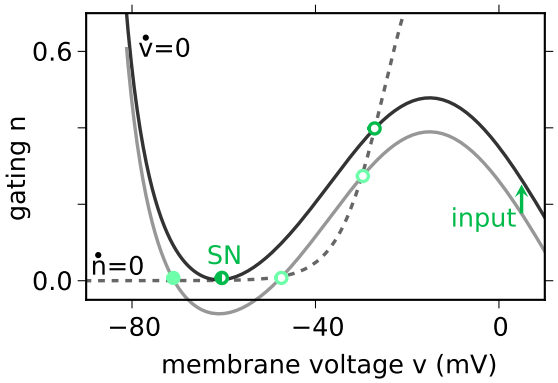

Figure 3.1.: Sketch of nullclines of a two dimensional conductance-based neuron model with membrane voltage v and gating variable n. Fixed points correspond to the intersection of the nullclines. With increasing input, the saddle (open circle) and stable node (filled circle) collide in a saddle-node (SN).

As already mentioned, the transition from rest to spiking, *i.e.*, from fixed point dynamics to limit cycle dynamics, requires the creation (or existence) of a limit cycle, and the destabilization (or destruction) of a fixed point. Fixed-point and limit-cycle bifurcation can occur simultaneously or in sequence. Relevant bifurcations are shortly introduced in the following paragraphs.

Bifurcations are associated with qualitative changes in fixed point dynamics. A stable fixed point, such as the resting state, can disappear in a saddle-node bifurcation, or it can lose stability at a Hopf bifurcation. The fixed-point bifurcation has functional implications on the subthreshold dynamics, *e.g.*, subthreshold oscillations that arise from Hopf bifurcations may be relevant for frequency selection, and also influence spiking [130, 144].

A Hopf bifurcation changes the stability of a focus, as the complex eigenvalues of the Jacobian (Eq. 3.2) cross the imaginary axis. A Hopf bifurcation furthermore involves the creation of a limit cycle that can be stable (*supercritical Hopf*) or unstable (*subcritical Hopf*) [97]. Limit cycles are introduced in the next section (Sec. 3.3.2).

Besides the Hopf bifurcation, also the saddle-node bifurcation is a common fixed-point bifurcation in neuronal models, which destroys a node and a saddle fixed point.

The node collides with a saddle in a saddle-node, as depicted in Fig. 3.1, and then disappears. For the Jacobian (Eq. 3.2), this corresponds to a zero-crossing of one eigenvalue along the real axis. The zero eigenvalue at the saddle-node bifurcation reflects infinitely slow dynamics in the direction of the associated eigenvector, along the so-called *semistable manifold*. When the input is adapted such that the limit cycle passes intimately close to the former location of the saddle-node (its *ghost*), the slow dynamics in the direction of the semistable manifold allows for arbitrary long inter-spike intervals (*i.e.*, limit cycle periods). In this case, the ghost of the saddle-node dominates the dynamics of any trajectory along the semistable manifold, in particular the limit cycle at spike onset, which is used in the derivation of the second publication.

3.3.2. Limit cycles

The second project assumes repetitively spiking neurons with a constant mean firing rate. Repetitive spiking is observed when the stable dynamics are attracted by a limit cycle, a closed trajectory in state space. This section introduces the saddle-node-loop bifurcation as transition between different limit-cycle bifurcations.

When a trajectory leaves the saddle-node along the semistable manifold, it can loop around and reenter the saddle-node, such that a *homoclinic orbit* is formed. This orbit can become a limit cycle once the saddle-node disappears. In biologically inspired model neurons, the homoclinic orbit typically approaches the saddle-node along the semistable manifold, and hence has a smooth shape as shown in Fig. 3.2. This limit-cycle bifurcation is called saddle-node on invariant cycle (SNIC) bifurcation (alternative names are, *e.g.*, SNIPER or saddle-node on a limit cycle, see Izhikevich [79]) and is often associated with so called *type-I* dynamics. In alternative to the approach along the semistable manifold, the homoclinic orbit can also approach the saddle-node along one of the other directions, which are called *strongly stable* manifolds (strongly stable compared to the weakly (in-)stable dynamics along the semistable manifold). This bifurcation, the saddle-node-loop bifurcation, occurs when the membrane capacitance is increased from $C_\mathrm{m} = 1\mu\mathrm{F/cm}^2$ to $C_\mathrm{m} \approx 1.3\mu\mathrm{F/cm}^2$, compare Fig. 3.2. As shown in detail in the second publication, for even higher capacitance values, a limit cycle is born already at lower inputs at a saddle-homoclinic orbit (HOM) bifurcation. In this case, unstable and stable manifold of the saddle (instead of the saddle-node) overlap and form a homoclinic orbit, which, when it detaches from the saddle, can give rise to a limit cycle. The saddle-node is in this case not associated with a homoclinic orbit, see Fig. 3.4B in contrast to the saddle-node on invariant cycle bifurcation illustrated in Fig. 3.4A. At the transition from saddle-node on invariant cycle to saddle-homoclinic orbit bifurcation lies a codimension-two bifurcation, the saddle-node-loop bifurcation. This bifurcation, and its properties, form the core of the second publication.

At the saddle-node-loop bifurcation, the homoclinic orbit switches its approach of the saddle-node from the semistable to the strongly stable manifold (compare the second publication, Fig. 3 and 4). Due to this flip in the trajectory, the saddle-node-loop bifurcation is also called *orbit flip* bifurcation [75].

The flip changes the spike shape when observing the membrane voltage over time (Fig. 3.3). A non-degenerated saddle-node on invariant cycle bifurcation always shows an *afterhyperpolarization*. In a model neuron stimulated with a constant current input

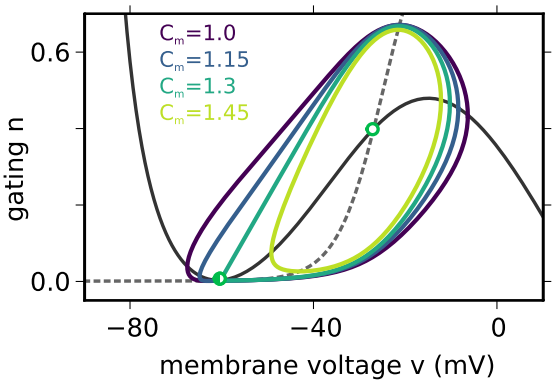

Figure 3.2.: An increase in capacitance deforms the limit cycle dynamics (two-dimensional sodium-potassium model from Izhikevich [79], units of the membrane capacitance C_m in $\mu\mathrm{F/cm^2}$). Around $C_\mathrm{m} = 1.3\mu\mathrm{F/cm^2}$, the homoclinic orbit switches from a saddle-node on invariant cycle to a saddle-homoclinic orbit bifurcation. This transition corresponds to the saddle-node-loop bifurcation.

just above threshold, this results in spikes that are followed by a period, in which the membrane potential is lower than the voltage observed in response to a constant, but subthreshold current input. The afterhyperpolarization can, potentially, be abolished by the orbit flip at the small saddle-node-loop bifurcation (Fig. 3.3). An afterhyperpolarization must be observed at a saddle-node on invariant cycle bifurcation, because the semistable manifold, along which the orbit moves, has a nonzero component in voltage direction, as is evident from the eigenvectors stated explicitly by Kirst et al. [90]. The flip at the small saddle-node-loop bifurcation abolishes the afterhyperpolarization if the angle between voltage direction and the strongly stable manifold (on which the dynamics jumps) is pointed. In the case of a small saddle-node-loop bifurcation[6], the membrane voltage can remain above the voltage of the saddle-node fixed point during the whole orbit, such that no afterhyperpolarization is observed. In contrast, afterhyperpolarization do always occur at the big saddle-node-loop bifurcation, where the generated limit cycle encircles the ghost of the saddle-node. A decrease in temperature has been reported to increase afterhyperpolarization in hippocampal neurons [162]. This might be related to an increased distance to the saddle-node-loop bifurcation, because, as shown below (Sec. 3.5.1), a lower temperature increases the distance to the small saddle-node-loop bifurcation similar to a decrease in capacitance. While such changes in afterhyperpolarization could, in principle, be related to a small saddle-node-loop bifurcation, there are several alternative explanations including adaptations in calcium concentration or ion channel composition [2].

In theory, the flip from the semistable manifold to the strongly stable manifold should also be visible in the speed of the voltage, $\frac{\mathrm{d}v}{\mathrm{d}t}$. Limit cycles arising from saddle-node on invariant cycle or saddle-node-loop bifurcations differ qualitatively in the velocity of the dynamics around the saddle-node. The speed on the exit of the saddle-node should

[6]The small (big, respectively) saddle-node-loop bifurcation refers to the transition at a small (big, respectively) saddle-homoclinic orbit bifurcation, such that the limit cycle does not (does, respectively) encircle the saddle fixed point to which the homoclinic orbit is formed (see Fig. 3 of the second publication).

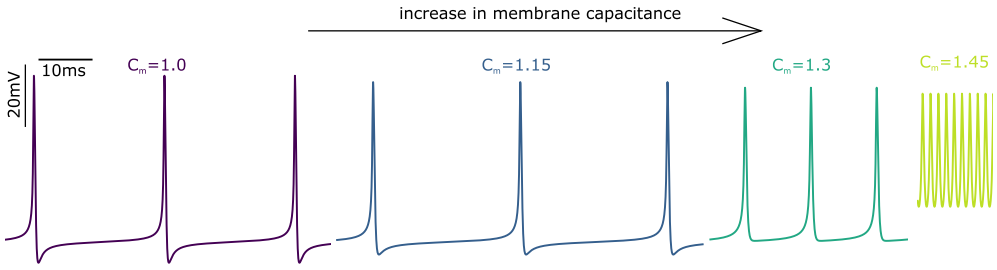

Figure 3.3.: An increase in capacitance deforms the spike shape, compare Fig. 3.2 (two-dimensional sodium-potassium model from Izhikevich [79], units of the membrane capacitance C_m in $\mu\mathrm{F/cm^2}$). The saddle-node-loop bifurcation happens around $C_\mathrm{m} = 1.3\mu\mathrm{F/cm^2}$.

be quadratic for both, while the approach should be quadratic for the saddle-node on invariant cycle, but linear for the saddle-node-loop bifurcation. In practice, this may be hard to observe, in particular in noisy systems, because the quadratic or linear dynamics are only expected in a small environment around the saddle-node.

In the second publication, spike onset in proximity of the saddle-node-loop bifurcation is contrasted with another bifurcation that is common in neuron models, and is often referred to as *type-II* dynamics [131]. Spike onset is in this case a sequence of two bifurcations with an intermittent region of bistability in between, a fold of limit cycles bifurcation followed by a subcritical Hopf bifurcation, see Fig. 3.4D. At the subcritical Hopf bifurcation, the stable fixed point (corresponding to the resting state) becomes unstable, and the dynamics relax to the limit cycle that was born at lower input, where it folds with the unstable limit cycle that was born at the Hopf bifurcation. Note that a supercritical Hopf bifurcation that directly creates a stable limit cycle is not a good model for the all-or-nothing spikes observed in biological models, because the resulting limit cycle implies infinitely small spikes. Also the unstable limit cycle that originates from the subcritical Hopf bifurcation is not relevant for neuronal dynamics, because neuronal dynamics typically fall on an already established, stable limit cycle at a subcritical Hopf bifurcation. Hence, the main contribution of the subcritical Hopf bifurcation in a neuronal context is the (de-)stabilization of a fixed point.

Spike onset at a subcritical Hopf bifurcation and fold of limit cycles bifurcation is for example observed in the original Hodgkin-Huxley model [73], which is used in the first publication as spike generation mechanism in the axon initial segment. A hallmark of this dynamics is a nonzero firing rate at spike onset. In contrast, spike onset at a saddle-node on invariant cycle bifurcation occurs with an infinite period, because the limit cycle dynamics is arbitrary slow in proximity of the saddle-node fixed point. This does not allow for the definition of a clear current threshold for finite simulation time, because a spike can or cannot be observed in a certain input range depending solely on the simulation duration [79]. The Hopf bifurcation with finite period at spike onset, however, allows for a clear current threshold. This is why the original Hodgkin-Huxley model [73] was used in the first publication for the models with active conductances. With a clear current threshold, and for long enough stimulation durations, the occurrence of a spike depends on the amplitude of the dendritic input and the signal transmission from dendrite to spike initiation zone, but not on the simulation duration. This allows for a clear definition of successful

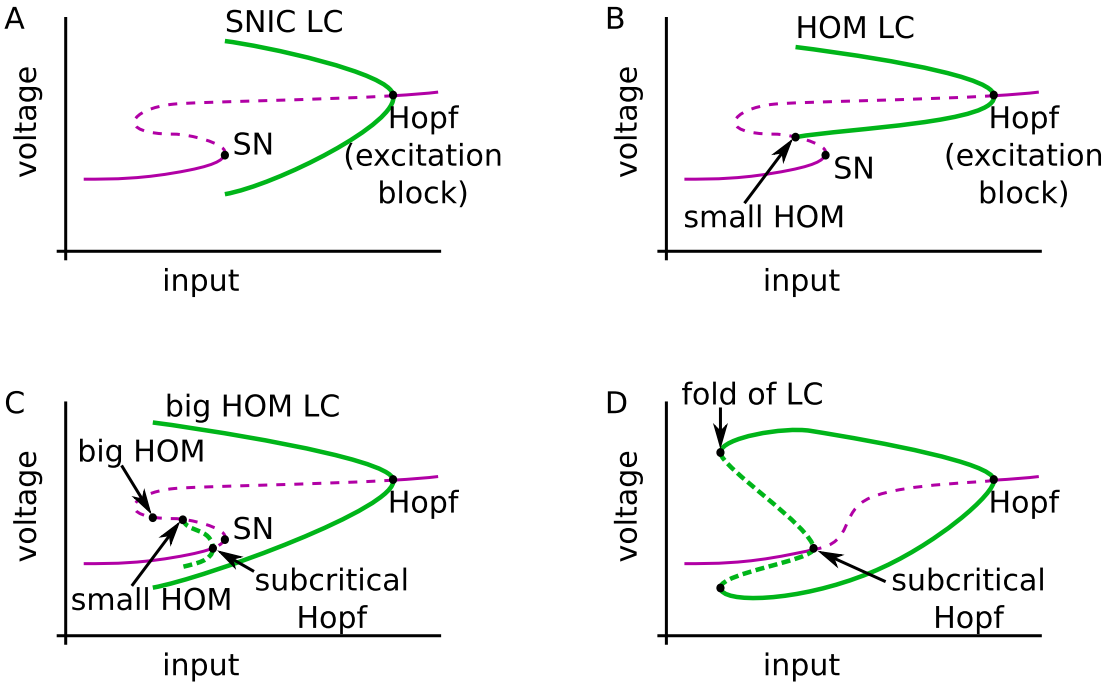

Figure 3.4.: Sketch of the relation between membrane voltage and input for different spike onset bifurcations. Fixed point voltage in violet, limit cycle (LC) maximal and minimal voltage in green. Straight lines denote linearly stable dynamics, dashed lines linear unstable dynamics. A: Saddle-node on invariant cycle bifurcation as typical for "type-I" neurons. B: Saddle-homoclinic orbit bifurcation (for an example, see Fig. 3.2 and Fig. 3.3 at the highest capacitance value). C: Bifurcation structure as observable below the Bogdanov-Takens point in the second publication, Figure 6. D: Subcritical Hopf bifurcation ("type-II") as in the original Hodgkin-Huxley model [73].

signal transmission in the first publication.

3.4. Phase dynamics

While conductance-based neuron models allow for a detailed analysis of neuronal dynamics, depending on a variety of biologically inspired parameters, particular assumptions allow to capture the essential spike dynamics of the (potentially multi-dimensional) dynamical system already with a single dynamical variable, the *phase* φ. The *phase reduction* is in general applicable to (stable) limit cycle dynamics that are weakly perturbed [96]. How weak the perturbation has to be depends on the limit cycle itself, more precisely on its attractiveness. The more attractive the limit cycle is in its immediate environment, the stronger the perturbations that are still admissible. As a result, the perturbation hardly influences the shape of the limit cycle, but only advances or delays the limit cycle dynamics in time.

The phase reduction can be applied to neurons that spike continuously in time. Perturbations, *i.e.*, input from synaptic coupling or stimulation electrode, are required to advance or delay the occurrence of the next spike (and only the next spike, to be strict), while leaving the spike shape mostly undisturbed.

These assumptions form the starting point for the analysis in the second project. The dynamics can then be captured with a considerably simpler equation compared to the original system in Eq. 3.1, which is given for the phase φ as

$$\dot{\varphi} = 1/T + Z(\varphi)s(t), \tag{3.3}$$

with limit cycle period T, a time-dependent input $s(t)$ and *phase-response curve* (PRC) $Z(\varphi)$, which is determined from the original system Eq. 3.1 [96]. The definition of the phase is translational invariant in time. As a convention, integer crossings of the phase are identified with the voltage maximum of subsequent spikes. In real time, spikes are correspondingly observed at times $T\varphi$ for $\varphi \in \mathbb{Z}$. For the unperturbed case, *i.e.*, $s(t) = 0$, the phase is just a scaled version of the time $\varphi = t/T$. With nonzero stimulus, the multiplication with the phase-response curve in Eq. 3.3 translates the stimulus into an advance or delay in the occurrence time of the next spike (*phase advance/delay*). The phase-response curve gives the phase advance or delay for a delta perturbation as sketched in Fig. 3.5, and the so called *infinitesimal* phase-response curve used in the following has a unit that is in Hz/[stim], where [stim] denotes the unit of the stimulus $s(t)$ [39]. The phase-response curve is also known by the names phase resetting curve, phase sensitivity or phase susceptibility. For mathematical details on the phase reduction and the phase-response curve please refer to the classical book by Kuramoto [96], or for an overview in the context of neuroscience to Ermentrout and Terman [38], as well as the references given in those.

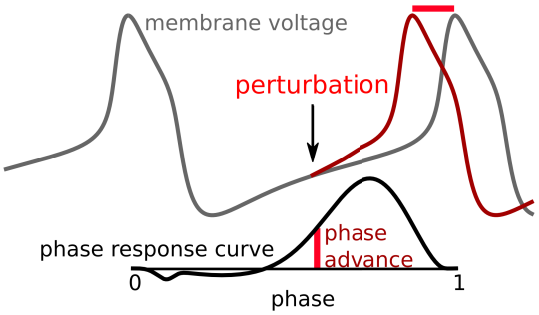

Figure 3.5.: The phase-response curve measures the phase advance (or delay) of the next spike in response to a delta perturbation.

The phase-response curve is, via its mathematical properties as solution to the adjoint equation of the dynamics, tightly related to the limit cycle period and the flow field around the limit cycle [142]. In the second publication, the membrane capacitance is changed, which directly affects the relaxation time of the voltage dynamics (Eq. 3.1). This changes the amplitude and the direction of the flow field in the phase space of voltage and each gating variable, and hence affects the phase-response curve in a direct way, both via the limit cycle period and the flow field. The phase-response curve changes particularly drastic around the saddle-node-loop bifurcation. The saddle-node-loop bifurcation not only deforms the flow field around the limit cycle, but the orbit flip lets the limit cycle (or at least half of it) jump to a new location, with a substantially different flow field than before. At the saddle-node-loop bifurcation, the orbit flips from the semistable manifold to the strongly stable manifold for the approach of the saddle-

node fixed point. This speeds up half of the limit cycle such that it can be effectively neglected in the phase description. This is also reflected in the phase-response curve, which is practically halved. This has drastic consequences for synchronization and other coding properties. A more detailed presentation of these points can be found in the second publication and Sec. 8.3.

3.4.1. Synchronization inferred from individual cells

The analysis in the second publication uses the phase-response curves around the saddle-node-loop bifurcation to derive drastic changes in the ability of cells to synchronize. What follows is an intuitive presentation of how synchronization on the network level can be inferred, via the phase-response curve, from properties of a single cell. The full mathematical derivation of the relation between synchronization and phase-response curve can be found in Kuramoto [96].

For a repetitively firing neuron, the phase-response curve measures how much a small input influences the timing of the next spike. When two neurons are synaptically coupled, they mutually affect each other's spiking. The interaction can synchronize the spiking, *i.e.*, the spikes occur at a fixed phase relation (the spike of one neuron occurs always at the same phase of the other). Note that this definition of synchronization (so-called *phase synchronization*) also includes what is sometimes called *anti-synchronization*, for which spiking alternates between both neurons. While anti-synchronization may not be easily recognized when observing more than a few units, *in-phase* synchronization has been proposed as a mechanism to link, for example, spatially separated representation of the same object [56]. Synchronization may also underlie rhythm generation in the hippocampus, important for memory [24], and has been related to several diseases such as schizophrenia, Parkinson's or epilepsy [168]. Spike synchronization to a common input, which is also facilitated around the saddle-node-loop bifurcation (see Sec. 8.3), is for example used to encode odors in the olfactory system [13, 77].

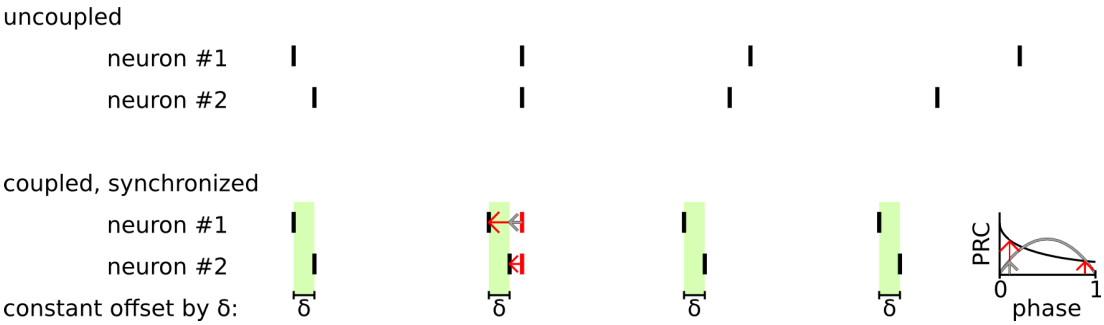

Figure 3.6.: Top: Spike times of two neurons with different but similar inter-spike-intervals. Bottom: Spike times of the same two neurons when coupled with delta-synapses such that the interaction is ruled by the asymmetric phase-response curve (black with red arrows). The symmetric phase-response curve would not lead to a constant phase difference δ, as both spikes would be advanced similarly (gray arrow), preserving the difference in the inter-spike-intervals.

In the example of Fig. 3.6, the two neurons synchronize when their mutual influence is asymmetric. Synchronization is reached when the neuron with the higher baseline firing rate is able to advance the spiking of the neuron with the lower baseline firing rate

more than *vice versa*. With excitatory coupling, the inter-spike-interval of each neuron will be shorter than the uncoupled inter-spike-interval due to the input it receives from the other neuron. A possible common inter-spike-interval duration is therefore shorter than both baseline inter-spike-interval. For synchronization, one neuron fires at a constant time delay δ before the other neuron. That implies that the first neuron receives the perturbation from the second neuron at a time δ *after* the first spikes, while the second neuron receives the perturbation from the first neuron at a time δ *before* the second spikes. A symmetric phase-response curve implies in such a symmetric coupling that the change in the inter-spike-intervals of both neurons is the same, and thus the difference between the baseline inter-spike-intervals cannot be reduced by the coupling. However, if the phase-response curve has an asymmetric component, this asymmetry can balance the asymmetry in the baseline inter-spike-intervals, and thereby allows for synchronization. Also in general, the asymmetry of the phase-response curve is related to the maximal frequency detuning (difference in firing rate) between two neurons that still allows them to synchronize. Assuming delta-synapses (coupling where a spike in one neurons induces an instantaneous increase in voltage in the other), the amplitude of the odd part of the phase-response curve is also related to their ability for synchronization in larger networks. In summary, (twice) the odd part of the phase-response curve corresponds to the *entrainment range* of two coupled oscillators, *i.e.*, the maximal phase difference (resulting from different baseline firing rates) that still allows for phase synchronization between the two. For details see Kuramoto [96].

While it seems at first glance counterintuitive to infer synchronization from a single cell, analog reasoning is used in everyday life. For example, for the Olympic discipline "synchronized swimming", the performance of the swimmers is evaluated based on their synchrony. While normally the synchrony is assessed from the actual performance of the whole group, it could, in principle, be already predicted based on the precision of one of the performers: The more professional each individual, the better the individual can be expected to observe the co-swimmers during his or her own action, and the more synchronous the group may perform. In a comparable way, synchronization of interacting neurons can also be estimated from the individual characteristics of the neurons.

3.5. Capacitance and temperature as bifurcation parameters for the saddle-node-loop bifurcation

As mentioned before, the saddle-node-loop bifurcation can be induced by various system parameters. While a considerable part of the discussion considers the temperature as bifurcation parameter (Chapter 10), the membrane capacitance, as an integral part of all conductance-based neuron models, is used as bifurcation parameter for the analysis in the second publication. The following sections establish the mathematical equivalence between membrane capacitance and a simplified temperature parameter, and set the latter into the broader context of temperature dependence in the nervous system.

3.5.1. Relative relaxation time constant as bifurcation parameter

The capacitance changes the velocities in the flow field of the dynamics in voltage dimension, while keeping the velocities in the gating dimensions unaffected. An increase in capacitance decreases the speed in voltage direction relative to the ion channel kinetics (Fig. 3.2). Slower dynamics in voltage direction effectively "squeezes" the flow field along the voltage dimension as the velocity vector becomes steeper, leading to a limit cycle that is less broad in the voltage dimension (Fig. 3.2). As shown in detail in the second publication, the deformation of the flow field by the membrane capacitance will, under mild assumptions, induce an saddle-node-loop bifurcation.

The second paper and Sec. 8.1 show that the capacitance as such is already an interesting parameter that could be regulated by nature. Yet, instead of using the capacitance to slow down the voltage dynamics, one can equally well use a parameter to speed up the gating dynamics. A prime candidate for this is the "temperature parameter" ϕ commonly introduced in conductance-based models [38] as prefactor to the right side of the gating dynamics. For example, for a gating variable a this gives

$$\frac{\mathrm{d}a}{\mathrm{d}t} = \phi \frac{a_\infty - a}{\tau_a}. \tag{3.4}$$

Whether the capacitance or ϕ is used as bifurcation parameter, one will observe the same bifurcations, because the capacitance can be transformed into a ϕ-like parameter by a simple scaling in time, $\tilde{t} = t/C_\mathrm{m}$. With this new time scale, Eq. 3.1 becomes

$$\frac{\mathrm{d}v}{\mathrm{d}\tilde{t}} = I_{input} - I_{ion(v,u)}, \tag{3.5}$$

$$\frac{\mathrm{d}m}{\mathrm{d}\tilde{t}} = 1/C_\mathrm{m} 1/\tau_\mathrm{m}(m_\infty - m), \tag{3.6}$$

$$\frac{\mathrm{d}n}{\mathrm{d}\tilde{t}} = 1/C_\mathrm{m} 1/\tau_\mathrm{n}(n_\infty - n), \tag{3.7}$$

$$..., \tag{3.8}$$

and with the identification $\phi = 1/C_\mathrm{m}$, a set of equations as in Eq. 3.4 is recovered. The parameter ϕ is called "temperature parameter" because, as reviewed in the next section, a scaling of the gating time constants is one of the main effects of temperature (Sec. 3.5.2).

3.5.2. Temperature affects the relative time constant

Temperature affects virtually any biological process, because an increase in temperature generically increases chemical reaction rates and diffusion. Hence, for conductance-based models of voltage-gated ion channels, basically all parameters should show some form of temperature dependence. Yet, experimental results suggest that the qualitatively strongest effect of temperature is on the opening and closing rates of the ion channels[7].

[7] Temperature influences not only ion channel kinetics and various other aspects of conductance-based ion channels, but also synaptic connections, neuronal properties and network dynamics, as reviewed

Observables such as gating rates tend to grow exponentially with an increase in temperature. A common measure for temperature dependence hence relies on the relative change in the parameter when the temperature is increased by 10°C, the so called Q_{10}-*values* [155]. Opening and closing rates typically show Q_{10} values between two and four [70]. Moreover, temperature has a medium effect on the maximal conductances of leak and ion channels, and a negligible effect on the membrane capacitance C_m and the reversal potentials V_k [70]. On the level of single neurons, these and potentially also other effects of temperature influence the resting membrane potential, the membrane time constant, and the firing rate, as reviewed by Wang et al. [174]. Action potentials and post-synaptic excitatory potentials (EPSPs) are faster and change in amplitude. For the conductance-based models used in Chapters 9 and 10, these various effects of temperature on neuronal dynamics are simplified, with a temperature dependency exclusively on the gating rates. To this end, the model definition Eq. 3.1 is augmented with the parameter ϕ introduced in Eq. 3.4. For simplicity, it is furthermore assumed that the scaling of the gating rates is equal for all gating variables, and that temperature does not affect the input. Note that a temperature dependence of the inputs would, for example, result from a network of connected, temperature-dependent neurons.

The assumption that the temperature dependence relies only on the gating rates (via the parameter ϕ) is quite restrictive. The following arguments show under which conditions this assumption can be relaxed. A rescaling of the time allows to take into account the temperature dependence of the maximal conductances and potentially the input current, and furthermore allows ion channel gating rates to differ between different gating variables, as reported experimentally. Temperature dependence is introduced in the general conductance-based model by scaling all conductances g_i by $\phi_{g\,i} = Q_{g\,i}^{\Delta T/10}$, input I_ext by $\phi_\mathrm{ext} = Q_\mathrm{ext}^{\Delta T/10}$ and all right-hand sides of the gating variables by $\phi_a = Q_a^{\Delta T/10}$ (where Q are different Q_{10} values for all parameters). Choosing $\phi_A = \min_a(\phi_a)$ for some fixed temperature difference ΔT, a rescaling of the time to $\tilde{t} = \phi_A t$ replaces Eq. 3.1 by

$$
\begin{aligned}
C_\mathrm{m}\frac{\mathrm{d}V}{\mathrm{d}\tilde{t}} &= \frac{1}{\phi_A}\left(\phi_\mathrm{ext}I_\mathrm{ext} + \phi_{g\,\mathrm{leak}}g_\mathrm{leak}\,(v - V_\mathrm{leak}) + \sum_\mathrm{k}\phi_{g\,k}g_k\,a_{k0}...a_{kj}\,(v - V_k)\right),\\
\frac{\mathrm{d}a}{\mathrm{d}\tilde{t}} &= \frac{\phi_a}{\phi_A}\frac{a_\infty - a}{\tau_a},\\
&....
\end{aligned}
$$

With this time scaling, it is obvious that, as long as $\max(\phi_\mathrm{ext}, \phi_{g\,i}) < \min_a(\phi_a) = \phi_A$, an increase in temperature will slow the voltage dynamics, and, for the gating variables, it will keep the rates constant or even increase them. Based on the results in the second publication, an approach of the saddle-node-loop bifurcation with temperature can hence be expected if $\max(Q_\mathrm{ext}, Q_{g\,i}) < \min_a(Q_a)$.

by Wang et al. [174], modulating for example brain rhythms [129].

3.6. Temperature variation in animals

If a change in brain temperature takes the dynamics of a neuron to the proximity of a saddle-node-loop bifurcation, this could have drastic consequences for neuronal processing. Below, examples for temperature dependence in animals as well as human pathologies are presented. The discussion of this thesis will in particular focus on the latter, suggesting that the saddle-node-loop bifurcation may act as a potential trigger for pathological brain states.

Variations in brain temperature are clearly critical for animals that do not actively regulate body temperature (*ectotherms*). Yet, variations in brain temperature also occur for *endotherms*, animals that control their body temperature. The brain temperature in endotherms depends on the brain metabolism, the cerebrospinal fluid and blood temperature, as reviewed by Wang et al. [174]. During ATP production for energy supply, about 33% of the energy is released as excess heat into the brain tissue [174]. The heat is emitted via blood-flow or via the surface of the head. Correspondingly, the temperature of deep brain areas is up to 1°C larger than the temperature of cortical brain areas (in rat even up to 1.5°C). The most superficial 2 to 3 cm of the cortex can be influenced by external heating and cooling (at least in monkeys), and in humans, the temperature gradient between brain tissue and blood can be up to 1°C [174].

In most ectotherms, brain and blood temperature are coupled, leading to an increase in brain temperature during physical exercise. Brain temperature in rat can increase by up to 2°C when the rat starts running [112], and significant increase in brain temperature during exercise has also been documented in humans [174]. Also without exercise, several experiments have shown physiological fluctuations in brain temperature in endotherms by 1 to 3°C [174].

In contrast to most animals that show an exercise-induced increase in brain temperature, certain mammals such as panting ungulates and carnivores have developed a mechanism that counters heating up: Air-cooled venous blood cools the arterial blood before it reaches the brain [5]. This allows them to keep their brain temperature 0.7 to 1.8°C below body core temperature even during physical activity. In my opinion, this highlights the importance of brain temperature for (endotherm) animals.

Functional alterations have already been reported for a change of 1°C, as reviewed by Wang et al. [174]. Compared to the physiological fluctuations of 1 to 3°C, this suggests that, even in healthy endotherms, temperature has a functional impact. In light of the results from the second project, drastic alteration in neuronal processing are expected when the change in temperature, acting as bifurcation parameter, drives neuronal dynamics into the proximity of saddle-node-loop bifurcations.

3.6.1. Medical conditions with temperature dependence

Temperature-induced alterations in brain function are particularly dramatic in pathology. The approach of a saddle-node-loop bifurcation with its drastic functional implications lends itself as one potential mechanism that could explain sudden transitions into a pathological state. The following presentation concentrates on pathologies where temperature can induces seizures. Seizures are devastating conditions during which controlled brain dynamics are replaced by abnormal enhanced and synchronous neuronal activity.

The most common type of temperature-dependent seizures are *febrile seizures*, also called *fever fits* or *fever cramps*. Around 5% of young children get, once in their life, a seizure during a period of high fever, with muscle cramps and, potentially, loss of consciousness [32]. Febrile seizures can have many causes, including temperature, inflammatory cytokines, mutated GABA receptors, or alkalosis, as reviewed by Cross [26], Dubé et al. [32]. Yet, rat experiments suggest that already an increase in brain temperature alone is sufficient to induce febrile seizure-like conditions. In wild-type rat, seizures are induced at a rectal temperature of a little above 42°C (commonly induced by hot air or bathing in hot water), see for example Gulec and Noyan [58], Klauenberg and Sparber [92], Mashimo et al. [105].

The precise mechanism for the induction of seizures with an increase in temperature is not yet known. One potential mechanism that emerges from this thesis is the approach of a (small) saddle-node-loop bifurcation, as discussed in Chapter 10.

Febrile seizures are particularly common in children with epileptic disorders. Temperature sensitivity is also known from other types of epilepsy, in which a hot bath ("hot-water epilepsy" [170]) or an abrupt change in air conditioning can be sufficient to induce seizures. In all these cases, an increase in temperature by just a few degree is sufficient to push brain dynamics into a seizure regime with abnormally enhanced and synchronous neuronal activity. On the other side, local cooling can stop emerging seizures, which is for example used during operations of patients with non-treatable epilepsy. As discussed later, the saddle-node-loop bifurcation may also be relevant for these conditions (Chapter 10).

3.7. Recapitulation

The last chapters have provided an overview over neuronal morphologies with different soma locations, spike generation mechanisms and signal processing. Going from dynamics over phase-response curves to synchronization, the second publication identifies the saddle-node-loop bifurcation as an interesting point for neuronal processing, accessible in a broad set of neuron models. The flexibility in spike-based coding that occurs at this transition point can also be interpreted as a lack of robustness, which may lead to system breakdowns such as observed during febrile seizures. With the temperature as bifurcation parameter, this perspective will be further elucidated later (Chapter 10). The main hypothesis of the first publication proposes energy-efficient signaling as a major driving force for different soma locations. This hypothesis is best assessed with the evolutionary outline and the alternative explanations reviewed in the last chapter in mind, and will be further considered in the discussion (Chapter 7).

Part II.

Publications

4. Externalization of neuronal somata as an evolutionary strategy for energy economization

CellPress

Current Biology
Magazine

Correspondence

Externalization of neuronal somata as an evolutionary strategy for energy economization

Janina Hesse[1,2]
and Susanne Schreiber[1,2,*]

Neuronal morphology of vertebrates and many invertebrates differs in a fundamental aspect: the location of neuronal cell bodies (somata) relative to their dendritic and axonal trees. The somata of most vertebrate neurons are located centrally between dendrites and axon. In contrast, neurons of various invertebrates, such as arthropods and cephalopods, typically externalize their somata to the end of a single process called a 'stem neurite' (Figure 1A). While this difference has been related to advantages of a spatial separation of neuropil and externalized somata [1–5], we here propose that the right soma location also reduces signal attenuation and consequently the energetic cost of signaling. Neurons commonly transfer signals from their dendrites to the axon, such that signals depolarize a centrally located soma before reaching the axon. The signal attenuation resulting from leakage through the soma membrane can be decreased through externalization of the soma, resulting in a reduction of the depolarized membrane area. In the light of evolutionary pressure towards energy-efficient signaling [6,7], we argue that an externalization of the soma is advantageous for relatively large somata. We support this hypothesis on the basis of compartmental models and previously published experimental data.

Typically, synaptic inputs depolarize the neuronal membrane. This signal propagates from the dendrites to the axon, where a spike can be initiated. On the way, depolarization amplitude is attenuated by passive properties of the membrane — a process that is counteracted by active membrane properties, such as voltage-activated sodium conductances. The lower the passive attenuation, the lower the amount of metabolic energy that needs to be invested in its compensation (either by boosting of the signal via active membrane properties or a larger synaptic input [8,9]). We here suggest that the right soma location decreases passive signal attenuation and hence also metabolic cost.

For a 'central soma' located between dendrites and axon, passive signal attenuation increases with the size of the soma membrane surface. A relocation of the soma to the end of a stem neurite (an 'externalized soma') removes the soma membrane from the signaling path (Figure 1A). Instead, signal attenuation occurs at the additional membrane provided by the stem neurite. An efficient soma location must therefore respect the trade-off between (central) soma surface and extra surface provided by the stem neurite.

In simulations of multicompartmental models with different soma locations and otherwise identical parameters (Figure S1A in Supplemental Information, published with this article online), we quantified the signal attenuation by the minimal dendritic signal amplitude required to reach a target depolarization in the axon (a spike, or, for passive models, a voltage threshold). The smaller this minimal dendritic signal, the smaller the signal attenuation between dendrites and axon. We show that the ratio of signal attenuation between models with central and externalized somata increases with the 'soma-to-neurite ratio', i.e., the ratio of the soma surface A and the 'depolarized' stem neurite surface, $A/\pi d\lambda$. The latter ratio depends on both morphological and electrophysiological parameters (see Supplemental Information). The critical soma-to-neurite ratio, defined as the value where attenuation in both models is equal, increases slightly with signal duration (Figure 1C, dashed curve). The simulations agree with corresponding analytical calculations (Figure 1C, solid curve). The calculations demonstrate that for short stimuli, externalized somata yield larger voltage responses than central somata (Figure 1B). All

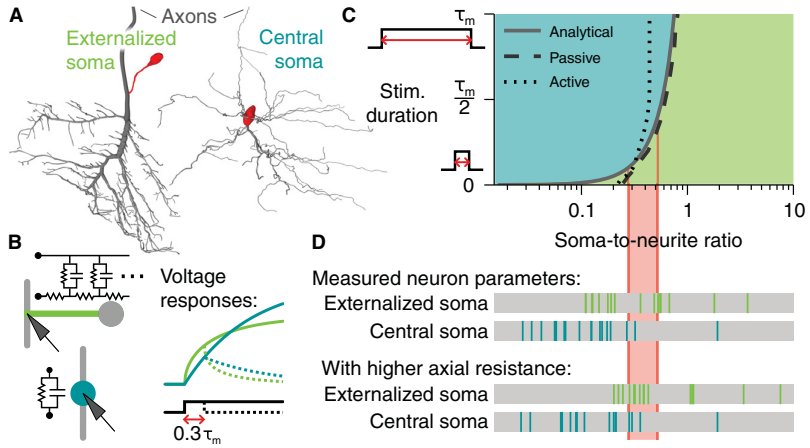

Figure 1. Signal attenuation in neurons with central or externalized soma location.
(A) Distinct morphology of neurons in the central nervous system of various invertebrates and vertebrates: in the former, the soma is externalized, while in the latter, a central location of the soma predominates (examples from blowfly and rat). (B) Left: circuit diagrams representing the analytical, simplified models. Right: voltage response to injected current pulses. The build-up of depolarization is initially faster for externalized somata, rendering them well adapted for the transmission of brief stimuli or high frequencies. (C) Color-coded morphology (either externalized in green, or central in blue) that is advantageous for signal attenuation as a function of the stimulus duration and the soma-to-neurite ratio for passive analytical models. Curves depict the critical soma-to-neurite ratios: analytical solution (solid curve), multicompartmental models with purely passive conductances (dashed), active models including spike generation (dotted). Above the critical soma-to-neurite ratio, externalization enhances energy efficiency. For illustration, the red box marks the soma-to-neurite interval corresponding to a biologically relevant range of stimulus durations ($0.1\tau_m$ – $0.4\tau_m$). (D) Experimental data on the soma-to-neurite ratio for neurons from various species (each vertical bar corresponding to one cell type; for details see Supplemental Information). Top: based on axial resistances as measured in dendrites or axons of the respective neurons, average soma-to-neurite ratio is larger in cells with externalized soma than in those with central soma. Bottom: assuming a higher axial resistance in the stem neurite (model prediction) increases this trend.

results qualitatively hold for models including active (Hodgkin–Huxley type) conductances in the axon (Figure 1C, dotted curve).

In summary, externalization of the soma reduces signal attenuation in cases of a large soma, a thin stem neurite, or a leaky membrane. Consequently, we predict that neurons with externalized soma tend to have a high soma-to-neurite ratio. For neurons with central soma, the soma-to-neurite ratio is not defined. Still, we can ask whether the central soma location would be more energy efficient, if the alternative was to move the soma to the end of a neurite whose diameter is assumed to scale with the diameter of the cell's proximal dendrites. Thus defining a soma-to-neurite ratio based on a 'virtual' stem neurite for neurons with central soma, we evaluate previously published morphological and electrophysiological data from various species and cell types (Table S1). Indeed, the soma-to-neurite ratio is significantly larger for neurons with externalized soma compared to neurons with central soma (Figure 1D, top traces, directed Mann-Whitney-U test with $p < 0.01$).

The soma-to-neurite ratio also depends on the length constant λ of the stem neurite, and hence on its axial resistance (see Supplemental Information). Experimental values of the latter were mostly derived from axons, where a low axial resistance facilitates signal propagation. A higher axial resistance in the stem neurite, however, would shield the soma and thus reduce signal attenuation. Based on our analysis, we hence predict that axial resistance in the stem neurite should be larger than in the axon. Assuming a higher, yet biologically plausible, axial resistance for the calculation of the soma-to-neurite ratio (250 Ωcm^2) allows for a better separation of soma-to-neurite ratios between central and externalized neurons (Figure 1D, bottom traces), in quantitative agreement with the optimal morphologies derived from the model (Figure 1C). This prediction on an electrophysiological parameter distinguishes our study from approaches based entirely on morphological aspects, and can be tested experimentally.

Our results suggest that an externalization of large somata decreases signal attenuation between dendrites and axon, benefiting information transfer in the context of noise, and saving metabolic energy otherwise required for an active boosting of neuronal signals. Previous work emphasized advantages of an externalization of the soma to the ganglion surface in the context of a separation of neuropil and soma layer, i.e., wiring length minimization [1,4], the use of graded potentials [5], and somatic access to nutrients [2,3]. Externalization has been proposed to shorten conduction times [1], which is a trend that is also found in our models. Our analysis adds a new perspective to the differential evolution of neuronal morphologies based on considerations of energy efficiency and reduced signal attenuation. While these effects hold for signals of different durations, quantitatively, externalization of the soma is particularly advantageous if inputs are short (Figure 1C).

Whether externalized somata of large size or central somata of small size — relative to the neurites — are favorable, is likely to be determined by additional factors. Those include constraints on the axial resistance of the stem neurite, the required soma volume for maintenance of the cell (such as for the synthesis machinery), the need for a central point of action for recurrent connections, and the frequency content of inputs.

It is noteworthy that even in mammals there are exceptions to the central soma location. Dorsal root ganglion cells transmit information from peripheral sensory areas along the spinal cord to the brain. These neurons exhibit large, externalized somata attached to stem neurites, the latter of which oftentimes are artificially prolonged by extensive wrapping around the soma [10]. We argue that this externalized morphology matches neuronal function: a central action point for recurrent connections is not required, somata can be larger to meet the maintenance demands of these extended cells, and a long stem neurite facilitates transmission of short signals (i.e., action potentials).

Interestingly, a look at the phylogenetic tree suggests that the Ur-bilaterian did not show an extensive externalization of neuronal somata (see Supplemental Information). Externalization of somata in higher invertebrates may hence have constituted an evolutionary strategy reducing neuronal energy consumption and signal attenuation while allowing for larger soma sizes (potentially desirable to accommodate more synthesis machinery for progressively elaborate nervous systems). Vertebrate neurons with central soma morphology may, on the other hand, have been preserved due to additional constraints and alternative optimization strategies, potentially including a higher recurrent connectivity or the outsourcing of organelles from soma into proximal dendrites.

SUPPLEMENTAL INFORMATION

Supplemental Information contains methods, one figure, and one table and can be found with this article online at http://dx.doi.org/10.1016/j.cub.2015.02.024.

REFERENCES

1. Ramón y Cajal, S. (1999). Texture of the Nervous System of Man and the Vertebrates, Volume I, P. Pasik and T. Pasik, eds. (New York: Springer).
2. Hanström, B. (1928). Some points on the phylogeny of nerve cells and of the central nervous system of invertebrates. J. Comp. Neurol. *46*, 475–493.
3. Sánchez-Soriano, N., Bottenberg, W., Fiala, A., Haessler, U., Kerassoviti, A., Knust, E., Löhr, R., and Prokop, A. (2005). Are dendrites in Drosophila homologous to vertebrate dendrites? Dev. Biol. *288*, 126–138.
4. Rivera-Alba, M., Peng, H., de Polavieja, G.G., and Chklovskii, D.B. (2014). Wiring economy can account for cell body placement across species and brain areas. Curr. Biol. *24*, R109–R110.
5. Niven, J.E., and Farris, S.M. (2012). Miniaturization of nervous systems and neurons. Curr. Biol. *22*, R323–R329.
6. Laughlin, S.B., and Sejnowski, T.J. (2003). Communication in neuronal networks. Science *301*, 1870–1874.
7. Niven, J.E., and Laughlin, S.B. (2008). Energy limitation as a selective pressure on the evolution of sensory systems. J. Exp. Biol. *211*, 1792–1804.
8. Attwell, D., and Laughlin, S.B. (2001). An energy budget for signaling in the grey matter of the brain. J. Cereb. Blood Flow Metab. *21*, 1133–1145.
9. Sengupta, B., Stemmler, M., Laughlin, S.B., and Niven, J.E. (2010). Action potential energy efficiency varies among neuron types in vertebrates and invertebrates. PLoS Comput. Biol. *6*, e1000840.
10. Matsuda, S., Kobayashi, N., Terashita, T., Shimokawa, T., Shigemoto, K., Mominoki, K., Wakisaka, H., Saito, S., Miyawaki, K., Saito, K., *et al*. (2005). Phylogenetic investigation of Dogiel's pericellular nests and Cajal's initial glomeruli in the dorsal root ganglion. J. Comp. Neurol. *491*, 234–245.

[1]Department of Biology, Institute for Theoretical Biology (ITB), Humboldt-Universität zu Berlin, 10115 Berlin, Germany. [2]Bernstein Center for Computational Neuroscience, 10115 Berlin, Germany.
*E-mail: s.schreiber@hu-berlin.de

Supplemental Information: Externalization of neuronal somata as an evolutionary strategy for energy economization

Janina Hesse, Susanne Schreiber

Supplemental Data

Based on our analysis, we predict that the soma-to-neurite ratio should be larger for neurons with externalized soma (also called (pseudo-)unipolar neurons) and smaller for neurons with central soma (also called bi- and multipolar neurons). To test this prediction, we scanned the literature for neurons with known morphological and electrophysiological data. The data in Table S1 were obtained from previously published experimental data. Table S1 summarizes soma surface area, axial resistance, specific membrane resistance, and soma location for neurons from different species. For neurons with externalized soma, the stem neurite diameter is provided in addition. For neurons with central soma, the equivalent *dendrite diameter* of the proximal dendrites is given instead, measured as the equivalent cylinder diameter after Rall's formula $d_{dend}^{3/2} = \sum d_i^{3/2}$, with d_i marking the diameter of proximal dendrite i.

For reconstruction data, soma surfaces could be obtained directly, while neurite diameters were quantified as the mean diameter along the proximal process until the first bifurcation. For two-dimensional stainings, soma surface was estimated as $A = \pi S$ if the somatic area S of the soma projection was provided in the original publication. Otherwise we assumed $A = \pi ab$, where a and b are the lengths of the two main axes of the soma projection. The neurite diameters were quantified proximal to the soma at a distance corresponding to the somatic radius.

Note that the surface area of externalized somata may be biased towards smaller values, and the data presented in Figure 1D may hence underestimate the corresponding soma-to-neurite ratios. This bias arises from a considerable increase of the surface of externalized somata due to invaginations [S1, S2]. Our estimates of the soma-to-neurite ratios of neurons with externalized soma hence are conservative.

Relation between stem neurite and dendrite diameter:

The soma-to-neurite ratio of neurons with externalized soma can be calculated based on the data given in Table S1. Neurons with central soma, however, lack a stem neurite. To allow for a comparison of both morphologies, we compared central morphologies to morphologies with a "virtual" stem neurite. Because the maintenance of axonal and dendritic trees requires proteins supplied by synthesis machinery predominantly located in the soma, it seemed reasonable to assume a relation between the diameter of the stem neurite and the dimensions of axonal and dendritic trees. Based on experimental data, we assumed that the stem neurite diameter d_{stem} is proportional to the equivalent diameter of the proximal dendrites d_{dend} (Figure S1F). Least-squares regression (excluding one outlier) results in $0.53 d_{\text{dend}} - 0.04$, with a correlation coefficient of $r = 0.97$. We hence assumed stem neurites with $d_{\text{stem}} = 0.5 d_{\text{dend}}$.

Supplemental Methods

Signal attenuation was compared in models with central or externalized soma, differing exclusively in the soma location. Multicompartmental models (Figure S1A) with purely passive membranes, as well as additional active conductances in the axon initial segment, were considered. Moreover, simplified single-compartment models were used to compare simulation results to analytical calculations (Figure 1B).

Signal attenuation was quantified based on the axonal membrane potential in response to dendritic current stimulation. Specifically, the amplitude of a dendritic current pulse was increased stepwise until a predefined depolarization (i.e., a voltage threshold) was reached in the axon for the passive models. For active models, the amplitude of the dendritic pulse was increased until a spike was initiated. The minimal dendritic current amplitude required to

reach the predefined voltage (or to elicit a spike) defined our estimate of signal attenuation. The larger the dendritic current required to elicit a specified axonal response, the larger the signal attenuation.

Our results showed for any model parameter combination whether a central or an externalized soma location implied less signal attenuation. Our interpretation relies on the assumption that a larger signal attenuation eventually entails a larger metabolic cost. In order to reach a given signal amplitude at the axon, neurons can counteract a passive attenuation of the signal by active ion channels that increase the signal either directly at the synapse, or along the signaling path. However, this kind of boosting is energetically costly. In fact, neurons have been found to spend large parts of their energy budget on reversing signal-related ion flow across the membrane both at synapses as well as along dendrites and axons [S3, S4, S5], for a discussion on the recent development of energy-efficient signaling also see [S6]. A minimization of signal attenuation may hence be desirable from an evolutionary perspective, benefiting an efficient usage of scarce energetic resources. Consequently, a soma location that decreases signal attenuation between dendrite and axon may be favored by evolution.

Multicompartmental models:

Multicompartmental models consisted of one dendrite and one axon, either with a central soma compartment in between, or with the soma compartment at the end of an additional stem neurite compartment (Figure S1A). Despite possible deviations from these morphologies, most neurons in both vertebrates and invertebrates exhibit one main output process with a spike initiation zone at its proximal end, see for example [S7, S8]. We replaced the elaborated axonal and dendritic trees found in vertebrates and invertebrates by single axon and dendrite cylinders. This simplification is exact for branched trees that follow Rall's $d^{3/2}$ constraint on branch diameters, such that the whole tree can be replaced by an equivalent cylinder. The axon comprised three compartments: a proximal axon initial segment (passive), a distal axon initial segment (the site of recording and, for the active model, spike initiation) and a long axon compartment (for the sake of simplicity passive and unmyelinated).

Model specification:

The passive membrane properties were given by the specific membrane capacitance of $C_m = 1\mu F/cm^2$, the passive reversal potential of $E_{passive} = -65mV$, and the specific membrane resistance R_m that was varied in the interval of $[3000,30000]\ \Omega cm^2$. The axial resistance R_a was varied in $[40,400]\ \Omega cm$.

In order to compare results from models with different axial and membrane resistances, we set the length of processes in electrotonic units. The space constant λ characterizes the spatial spread of a depolarization; it is defined as $\lambda = \sqrt{\frac{R_m}{R_a}\frac{d}{4}}$, with d specifying the process diameter. Axonal and dendritic d was set to $2\mu m$. The two proximal axon compartments (axon initial segment compartments) had a length of 0.05λ; lengths of dendritic and distal axon compartment were set to 2λ, which was sufficient to prevent boundary effects.

For the active models, the distal axon initial segment compartment was equipped with original Hodgkin-Huxley ion channels [S9]. Their density was adapted to allow for action potential initiation in the relatively small axon initial segment (peak sodium conductance $\bar{g}_{Na} = 1/R_m\ 50666 S/cm^2$, a proportional peak potassium conductance of $\bar{g}_K = 0.3\,\bar{g}_{Na}$, and no additional leak, $\bar{g}_L = 0$). Temperature was set to 23°C.

The stem neurite diameter d_{stem} was investigated in the interval $[0.8,15]\ \mu m$. Stem neurite length was fixed to $L_{stem} = 0.5\lambda$ unless stated otherwise. The soma diameter and length were identical (matching the surface area of a sphere with the same diameter) and were explored in the interval $[4,100]\ \mu m$, i.e., the soma surface ranged from around $200\mu m^2$ to more than $10^5\mu m^2$.

The models were implemented in NEURON [S10] via its python interface [S11]. Temporal resolution was 0.01ms. The stimulation electrode (current clamp of NEURON) was located in the dendrite compartment, 0.1λ from the proximal end. This location was required to prevent a broadening of the dendritic signal due to the passive cable properties of the dendrite. For stimulation, step currents of fixed duration were used. Stimulus duration was adapted to the membrane time constant, $\tau_m = C_m R_m$, to allow for a comparison between models of different specific membrane resistance. Voltage responses were recorded in the distal axon initial segment.

Measurements:

We compared signal attenuation in models with central or externalized soma location: axon and dendrite compartments were either both attached to the soma compartment (central soma), or to the stem neurite compartment at the end opposite the soma (externalized soma). For all parameter combinations of axial resistance, specific membrane resistance, soma diameter, and stem neurite diameter, we evaluated the relative signal attenuation of the models with central versus externalized soma. Parameter ranges (as specified above) were sampled equidistantly with at least 10 data points for each parameter.

Minimal dendritic stimulation was used to measure signal attenuation (requiring a crossing of the voltage threshold set to 30mV in passive models, or the initiation of a spike in active models). Spikes were identified by voltage changes faster than 100V/s, $dV/dt > 100$V/s. *Relative attenuation* was defined as the ratio of the minimal dendritic current amplitude measured in the model with central soma and the minimal dendritic current amplitude measured in the model with externalized soma (Figure S1B).

We note that in our model the relative minimal dendritic stimulation is (approximately) equivalent to the relative axonal signal strength (i.e., the ratio of the maximal voltage observed in response to a dendritic current step of equal amplitude). The latter data are depicted in the inset to Figure S1C, showing the relative maximal axonal depolarization without noise, and – as measure of the signal-to-noise level – the relative mean axonal depolarization normalized by the standard deviation of the voltage fluctuation for the case with an additional white noise current input in the axon initial segment. Our measure hence quantifies either energy consumption (assuming a signal is boosted) or signal attenuation (i.e., the extend by which the signal is reduced if not actively amplified). In the presence of axonal noise, smaller axonal signal amplitudes reduce the signal-to-noise ratio and hence information transfer.

Supplemental Results

Multicompartmental models:

Relative attenuation substantially increased with soma-to-neurite ratio for both passive and active models (Figure S1C and Figure S1D). This effect prevailed when prolonging the stimulus duration, shortening the stem neurite, or increasing dendrite and axon diameter, though the curves became shallower. For soma-to-neurite ratios above the critical value (i.e. favorable externalization), longer stem neurites led to better shielding of the externalized soma and thus to larger relative signal attenuation, and relative signal attenuation also increased for shorter stimuli (Figure S1E). The effect of signal duration on relative attenuation is explained by differences in the total capacitive current between models with central versus externalized soma. In the central morphology, the whole soma is depolarized when a signal passes, and hence contributes to the capacitive current (and to signal attenuation). In the externalized morphology, only those parts of the stem neurite that are depolarized contribute. For shorter stimuli, spread of the depolarization into the stem neurite is smaller and hence also the total capacitive current. This effect explained the dependence of the critical soma-to-neurite ratio on the duration of the stimulus pulse (Figure 1C), and may contribute to the reliable transmission of action potentials reported for dorsal root ganglion cells [S12]. Furthermore, the critical soma-to-neurite ratio showed a weak dependence on stem neurite

length (data not shown) and was mostly independent of dendrite and axon diameter as well as specific membrane capacitance.

While in passive models the critical soma-to-neurite ratio was well confined, it more strongly depended on model parameters in active models (exemplified by the larger horizontal width of the gray area at an attenuation ratio of 1, Figure S1D). In the main text, the dotted curve in Figure 1C depicts the mean critical soma-to-neurite ratio across active models.

For completeness, we note that in general, our results also hold for somata with active conductances. Active somatic conductances can boost the propagating signal and hence reduce signal attenuation. This process is comparable to a boosting of the signal in the dendrite (like in the minimal-dendritic-stimulation paradigm). In both cases, it is the ionic charges "lost" through the membrane leak that are compensated for by a flow of charges, either via the dendritic or somatic membrane. The energetic cost in both scenarios is directly related to this charge transfer, and for the most energy-efficient location of the soma, it is of minor relevance whether the signal is boosted at the dendrite or at the soma.

Single-compartment models:

Simplification of the multicompartment models allowed us to derive an analytical formula for the critical soma-to-neurite ratio that almost precisely matched the passive models with long stem neurite (Figure 1C, dashed and straight curve). The central soma amounted to an iso-potential sphere of surface area A. The externalized soma was not explicitly included under the assumption that a long stem neurite shielded the soma. The stem neurite corresponded to a semi-infinite cable of diameter d and with length constant λ. See Figure 1B for corresponding circuit diagrams.

For both models, the relation between a current step input and the resulting voltage are known [S13]. The maximal depolarization in response to a step current (amplitude I and duration $\Delta \cdot \tau_m$) for the central soma model is given by $V_{central} = I\left(1-e^{-\Delta}\right)R_m / A$. For the externalized soma model it is given by $V_{external} = I\mathrm{erf}\left(\sqrt{\Delta}\right)4R_a\lambda/\left(\pi d^2\right)$, where *erf* denotes the error function.

At the critical soma-to-neurite ratio, current amplitudes and maximal voltage responses of both models have to be equal in the minimal stimulation paradigm. Consequently, the critical soma-to-neurite ratio was given by $A/\left(\pi d\lambda\right) = \left(1-e^{-\Delta}\right)/\mathrm{erf}\left(\sqrt{\Delta}\right)$. Note that the analytical model showed directly that the effect of stimulus duration on the critical soma-to-neurite ratio (Figure 1C) agrees to the dependence of depolarization spread on stimulus frequencies in passive cables [S14]; stimuli of lower frequency spread further.

Intuitively, the soma-to-neurite ratio can be interpreted as the ratio of the soma surface A to the depolarized parts of the stem neurite surface (i.e., $\pi d\lambda$). For step current inputs of infinite duration, the critical soma-to-neurite ratio is one. In this case, signal attenuation at the central soma is larger than at the stem neurite because the soma surface, and thereby the total somatic leak current, is larger than the depolarized surface of the stem neurite and the corresponding leak current.

The equation $V_{central} = I\left(1-e^{-\Delta}\right)R_m / A$ shows that, in principle, for a central soma location signal attenuation could also be reduced by increasing the somatic membrane resistance (corresponding to a decrease in leak conductance). While such a strategy may help to maintain a large signal amplitude despite a central soma location, the increase in membrane resistance results in an increase of the membrane time constant and hence significantly slows down processing. In contrast, the externalization of the soma advocated in this study does not require an increase in membrane resistance, and increases processing speed even further by a reduction of the capacitive load.

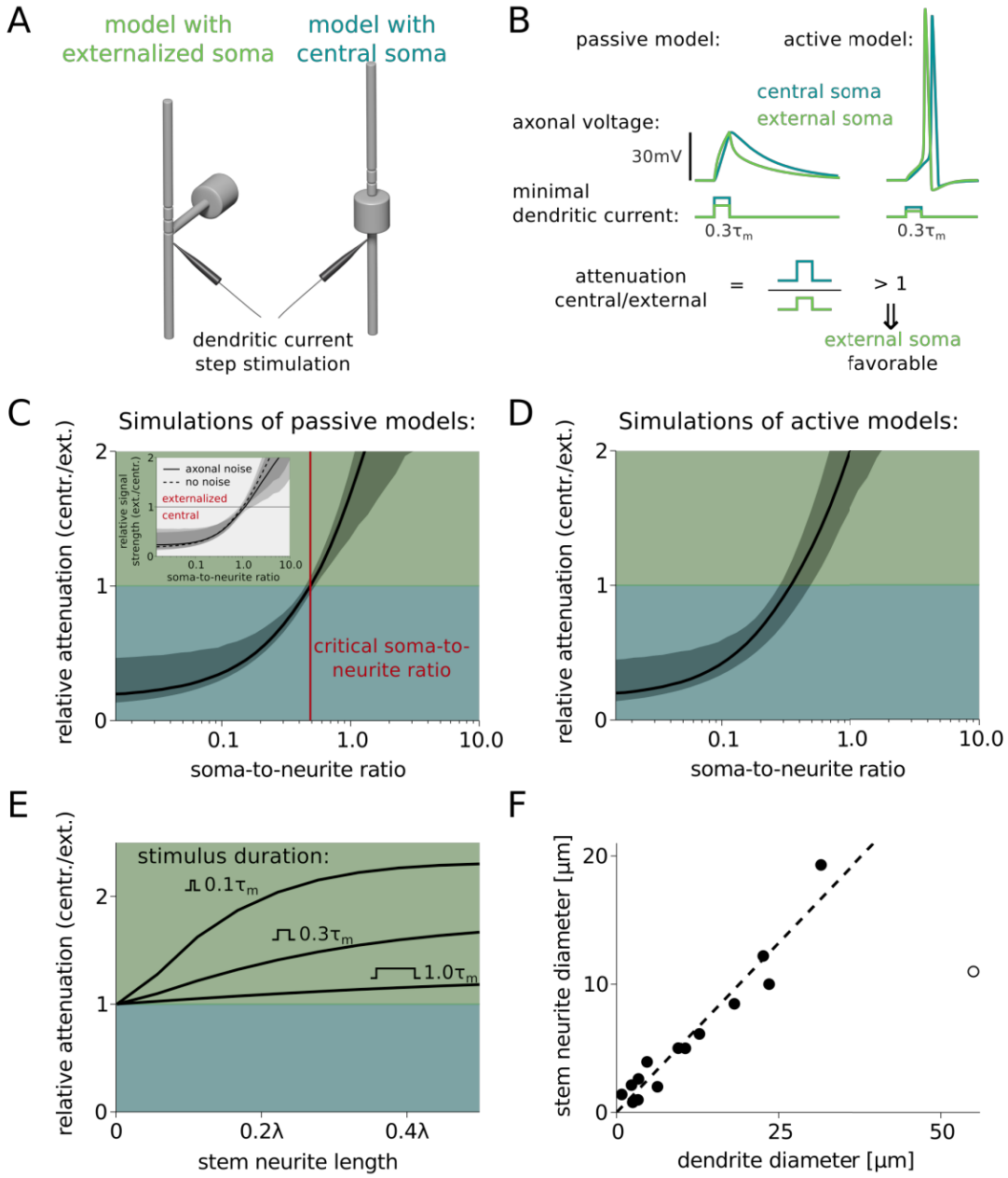

Figure S1: (A) Structure of multicompartmental model neurons with central and externalized soma. (B) Minimal dendritic stimulation paradigm. Signal attenuation is derived from the minimal amplitude of a current pulse required to cross a predefined voltage threshold (passive models) or to elicit a spike (active models). (C) Relative attenuation across models with different soma-to-neurite ratio (across all parameter combinations of soma diameter, stem neurite diameter, axial resistance and specific membrane resistance, with a stimulus duration of $0.3\tau_m$); medians (black curve) and 10th and 90th percentiles (gray area). Inset: Same analysis for the relative signal strength with and without noise for a constant dendritic current injection. Externalization is favorable for relative signal strengths above one. (D) Active models; same analysis as in C. (E) Relative signal attenuation as a function of stem neurite length for three different stimulus pulse durations. Example with a soma-to-neurite ratio that favors the externalized morphology. (F) Stem neurite diameter correlates well with primary dendrite diameter. Data points corresponding to all experimental data from neurons with externalized soma location (Table S1, with the exception of one cell not exhibiting a primary dendrite). Linear regression, excluding the outlier (open circle), yielded a slope of 0.53 (intercept = –0.04, r = 0.97).

Supplemental Discussion

Neurons with externalized soma (unipolar neurons) or with central soma (bi- and multipolar neurons) are observed in various phyla. While a detailed analysis goes beyond the scope of our study, the following picture emerged from an investigation of a subset of species. Cnidaria and Ctenophora, which are derived earlier than all Bilateria, have multipolar neurons with processes that do not show neuronal polarity (no clear dendrites and axons) (e.g., [S15, S16, S17]). The Bilateria are separated into the Deuterostomia and Protostomia. Within the Deuterostomia (e.g., vertebrates [S18], Echinodermata [S15, S19], lencelet [S20]), animals seem to have predominantly bi- and multipolar neurons. Within the Protostomia, a clear predominance of unipolar neurons within the central nervous system is observed for Arthropoda (e.g., [S21]), Nemertea (e.g., [S22]), and Rotifera (e.g., Asplanchna brightwellii [S23]). A mixture of unipolar, bi- and multipolar neurons with a predominance of unipolar neurons is found for Annelida (e.g., Pogonophora [S24]) and Mollusca (e.g., [S25]). A mixture of both morhologies, but with clear predominance of bi- and multipolar neurons, is found for Platyhelminthes (flat worms, e.g., Mesostoma [S26], policlads, and probably other Turbellaria [S27]) and Nematoda (e.g., C. elegans [S24]).

We conclude that it is highly unlikely that the evolutionary older morphology is the unipolar one, because

- bi- and multipolar neurons dominate in certain species from both Deuterostomia and Protostomia, especially in earlier derived branches,
- unipolar neurons do not dominate in any Deuterostomia,
- and non-Bilaterian phyla do not show unipolar neurons at all.

Neuron example images:

The neurons with central and externalized soma shown in Figure 1A were drawn with Py3DN [S28] and Blender (blender.org) based on reconstructions from NeuroMorpho.Org [S60]. The neuron with externalized soma on the left is a tangential cell (interneuron) from the blowfly visual lobe (lobula plate) from [S29], NeuroMorpho.Org ID: NMO_06636. The neuron with central soma on the right is a layer 2/3 pyramidal cell from rat neocortex (medial prefrontal cortex) from [S30], NeuroMorpho.Org ID: NMO_09626.

Neurons with externalized soma	R_a [Ωcm]	R_m [Ωcm^2]	Soma area [μm^2]	Stem diameter [μm]	Source
blowfly CH cell	60	2500	2265	2.6	[S31, S29][a]
blowfly HS cell	40	2000	2113	6.1	[S31, S29][a]
blowfly VS cell	40	2000	1600	5.0	[S31, S29][a]
fruit fly DM1 neuron	178	16500	385	0.8	[S32][b]
fruit fly HS cell	400	8166	336	1.0	[S33][c]
locust ocellar L-neuron	24	2000	13397	19.3	[S34]
locust LGMD neuron	60	4500	8214	10.0	[S35][d]
cricket MG interneuron	100	4000	7521	5.0	[S36, S37]
cockroach motorneuron (nymphal)	130	30000	1087	2.1	[S38]
cockroach motorneuron (adult)	130	30000	3318	3.9	[S38]
cockroach giant interneuron	132	16200	8874	8.5	[S39, S40]
lobster motorneuron	60	2290	19254	10.8	[S41, S42][a]
crayfish MG neuron	60	1996	122554	11.0	[S43]
crayfish LG interneuron (nymphal)	60	8600	2942	2.0	[S44]
crayfish LG interneuron (adult)	60	20900	13685	12.2	[S44]
rat DRG cell (cultured)	70	3300	3217	1.4	[S12]
Neurons with central soma	R_a [Ωcm]	R_m [Ωcm^2]	Soma area [μm^2]	Dendrite diameter [μm]	Source
goldfish area II neuron	150	33333	2679	7.5	[S45]
turtle granule cell	100	30300	79	1.6	[S46]
guinea-pig Purkinje neuron	250	500	1948	5.5	[S47][a]
mouse granule cell	194	38000	514	5.2	[S48][b]
rat DG interneuron (GCLP)	200	10300	1520	5.2	[S49][a]
rat DG interneuron (IMLP)	200	15100	1100	5.3	[S49][a]
rat DG interneuron (OMLP)	200	23400	1890	5.2	[S49][a]
rat DG interneuron (TMLP)	200	13400	740	9.2	[S49][a]
rat Purkinje neuron	115	122000	1214	3.1	[S50]
rat ventral horn neuron	87	5300	2064	11.4	[S51]
rat DG basket cell	172	7600	1051	6.4	[S52][b]
rat pyramidal cell (CA1)	178	87736	578	6.5	[S53][b]
rat pyramidal cell (visual cortex)	390	120000	1500	12.6	[S54]
rat pyramidal cell (neo-cortex)	100	25000	1566	9.9	[S55][b]
rat pyramidal cell (barrel cortex)	150	4500	349	6.5	[S56][e]
cat X cell	200	5534	688	10.3	[S57, S58]
cat Y cell	200	4451	1549	15.6	[S57, S58]
cat motorneuron	70	2500	10000	34.3	[S59]

Table S1: Parameters of all neurons used in the study; morphological and electrophysiological data taken from the literature, references noted under *Source*. *Soma area* specifies the surface area of the soma. Axial resistance R_a and specific membrane resistance R_m are stated as reported in the corresponding publications (noted under *Source*). *Dendrite diameter* refers to the equivalent cylinder diameter representing all proximal dendrites.

[a] Reconstructions from NeuroMorpho.Org [S60].
[b] Neuronal parameters from ModelDB [S61].
[c] Data kindly provided by Hermann Cuntz.
[d] Data kindly provided by Fabrizio Gabbiani.
[e] Data kindly provided by Guy Leyal and Idan Segev.

Supplemental References

[S1] Trujillo-Cenóz, O. (1962). Some aspects of the structural organization of the arthropod ganglia. Zeitschrift für Zellforschung und Mikroskopische Anatomie 56, 5, 649–682.

[S2] Gwilliam, G. F. and Burrows, M. (1980). Electrical characteristics of the membrane of an identified insect motor neurone. J Exp Biol 86, 1, 49–61.

[S3] Attwell, D. and Laughlin, S. B. (2001). An energy budget for signaling in the grey matter of the brain. J. Cereb. Blood Flow Metab. 21, 10, 1133–1145.

[S4] Alle, H., Roth, A., and Geiger, J. R. P. (2009). Energy-efficient action potentials in hippocampal mossy fibers. Science 325, 5946, 1405–1408.

[S5] Sengupta, B., Stemmler, M., Laughlin, S. B., and Niven, J. E. (2010). Action potential energy efficiency varies among neuron types in vertebrates and invertebrates. PLoS Comput Biol 6, 7, e1000840.

[S6] Sengupta, B., Stemmler, M. B., and Friston, K. J. (2013). Information and efficiency in the nervous system – a synthesis. PLoS Comput Biol 9, 7, e1003157.

[S7] Bucher, D. and Goaillard, J.-M. (2011). Beyond faithful conduction: Short-term dynamics, neuromodulation, and long-term regulation of spike propagation in the axon. Progress in Neurobiology 94, 4, 307–346.

[S8] Trunova, S., Baek, B., and Giniger, E. (2011). Cdk5 regulates the size of an AIS-like compartment in mushroom body neurons of the Drosophila central brain. J Neurosci 31, 29, 10451–10462.

[S9] Hodgkin, A. L. and Huxley, A. F. (1952). A quantitative description of membrane current and its application to conduction and excitation in nerve. J Physiol 117, 4, 500–544.

[S10] Carnevale, N. T. and Hines, M. L. (2006). The NEURON Book (Cambridge: Cambridge University Press).

[S11] Hines, M. L., Davison, A. P., and Muller, E. (2009). NEURON and python. Front Neuroinformatics 3.

[S12] Luscher, C., Streit, J., Quadroni, R., and Luscher, H. R. (1994). Action potential propagation through embryonic dorsal root ganglion cells in culture. I. Influence of the cell morphology on propagation properties. Journal of Neurophysiology 72, 2, 622–633.

[S13] Jack, J. J. B., Noble, D., and Tsien, R. W. (1975). Electric current flow in excitable cells (Oxford: Clarendon Press).

[S14] Koch, C. (2004). Biophysics of Computation: Information Processing in Single Neurons (Oxford: Oxford University Press).

[S15] Dudel, J., Menzel, R., and Schmidt, R. F. (2001). Neurowissenschaft: Vom Molekül zur Kognition (Berlin: Springer).

[S16] Holland, N. D. (2003). Early central nervous system evolution: An era of skin brains? Nature Reviews Neuroscience 4, 8, 617–627.

[S17] Craig, A. M. and Banker, G. (1994). Neuronal polarity. Annual Review of Neuroscience 17, 1, 267–310.

[S18] Kandel, E. R., Schwartz, J. H., and Jessell, T. M. (2000). Principles of neural science (New York: McGraw-Hill, Health Professions Division).

[S19] Cobb, J. L. S. (1985). The neurobiology of the ectoneural/hyponeural synaptic connection in an echinoderm. The Biological Bulletin 168, 3, 432–446.

[S20] Bone, Q. (1960). The central nervous system in Amphioxus. The Journal of Comparative Neurology 115, 1, 27–64.

[S21] Roeder, K. D. (1998). Nerve Cells and Insect Behavior (Cambridge, MA: Harvard University Press).

[S22] Hanström, B. (1928). Some points on the phylogeny of nerve cells and of the central nervous system of invertebrates. The Journal of Comparative Neurology 46, 2, 475–493.

[S23] Hochberg, R. (2009). Three-dimensional reconstruction and neural map of the serotonergic brain of Asplanchna brightwellii (Rotifera, Monogononta). Journal of Morphology 270, 4, 430–441.

[S24] Harrison, F. W. and Rice, M. E. (1993). Microscopic Anatomy of Invertebrates, Onychophora, Chilopoda, and Lesser Protostomata (New York: John Wiley & Sons, Ltd).

[S25] Tauc, L. (1966). Brains to Cells: The Neuroanatomy of Selected Gastropod Species. In Wilbur, K. M. and Yonge, C. M., eds., Physiology of Mollusca. (San Diego: Academic Press). pp. 387–454.
[S26] Koopowitz, H., Elvin, M., and Bae, T. (1995). Comparison of the nervous system of the rhabdocoel Mesostoma ehrenbergii with that of the polyclad Notoplana acticola. Hydrobiologia 305, 1-3, 127–133.
[S27] Koopowitz, H. (1989). Polyclad Neurobiology and the Evolution of Central Nervous Systems. In Anderson, P. A. V., ed., Evolution of the First Nervous Systems. (New York: Springer US), 188. pp. 315–328.
[S28] Aguiar, P., Sousa, M., and Szucs, P. (2013). Versatile morphometric analysis and visualization of the three-dimensional structure of neurons. Neuroinform 11, 4, 393–403.
[S29] Cuntz, H., Forstner, F., Haag, J., and Borst, A. (2008). The morphological identity of insect dendrites. PLoS Comput. Biol. 4, 12, e1000251.
[S30] Bories, C., Husson, Z., Guitton, M. J., and Koninck, Y. D. (2013). Differential balance of prefrontal synaptic activity in successful versus unsuccessful cognitive aging. J. Neurosci. 33, 4, 1344–1356.
[S31] Borst, A. and Haag, J. (1996). The intrinsic electrophysiological characteristics of fly lobula plate tangential cells: I. Passive membrane properties. Journal of Computational Neuroscience 3, 4, 313–336.
[S32] Gouwens, N. W. and Wilson, R. I. (2009). Signal propagation in Drosophila central neurons. J. Neurosci. 29, 19, 6239–6249.
[S33] Cuntz, H., Forstner, F., Schnell, B., Ammer, G., Raghu, S. V., and Borst, A. (2013). Preserving neural function under extreme scaling. PLoS ONE 8, 8, e71540.
[S34] Ammermüller, J. (1986). Passive cable properties of locust ocellar L-neurons. Journal of Comparative Physiology A: Neuroethology, Sensory, Neural, and Behavioral Physiology 158, 3, 339–344.
[S35] Peron, S. P., Krapp, H. G., and Gabbiani, F. (2007). Influence of electrotonic structure and synaptic mapping on the receptive field properties of a collision-detecting neuron. J. Neurophysiol. 97, 1, 159–177.
[S36] Hill, A. A. V., Edwards, D. H., and Murphey, R. K. (1994). The effect of neuronal growth on synaptic integration. Journal of Computational Neuroscience 1, 3, 239–254.
[S37] Jacobs, G. A. and Murphey, R. K. (1987). Segmental origins of the cricket giant interneuron system. J. Comp. Neurol. 265, 1, 145–157.
[S38] Hochner, B. and Spira, M. E. (1987). Preservation of motoneuron electrotonic characteristics during postembryonic growth. J. Neurosci. 7, 1, 261–270.
[S39] Harrow, I. D., Hue, B., Pelhate, M., and Sattelle, D. B. (1980). Cockroach giant interneurones stained by cobalt-backfilling of dissected axons. J. Exp. Biol. 84, 341–343.
[S40] Yarom, Y. and Spira, M. E. (1983). Morphological and electrophysiological properties of giant interneurons during the postembryonic development of the cockroach CNS. Developmental Brain Research 8, 2–3, 321–334.
[S41] Hodgkin, A. L. and Rushton, W. A. H. (1946). The electrical constants of a crustacean nerve fibre. Proc. R. Soc. Lond. B 133, 873, 444–479.
[S42] Oginsky, M. F., Rodgers, E. W., Clark, M. C., Simmons, R., Krenz, W.-D. C., and Baro, D. J. (2010). D(2) receptors receive paracrine neurotransmission and are consistently targeted to a subset of synaptic structures in an identified neuron of the crustacean stomatogastric nervous system. J. Comp. Neurol. 518, 3, 255–276.
[S43] Glantz, R. M. and Viancour, T. (1983). Integrative properties of crayfish medial giant neuron: steady-state model. J Neurophysiol 50, 5, 1122–1142.
[S44] Edwards, D. H., Yeh, S. R., Barnett, L. D., and Nagappan, P. R. (1994). Changes in synaptic integration during the growth of the lateral giant neuron of crayfish. Journal of Neurophysiology 72, 2, 899–908.
[S45] Weaver, C. M. and Wearne, S. L. (2008). Neuronal firing sensitivity to morphologic and active membrane parameters. PLoS Comput Biol 4, 1, e11.
[S46] Gabbiani, F., Midtgaard, J., and Knopfel, T. (1994). Synaptic integration in a model of cerebellar granule cells. Journal of Neurophysiology 72, 2, 999–1009.

[S47] Rapp, M., Segev, I., and Yarom, Y. (1994). Physiology, morphology and detailed passive models of guinea-pig cerebellar purkinje cells. J Physiol 474, 1, 101–118.
[S48] Schmidt-Hieber, C., Jonas, P., and Bischofberger, J. (2007). Subthreshold dendritic signal processing and coincidence detection in dentate gyrus granule cells. J. Neurosci. 27, 31, 8430–8441.
[S49] Mott, D. D., Turner, D. A., Okazaki, M. M., and Lewis, D. V. (1997). Interneurons of the dentate–hilus border of the rat dentate gyrus: Morphological and electrophysiological heterogeneity. J. Neurosci. 17, 11, 3990–4005.
[S50] Roth, A. and Häusser, M. (2001). Compartmental models of rat cerebellar purkinje cells based on simultaneous somatic and dendritic patch-clamp recordings. J Physiol 535, 2, 445–472.
[S51] Thurbon, D., Lüscher, H.-R., Hofstetter, T., and Redman, S. J. (1998). Passive electrical properties of ventral horn neurons in rat spinal cord slices. Journal of Neurophysiology 79, 5, 2485–2502.
[S52] Nörenberg, A., Hu, H., Vida, I., Bartos, M., and Jonas, P. (2009). Distinct nonuniform cable properties optimize rapid and efficient activation of fast-spiking GABAergic interneurons. PNAS, 200910716.
[S53] Golding, N. L., Mickus, T. J., Katz, Y., Kath, W. L., and Spruston, N. (2005). Factors mediating powerful voltage attenuation along CA1 pyramidal neuron dendrites. J Physiol 568, 1, 69–82.
[S54] Major, G., Larkman, A. U., Jonas, P., Sakmann, B., and Jack, J. J. (1994). Detailed passive cable models of whole-cell recorded CA3 pyramidal neurons in rat hippocampal slices. J. Neurosci. 14, 8, 4613–4638.
[S55] Hay, E., Schürmann, F., Markram, H., and Segev, I. (2013). Preserving axosomatic spiking features despite diverse dendritic morphology. Journal of Neurophysiology 109, 12, 2972–2981.
[S56] Sarid, L., Feldmeyer, D., Gidon, A., Sakmann, B., and Segev, I. (2013). Contribution of intracolumnar layer 2/3-to-layer 2/3 excitatory connections in shaping the response to whisker deflection in rat barrel cortex. Cereb. Cortex, bht268.
[S57] Bloomfield, S. A., Hamos, J. E., and Sherman, S. M. (1987). Passive cable properties and morphological correlates of neurones in the lateral geniculate nucleus of the cat. J Physiol 383, 1, 653–692.
[S58] Friedlander, M. J., Lin, C. S., Stanford, L. R., and Sherman, S. M. (1981). Morphology of functionally identified neurons in lateral geniculate nucleus of the cat. J. Neurophysiol. 46, 1, 80–129.
[S59] Rall, W. (1977). Core Conductor Theory and Cable Properties of Neurons. In Kandel, E.R., Brookhardt, J.M., and Mountcastle, V.M., eds., Handbook of physiology, cellular biology of neurons. (Bethesda, MD: American Physiological Society). pp. 39–97.
[S60] Ascoli, G. A., Donohue, D. E., and Halavi, M. (2007). NeuroMorpho.org: A central resource for neuronal morphologies. J. Neurosci. 27, 35, 9247–9251.
[S61] Hines, M. L., Morse, T., Migliore, M., Carnevale, N. T., and Shepherd, G. M. (2004). ModelDB: A database to support computational neuroscience. J Comput Neurosci 17, 1, 7–11.

Acknowledgments
We are grateful to Fabrizio Gabbiani, Hermann Cuntz, Guy Leyal, and Idan Segev for kindly sharing data. We thank Jan-Hendrik Schleimer for feedback on the manuscript. This work was funded by grants from the Federal Ministry of Education and Research, Germany (01GQ1001A, 01GQ0901, 01GQ0972, 01GQ1403) and the Deutsche Forschungsgemeinschaft (SFB618/B1, GK1589/1).

5. Qualitative changes in phase-response curve and synchronization at the saddle-node-loop bifurcation

PHYSICAL REVIEW E **95**, 052203 (2017)

Qualitative changes in phase-response curve and synchronization at the saddle-node-loop bifurcation

Janina Hesse,[*] Jan-Hendrik Schleimer,[†] and Susanne Schreiber[‡]
Institute for Theoretical Biology, Department of Biology, Humboldt-Universität zu Berlin, Philippstrasse 13, Haus 4, 10115 Berlin, Germany
and Bernstein Center for Computational Neuroscience Berlin, Berlin, Germany
(Received 24 June 2016; revised manuscript received 12 November 2016; published 3 May 2017)

Prominent changes in neuronal dynamics have previously been attributed to a specific switch in onset bifurcation, the Bogdanov-Takens (BT) point. This study unveils another, relevant and so far underestimated transition point: the saddle-node-loop bifurcation, which can be reached by several parameters, including capacitance, leak conductance, and temperature. This bifurcation turns out to induce even more drastic changes in synchronization than the BT transition. This result arises from a direct effect of the saddle-node-loop bifurcation on the limit cycle and hence spike dynamics. In contrast, the BT bifurcation exerts its immediate influence upon the subthreshold dynamics and hence only indirectly relates to spiking. We specifically demonstrate that the saddle-node-loop bifurcation (i) ubiquitously occurs in planar neuron models with a saddle node on invariant cycle onset bifurcation, and (ii) results in a symmetry breaking of the system's phase-response curve. The latter entails an increase in synchronization range in pulse-coupled oscillators, such as neurons. The derived bifurcation structure is of interest in any system for which a relaxation limit is admissible, such as Josephson junctions and chemical oscillators.

DOI: 10.1103/PhysRevE.95.052203

I. INTRODUCTION

Different states of macroscopic network dynamics are a hallmark of complex systems such as the brain. In nervous systems, transitions between dynamical states constitute important switch points. For example, the emergence of so-called frustrated synchronization states (i.e., high-entropic, multistable network states verging between order and disorder) is thought to play a role in neural function and its pathologies [1]. Such transitions can, on the one hand, emerge as a consequence of the network topology, as it is found in the human connectome [2]. Here, we present a general case where a specific variation in single-neuron properties can drastically switch network synchronization properties, provided the cells' parameters are close to a critical transition point: the saddle-node-loop (SNL) bifurcation.

While this bifurcation is not unknown [3], our results demonstrate that its substantial, qualitative consequences for neural dynamics have so far not been sufficiently acknowledged. Moreover, we show that the SNL bifurcation is a ubiquitous feature in (planar) type I neuron models. Because a vast proportion of models [4–6] belongs to this class (describing neurons ranging from isolated gastropod somata [7] to hippocampal neurons [8,9]), this transition point and its implication need to be taken into account for biological function.

Different types of spike generation were first classified by Hodgkin [10] and later linked to particular bifurcations ruling the transition from rest to spiking [11,12]. Recently, the ability of neurons to change the mechanism of spike generation under physiological conditions has attracted the interest of both theoreticians and experimentalists [13–16]. Attention was mostly directed at the transition between the two traditional excitability types, which involve either a *fold* (saddle node) or a *Hopf* bifurcation [Fig. 1(a)], along with their differential subthreshold filtering properties [17–20]. Here, we investigate an alternative transition, which switches the spike onset from a *saddle node on an invariant cycle* (SNIC) bifurcation to a *saddle homoclinic orbit* (HOM) bifurcation [Fig. 1(b)]. This transition is organized by a codimension-two bifurcation: the SNL bifurcation [21,22]. As we demonstrate, the SNL bifurcation causes an abrupt change in the phase-response curve, with far-reaching functional consequences. For example, the increased ability of individual cells to form antiphase synchronization observed at an SNL bifurcation affects the dynamics of networks (Fig. 2), with potential relevance for various pathological conditions ranging from epilepsy to Parkinson's disease [25,26].

SNL bifurcations can occur with several bifurcation parameters, including the time constant of the gating kinetics [23]. In this study, we identify the separation of time scales between voltage and gating dynamics as the decisive bifurcation parameter, underlying the effect of other parameters, such as capacitance or temperature. Starting at a SNIC bifurcation in planar general neuron models, we demonstrate that a variation in the separation of time scales provokes a generic sequence of firing onset bifurcations. Compared to other bifurcation studies, which rely on a *local* unfolding of a codimension-three bifurcation [27,28], our approach proves the generic bifurcation structure including the appearance and ordering of codimension-two bifurcations on a *global* scale not restricted to local analysis. The composed bifurcation diagram hence

[*]janina.hesse@bccn-berlin.de
[†]jh.schleimer@hu-berlin.de
[‡]www.neuron-science.de

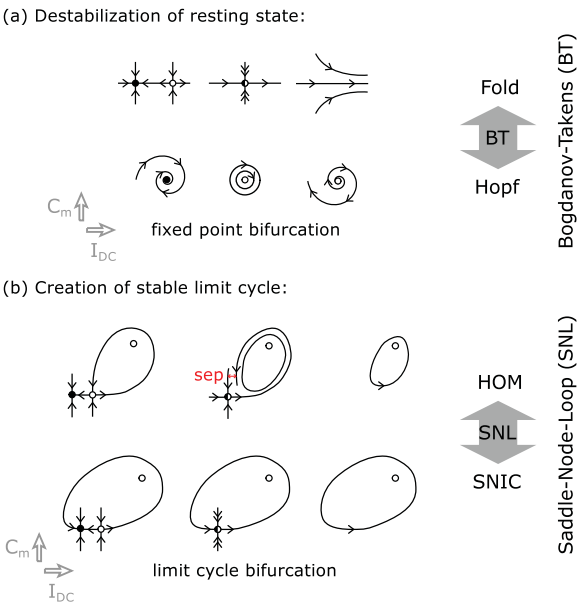

FIG. 1. The transition from rest to spiking in response to an increase in input current I_{DC} requires (a) that the resting state loses stability (illustrated are fold and subcritical Hopf bifurcations) and (b) the creation of a limit cycle [illustrated are saddle homoclinic orbit (HOM) and SNIC bifurcations]. The membrane capacitance C_m makes it possible to switch between these bifurcations. The separation function, sep, marked in red, measures the distance between the stable and unstable manifold of the saddle. The overlap of both, i.e., sep $= 0$, results in a homoclinic orbit.

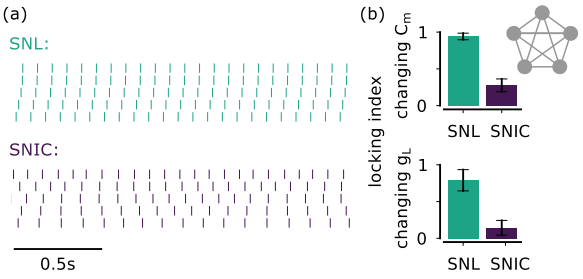

FIG. 2. (a) Spike raster plot of two small globally coupled networks of five Wang-Buzsaki models (see Appendix A), one close to the SNL bifurcation with $C_m = 1.47$ μF/cm^2, the other at a SNIC bifurcation with $C_m = 1$ μF/cm^2. Synaptic connections are modeled as voltage perturbations of $\varepsilon = 0.39$ mV. The frequency detuning of the neurons is approximately equally spaced between 5 and 11 Hz. (b) Phase-locking index, calculated between pairwise neurons i and j with phase $\phi_{i,j}$ as $\langle e^{i2\pi(\phi_i-\phi_j)}\rangle$, where brackets denote temporal averaging. Error bars denote standard deviations. (Top) Locking index for the network when the capacitance is changed [as in panel (a)]. (Bottom) Locking index for the network when the leak conductance g_L is changed (instead of capacitance). $\varepsilon = 0.08$ mV, $C_m = 1$ μF/cm^2, and SNIC at $g_L = 0.1$ mS/cm^2 and SNL at $g_L \approx 0.57$ mS/cm^2; all other parameters are identical to those in the top panel. Locking at both SNL bifurcations exceeds locking at the corresponding SNIC bifurcation.

predicts the behavior of a class of neurons over the whole range of time-scale parameters and thereby warrants a direct comparison with biological neurons.

The organization of this article is as follows. Section II describes how the phase-response curve can be identified from the limit cycle of a dynamical system. With this relation established, Sec. III proves that a symmetry breaking of the phase-response curve occurs at SNL bifurcations. The functional consequences for synchronization in spiking systems are discussed in Sec. IV. The significance of these consequences is perpetuated by the results in Sec. V, where we prove that SNL bifurcations generically occur in planar neuron models.

II. CONDUCTANCE-BASED NEURON MODEL AND PHASE REDUCTION

To investigate spike-based synchronization, our detailed, conductance-based model neurons are reduced to a phase description. The latter assumes tonic responses of a mean-driven neuron [18]; i.e., spikes are emitted with a mean spike rate, f, in response to a constant mean intensity, I_{DC}, and their occurrence is modulated by inputs sufficiently weak to only shift spike times $\{t_k^{sp}\}$. The spike train is $y(t) = \sum_k \delta(t_k^{sp} - t)$.

The dynamics of the membrane voltage v follows a current balance equation, $I_{DC} = I_{cap} + I_{ion}$. The input equals the capacitive current, $I_{cap} = \frac{dC_m v}{dt}$ (with membrane capacitance C_m) and an ionic current, $I_{ion} = I_{ion}(v, m_i, ...)$, which is a function of v itself and the open probability of ion channels given by their *gating variables*, m_i. Combined, this *conductance-based neuron model* forms a dynamical system, $\dot{X} = F(X)$, with the structure

$$\begin{pmatrix} \dot{v} \\ \dot{m}_i \\ \dots \end{pmatrix} = \begin{pmatrix} \frac{1}{C_m}[I_{DC} - I_{ion}(v, m_i, ...)] \\ \frac{m_i^\infty(v) - m_i}{\tau_{m_i}(v)} \\ \dots \end{pmatrix}, \quad (1)$$

where the overdot denotes the derivative with respect to time and F determines the dynamics of the unperturbed system. Synaptic inputs are modeled as instantaneous voltage perturbations: If a spike occurs at time t^{sp} in the presynaptic neuron, then $v_{post}(t_{pre}^{sp}) \mapsto v_{post}(t_{pre}^{sp}) + \varepsilon$, where $\varepsilon = I_{syn} C_m^{-1} \int_{t^{sp}-\Delta}^{t^{sp}+\Delta} dr\, \delta(r - t^{sp})$ results from the integration of δ currents of amplitude I_{syn}. The dynamical variables consist of the voltage and the gating variables. The gating is typically modeled by first-order kinetics (for details, see Appendix A).

The input I_{DC} acts as bifurcation parameter for both the fixed-point destabilization and the limit-cycle creation (Fig. 1). For our analysis, we focus on neuron models in which the fixed point loses stability at a fold bifurcation.

The study of spike synchronization is facilitated by reducing the high-dimensional dynamics to a single phase equation. One way to formally obtain such a reduction from a biophysical model of membrane-voltage dynamics is to find the *input-output* (I/O) *equivalent* phase oscillator [29]. The mapping of input to spike times is given by the *phase-response curve (PRC)* of the neuron [30]. The PRC, Z, relates the timing of the occurrence of a weak perturbation to the resulting temporal advance or delay of the following spike, $Z : \phi \mapsto \Delta\phi$. The spike times $\{t_k^{sp}\}$ correspond to the level

crossings of the phase, $\phi(t_k^{\rm sp}) = k$ for $k \in \mathbb{Z}$, so that the spike train can be written as $y[\phi(t)] = \sum_k \delta[\phi(t) - k]$. The occurrence of spikes in neuron i, if receiving inputs from another neuron j, is governed by the phase equation

$$\dot{\phi}_i = f_i + Z(\phi_i) y(\phi_j) + \xi_i(t). \tag{2}$$

The intrinsic noise $\xi_i(t)$ of each neuron is assumed to be a zero-mean white-noise process, $\langle \xi_i(0)\xi_i(\Delta t)\rangle = \sigma^2\delta(\Delta t)$.

In the following, the mean spike rate, f, in response to the mean drive, $I_{\rm DC}$, and the PRC, $Z(\phi)$, are implicitly taken to be functions of the parameters of the detailed neuron model introduced above in Eq. (1). The phase oscillator in Eq. (2) is then used throughout the paper to predict synchronization properties of neurons.

To identify the I/O equivalent phase model in Eq. (2), the PRC needs to be calculated for the conductance-based model in Eq. (1). From a dynamical systems perspective, the PRC Z is the periodic solution to the adjoint of the first variational equation of the unperturbed dynamics in Eq. (1), $\dot{X} = F(X)$,

$$\frac{dZ}{d\phi}(\phi) = -J^{\top}(\phi) Z(\phi), \tag{3}$$

where $\top$ denotes the matrix transpose and $J = \frac{\partial F}{\partial X}$ is the *Jacobian* evaluated on the limit cycle. To comply with Eq. (2), the PRC associated with voltage perturbations needs to be normalized as $Z(\phi)F(\phi) = f, \forall\ \phi$. The resulting relation between PRC and parameters of the conductance-based neuron model allows us to consider synchronization at different firing onset bifurcations. In the following, we use the dynamics on the homoclinic orbit to deduce PRC properties of the limit cycle that arises from the homoclinic orbit, and, for convenience, we refer to the limit cycle PRC as the PRC *at* the limit-cycle bifurcation (SNIC or SNL), i.e., $Z_{\rm SNIC}$ or $Z_{\rm SNL}$.

III. A FLIP IN THE DYNAMICS ALTERS THE PRC SYMMETRY AT AN SNL BIFURCATION

In a first step, we infer the PRC from the dynamics at firing onset bifurcations, in particular around the SNL bifurcation. As bifurcations imply in general qualitatively different dynamics [31], limit-cycle dynamics are expected to change at the switch in firing onset dynamics at the SNL bifurcation. However, what are the specific consequences for the PRC and hence the synchronization ability of neurons? To answer this question, we start by discussing changes in limit-cycle dynamics at the SNL bifurcation. We then show that this also alters the PRC in such a profound way that it has, in turn, drastic implications for the resulting synchronization ability discussed in Sec. IV.

A. Orbit flip

We consider models with classical type I excitability where the transition from rest to repetitive firing is marked by (i) the elimination of the resting state in a fold bifurcation and (ii) the existence of a limit cycle to which the dynamics relax instead. This limit cycle is born at a *limit-cycle bifurcation*, which is in type I neurons typically a SNIC bifurcation. At a codimension-two SNL bifurcation, the limit-cycle bifurcation switches between a SNIC and a HOM bifurcation [Fig. 1(b)].

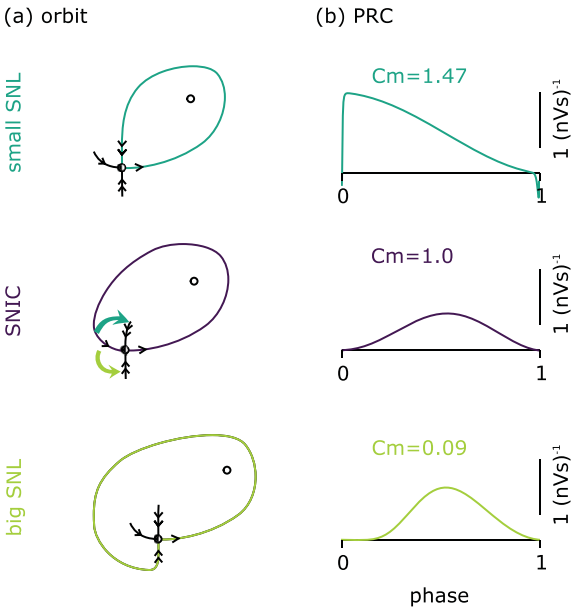

FIG. 3. (Top to bottom) (a) Schematic illustration of the orbits at small SNL bifurcation, nondegenerated SNIC bifurcation, and big SNL bifurcation, with semistable (small single arrow) and strongly stable manifold (double arrows). These bifurcations occur in the Wang-Buzsaki model for $I_{\rm DC} \approx 0.16\ \mu$A/cm^2, $C_{\rm m} \approx [1.47, 1, 0.09]\ \mu$F/cm^2. (b) The associated phase-response curves measured for $I_{\rm DC}$ 2% above the fold bifurcation.

The following, model-independent analysis focuses on the *small* SNL bifurcation that transitions from a SNIC orbit to a small HOM orbit [Fig. 3(a)], because it entails more drastic changes in PRC shape, as discussed later. The *big* SNL bifurcation (transitioning to a big HOM orbit) will be studied with numerical continuation (Sec. IV).

The limit cycle created at a HOM, SNIC, or SNL bifurcation arises from a homoclinic orbit to a saddle (HOM) or saddle node (SNIC, and also SNL). Under the assumption of sufficiently large limit-cycle periods, the slow velocity in the vicinity of these fixed points contracts the dynamics such that limit-cycle properties, e.g., period or PRC, can be extracted from a linear approximation around the fixed point.

The linearized dynamics around the saddle-node fixed point is given by its Jacobian. Assuming nondegeneracy, the Jacobian has a single zero eigenvalue, associated with the *semistable* manifold, while the other eigenvalues are strictly negative (*strongly stable* manifolds). Trajectories always leave the saddle node along the semistable manifold. When a trajectory loops around in a homoclinic orbit, it can either reapproach the saddle node along the same manifold (SNIC bifurcation) or along the much faster, strongly stable manifold (SNL bifurcation). The approach of the saddle node at an SNL bifurcation flips from the semistable manifold to one of the strongly stable manifolds (hence, *orbit flip* bifurcation [24]) [Fig. 3(a)]. For neuron models, this flip can be induced by a scaling of the relative speed in the voltage and gating kinetics (Fig. 4). When the saddle node disappears after the fold

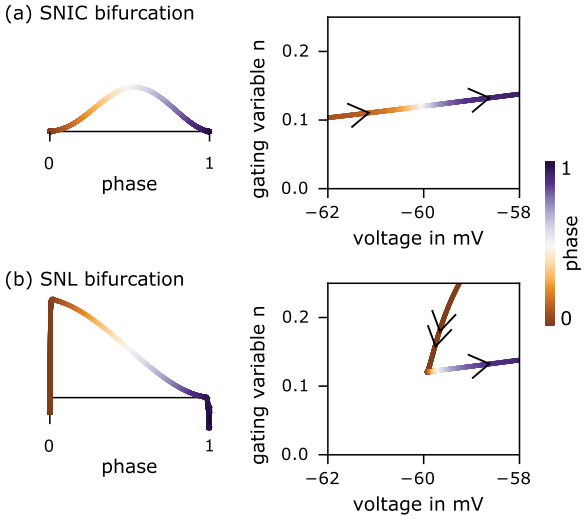

FIG. 4. Phase-response curve (left) and phase plot around the saddle node (right) for (a) a nondegenerated SNIC bifurcation with $C_m = 1\ \mu\text{F/cm}^2$ and (b) a small SNL bifurcation with $C_m \approx 1.47\ \mu\text{F/cm}^2$ in the Wang-Buzsaki model with the limit-cycle period fixed in both cases to 2 Hz.

bifurcation, its remaining *ghost* still dominates the resulting limit-cycle dynamics. The limit-cycle period drastically decreases around the SNL bifurcation (Fig. 5(a); see also [3]), mainly because of the separation of time scales between strongly stable and semistable manifold, which renders the approach along the strongly stable manifold much faster than the approach along the semistable manifold.

B. PRC symmetry and Fourier modes

Numerical continuation of several neuron models shows that the PRC is drastically altered at the SNL bifurcation. Exemplified in Fig. 3(b) for the Wang-Buzsaki model (Appendix A), the symmetric PRC at a (nondegenerated) SNIC bifurcation becomes increasingly asymmetric when an

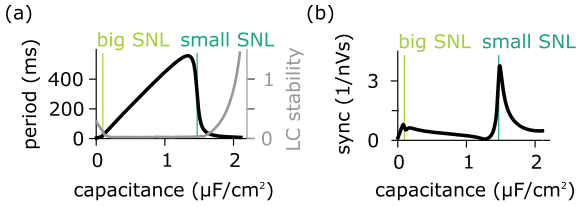

FIG. 5. Variation of the membrane capacitance C_m for the Wang-Buzsaki model with input fixed at 2% above limit-cycle onset at $I_{DC} \approx 0.16\ \mu\text{A/cm}^2$. (a) Limit-cycle period (black) and relative limit-cycle (LC) stability (gray) given by the ratio of the limit-cycle attraction time (inverse of the Floquet exponent) and the period. A small LC stability supports the validity of the phase description [36]. (b) Maximal amplitude of the odd part of the PRC, corresponding to the entrainment range when normalized by the coupling strength assuming δ coupling (abbreviated sync).

increase in membrane capacitance tunes the model towards the SNL bifurcation. The strong asymmetry at the SNL bifurcation directly affects the synchronization ability of the neuron (see Sec. IV).

The sudden occurrence of PRC asymmetry at an SNL bifurcation can be directly inferred from the orbit flip in the dynamics described in the last section (Sec. III A). The PRC peaks when the phase reaches the ghost of the saddle node, where the slow dynamics allow infinitesimal perturbations to maximally advance phase. In the case of the SNIC bifurcation, the same velocity governs the approach and exit of the ghost, both aligned with the semistable manifold (Fig. 4; for details, see Appendix B). The orbit flip to the strongly stable manifold at the SNL bifurcation either decreases or increases the time spent on the approach compared to exit for the small or big SNL, respectively. This, in turn, breaks the symmetry of the PRC at the SNIC bifurcation by advancing or delaying the phase at which the maximum of the PRC resides.

Neglecting the fast approach at the small SNL bifurcation, it seems as if the flow of the limit-cycle trajectory is directly injected at the ghost. Because the exit dynamics at SNL and SNIC bifurcations are similar, the PRC at the small SNL bifurcation appears as a rescaled version of the second half of the PRC at the SNIC bifurcation, $Z_{\text{small SNL}}(\phi) \propto Z_{\text{SNIC}}(0.5\phi + 0.5)$. This reasoning is supported by numerical continuation [Figs. 3(b) and 4] and explains the observation that the limit-cycle period is approximately halved at the SNL bifurcation [Fig. 5(a)].

The necessity of the PRC symmetry breaking at the SNL bifurcation can also be seen from normal form theory. For the SNIC bifurcation (and the supercritical Hopf bifurcation), the PRC is a simple trigonometric function, $Z_{\text{SNIC}}(\phi) \propto 1 - \cos(2\pi\phi)$ [$Z_{\text{Hopf}}(\phi) \propto \sin(2\pi\phi)$] [11,32,33]. Approached from the SNIC, the small SNL bifurcation, however, registers a sudden emergence of higher Fourier modes in the PRC. On the other side of the small SNL bifurcation, the canonical PRC at a small HOM bifurcation is an exponential with some decay constant τ, $Z_{\text{HOM}}(\phi) \propto \exp(-\phi/\tau)$ [33,34]. Hence, in contrast to the trigonometric PRCs with a single Fourier mode at the SNIC or supercritical Hopf bifurcations, the PRCs at HOM and small SNL bifurcations have an infinite amount of Fourier modes. This results in Gibb's phenomenon if finite approximations are used.

The significant increase in PRC Fourier modes, as well as the breaking in PRC symmetry, are generic properties of SNL bifurcations.

IV. SYNCHRONIZATION PEAKS AROUND SNL BIFURCATIONS

The asymmetry of the PRC scales the frequency detuning over which a neuron entrains to its input (the width of the Arnold tongue [35,36]). The input can be either a periodic signal or the recurrent input from other neurons in a network. Here, we use synchronization in the sense of a constant phase relation between oscillators; compare Fig. 2. The relation between PRC and synchronization can be illustrated by two δ-coupled phase oscillators, $\phi_{1,2}$, as defined in Eq. (2),

$$\dot{\phi}_{1,2} = f_{1,2} + Q(\phi_{1,2} - \phi_{2,1}) + \xi_{1,2}, \tag{4}$$

where the coupling function Q results from an averaging step if the interaction between both oscillators are assumed to be weak [37]. In the present pulse-coupled case this means

$$Q(\Delta) = \int_0^\infty Z(\varphi)\delta(\varphi + \Delta)d\varphi = Z(\Delta).$$

The phase difference, $\psi = \phi_1 - \phi_2$, evolves as $\dot{\psi} = \Delta f + Q_{\text{odd}}(\psi)$, where $Q_{\text{odd}}(\psi) = Q(\psi) - Q(-\psi)$ is twice the odd part of the coupling function. Synchronization (i.e., a constant phase lag ψ) requires $\dot{\psi} = 0$, and the maximal admissible frequency detuning $\Delta f = f_1 - f_2$ is given by the image of Q_{odd}. In the case of δ coupling, Q_{odd} is equal to twice the odd part of the PRC, Z_{odd}, so that phase locking occurs only if $\Delta f \in [\min Z_{\text{odd}}, \max Z_{\text{odd}}]$. In Fig. 5(b), the synchronization range $\max Z_{\text{odd}} - \min Z_{\text{odd}}$ is plotted. The increased synchronization range will also manifest itself in globally coupled networks of the type studied in Refs. [38,39]. For two coupled oscillators, a small SNL bifurcation favors alternated spiking, which is sometimes called *antiphase synchronization*. This is in contrast to the stable in-phase locking that is observed for PRCs shaped like a negative sine (see Supplemental Material in Ref. [27]).

The decisive factor for increased synchronization around the SNL points is the PRC symmetry breaking with the emergence of high-frequency Fourier modes, which govern the existence and stability of fixed points in the phase differences between oscillators. Of minor importance for the peak observed in Fig. 5(b) is the period reduction observed in Fig. 5(a), which counteracts the increase in synchronization in approach of the SNL points by scaling the PRC with the period. The network example from Fig. 2 also shows a significant change in synchronization when the period is held constant by a fixation of the mean firing rate. The PRC symmetry breaking with the emergence of high-frequency Fourier modes occurs generically at SNL bifurcations (Sec. III), such that the consequences derived in this section generalize to other oscillators beyond neuroscience. In particular, neurons close to an SNL bifurcation synchronize differently from what is expected for SNIC neurons that show traditional type I excitability.

V. GENERIC OCCURRENCE OF SNL BIFURCATIONS

The consequences of the SNL bifurcation discussed in Sec. IV will be of particular relevance for neuronal processing [40] if the SNL bifurcation generally occurs in realistic neuron models. Next, we demonstrate that indeed any two-dimensional, type I conductance-based neuron model can always be tuned to SNL bifurcations. More precisely, we show that the SNL bifurcation is an essential element in the bifurcation diagram that uses input current and membrane capacitance as control parameters. This bifurcation diagram also allows us to relate the SNL bifurcation to other bifurcations such as the Bogdanov-Takens (BT) bifurcation, classically termed the switch of type I/II excitability [37,41].

Concentrating on bifurcations relevant for neuronal spiking (i.e., bifurcations affecting a stable limit cycle), Fig. 6 shows a bifurcation diagram of the Wang-Buzsaki model (Appendix A) with input current and membrane capacitance as control parameters. Along the dimension spanned by the capacitance, two SNL bifurcations enclose the SNIC bifurcation. The lower SNL bifurcation corresponds to a big SNL bifurcation for which the arising limit cycle encircles the ghost of the saddle node and the upper SNL bifurcation corresponds to a small SNL bifurcation for which the ghost of the saddle node lies outside of the limit cycle [Fig. 3(a)]. In particular, decreasing the capacitance, an SNL point is passed *before* the BT bifurcation is reached.

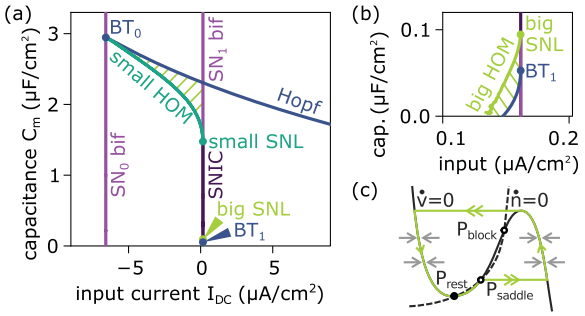

FIG. 6. (a) Bifurcation diagram of the Wang-Buzsaki model under variation of membrane capacitance C_m and input current I_{DC}. With $C_m = 1\ \mu\text{F/cm}^2$, the limit cycle arises from a SNIC bifurcation. Increasing C_m leads to the small SNL at $C_m \approx 1.47\ \mu\text{F/cm}^2$. Hatched areas mark bistability. (b) Decreasing C_m leads to the big SNL and then to a Bogdanov-Takens (BT) bifurcation. Note that a change of stability in the big HOM branch, not shown here, follows from Ref. [42]. (c) Schematic illustration for the limit $C_m \to 0$, in which the system corresponds to a relaxation oscillator. Drawn in the state space of gating variable n versus voltage v, the solid line with an inverted N shape represents the voltage nullcline, and the dashed line represents the gating nullcline. At some I_{DC}, the resting state loses stability and a big HOM orbit around all fixed points (green) is created.

We show in Appendix C that this bifurcation structure generalizes (under mild assumptions) to planar neuron models. The membrane capacitance C_m is used as a bifurcation parameter in the general bifurcation diagram that we construe, because it simply changes the time scale of the voltage dynamics [Eq. (1)]. The proof separately considers the lower and the upper parts of the bifurcation diagram. The lower part is based on the so-called *relaxation limit* with infinitely fast voltage dynamics that arises from the limit $C_m \to 0$ [Fig. 6(c)], where the bifurcation structure is known [42]. Nonzero capacitance values are deduced from several observations that restrict the path of limit-cycle bifurcation branches in planar systems. The upper part of the bifurcation diagram is extracted from the unfolding of a BT point.

Our derivation may be an interesting starting point for similar results in other dynamical systems in which the time scale of a single dynamical variable is used as a bifurcation parameter. For our planar neuron models, we find that the SNIC bifurcation branch is generically enclosed by two SNL bifurcations that are reached by an adaptation of the voltage time scale. In particular, our results show that a continuous variation of the voltage time scale reaches the BT point only *after* passing one of the SNL bifurcations.

VI. DISCUSSION

This article explores the intricate relation between SNL bifurcations, the changes in associated PRCs, and the resulting consequences for the ability of neurons to synchronize (Fig. 5).

In a mean-driven regime [18] (i.e., in the presence of a stable limit cycle), drastic changes in neuronal processing in general [40], and synchronization in particular, can be expected if a bifurcation directly affects the stable limit cycle (and not only the fixed points). This is the case for the SNL bifurcation, with strong implications for synchronization, as we have shown here. In contrast, at a Bogdanov-Takens bifurcation, which is classically regarded as the transition point between type I and type II excitability, stable limit cycles are not directly involved. The BT-associated Hopf bifurcation in neuron models is typically subcritical, and the limit cycle arising at the subcritical Hopf bifurcation is unstable. Hence, the limit cycle changes bear only indirect relevance for mean-driven spiking. This provides an intuitive explanation for why the changes in synchronization we observed at the BT transition are minor compared to those of the saddle-node-loop bifurcation [Fig. 5(b)]. While the subcritical Hopf bifurcation can lead to substantial changes in subthreshold dynamics and filtering [17,19,27,37,43], synchronization is modified only if the system behaves like a fluctuation-driven escape problem [44,45], and not like the mean-driven regime considered here.

Moreover, we note that models in the vicinity of a BT point have a different bifurcation structure than the original Hodgkin-Huxley (HH) model [46]. In the HH model, the unstable limit cycle is born at a fold of limit cycles bifurcation (together with the stable limit cycle) and terminates in the subcritical Hopf bifurcation (destabilizing the fixed point). In contrast, in the normal form of the BT bifurcation, the unstable limit cycle is born at a HOM bifurcation [47]. This difference will probably affect the PRC of the stable limit cycle, for which the canonical shape is still unresolved [48]. Furthermore, the identified generic bifurcation sequence shows that a smooth change in time-scale parameters does not justify the previously used heuristic formula that exploits a single Fourier mode to interpolate between Z_{SNIC} and Z_{Hopf} [40,49,50].

As codimension-two bifurcation, the SNL bifurcation is reached in neuron models by an appropriate tuning of both the input current and one additional model parameter. Examples for the second control parameter are the membrane capacitance, maximal gating conductances, tonic inhibition [27], neuromodulators [14], or gating time constants [23]. With the membrane capacitance as a bifurcation parameter, we demonstrate for planar conductance-based models with a SNIC bifurcation that, ubiquitously, an SNL bifurcation is the first bifurcation reached for lowered or increased capacitance, respectively. With the three bifurcation parameters—capacitance, input, and leak conductance—the identified sequence of bifurcations collapses into a codimension-three cusp BT point [27,28]. This potentially generalizes the described bifurcation structure beyond the planar case.

Focusing on neuron models that spike at low firing rates, where the dynamics is dominated by the bifurcation that creates the limit cycle, allows us to draw model-independent conclusions. Furthermore, the phase description employed here demands for small inputs compared to the limit-cycle stability. The strong stability of the limit cycle around the SNL point [Fig. 5(a)] validates the phase reduction even for reasonably sized inputs. The low firing rates required for the center manifold reduction to be valid and the relatively weak synaptic connections are typical for cortical neurons [4,5].

Our mathematical arguments (Appendix C) require one bifurcation parameter to be the relative time scale between state variables, which can take us to the relaxation limit. The membrane capacitance is one such parameter. The effective membrane capacitance depends on cell parameters, such as the morphology of the neuron or the myelination of its axon [51], and may hence be adapted on developmental or evolutionary time scales. Recent studies report reduced capacitance in human neurons [52,53], potentially due to the lipid composition of the membrane. While these studies consider mainly passive membrane properties, our work extends beyond and reports the implications of changed capacitance for spike dynamics. In contrast to the general assumption that the membrane capacitance is constant across all neurons, the reported variability in membrane capacitance suggests that evolution could directly tune the membrane capacitance to the proximity of an SNL point. Indeed, it seems that not only evolution, but also development acts on the membrane capacitance; for example, aging reduces C_{m} in rhesus monkeys [54].

Among the biologically relevant bifurcation parameters is the leak conductance g_{L}, which affects the time-scale separation in a more indirect way than capacitance. Changes in leak can equally lead to an SNL bifurcation [27], with the accompanying increase in (antiphase) synchronization [Fig. 2(b)]. For example, the effective leak conductance can be changed by the amount of inhibition the neurons receives (*shunting inhibition*) [27] or by certain neuromodulators [55,56].

Based on our results, we predict that SNL points can be identified experimentally via the characteristic breaking of PRC symmetry. Experimental measurement of PRCs [27,57–61] can help to assess whether cellular dynamics are close to an SNL bifurcation. Moreover, our analysis suggests that a specific experimental technique—infrared neural stimulation—may require a careful interpretation. Specifically, infrared neural stimulation could not only excite neuronal tissue, but potentially also alter neuronal dynamics, because it has been shown to rely on a change in membrane capacitance, C_{m}, to depolarize neurons and thus stimulate networks [62]. Hence, during infrared neural stimulation extended changes in capacitance could push the neurons closer to an SNL bifurcation, with consequences for neuronal dynamics and functionality exceeding a pure excitation.

Last but not least, our results provoke the question as to why neurons should, under natural conditions, favor a position close to an SNL point. On the one hand, the facilitation of antiphase synchronization around the SNL point may result in a frustrated network state with rich dynamical attractors for memory or information processing [1,65]. On the other hand, SNL bifurcations may also be relevant in pathology (e.g., epilepsy). Beyond neural networks [66], frustrated systems also underlie power blackouts [71], repressive gene networks [65], and social networks [72].

In summary, our study consists of two parts. First, we extracted the phase-response curve from the dynamics at an SNL bifurcation and used this knowledge to infer the associated synchronization abilities. Both the PRC asymmetry

and its high Fourier modes are generic properties at SNL bifurcations. Thereby, our results generalize across neuron models, and are equally applicable to any system that allows for a phase reduction. Second, we have demonstrated that SNL bifurcations occur ubiquitously in a set of planar neuron models. With the time scale of one dynamical variable as bifurcation parameter, the structure of our proof is likely to extend to other systems with a subcritical Hopf bifurcation in the relaxation limit, such as lasers [73,74], Josephson junctions [75–78], and chemical reactions [79,80]. Together, both parts highlight the SNL bifurcation as a hitherto underestimated bifurcation with prominent importance for neuronal dynamics.

ACKNOWLEDGMENTS

We thank Martin Wechselberger for inspiring discussions and pointing out the connection to his work on the relaxation limit and Grigory Bordyugov for advice on numerical continuation with AUTO [81] and homoclinic bifurcations. Funded by the German Federal Ministry of Education and Research (Grants No. 01GQ0901 and No. 01GQ1403).

Authors J.H. and J-H.S. contributed equally to this work.

APPENDIX A: GENERIC DEFINITION OF CONDUCTANCE-BASED NEURON MODELS

We consider a generic class of conductance-based neuron models [27],

$$\dot{v} = \frac{I_{\mathrm{cap}}(v,\ldots)}{C_{\mathrm{m}}} = \frac{1}{C_{\mathrm{m}}}[I_{\mathrm{in}} - g_{\mathrm{L}}(v - v_{\mathrm{L}}) - I_{\mathrm{gating}}], \tag{A1}$$

$$I_{\mathrm{gating}} = \sum_{i=0}^{n} g_i(v - v_i) \prod_{k=0}^{K} m_{ik}^{p_{ik}}, \tag{A2}$$

where ion channel i has maximal conductance g_i and reversal potential v_i and its open probability is given by a product of gating variables (potentially to some power of p_{ik}). Each gating variable m_{ik} of ion channel i is either a function of the voltage, $m_{ik} = m_{ik\infty}(v)$, or relaxes exponentially to its steady state value $m_{ik\infty}(v)$, with gating kinetics given by

$$\dot{m_{ik}} = \frac{m_{ik\infty}(v) - m_{ik}}{\tau_{ik}(v)}. \tag{A3}$$

For numerical continuation, we use a single-compartmental version of the Wang-Buzsaki model for hippocampal pyramidal cells [9] with the dynamics

$$\begin{aligned}
\dot{v} &= [I + g_{\mathrm{L}}(E_{\mathrm{L}} - v) + I_{\mathrm{gate}}]/C_{\mathrm{m}},\\
\dot{h} &= 5\,[\alpha_h(v)(1-h) - \beta_h(v)\,h],\\
\dot{n} &= 5\,[\alpha_n(v)(1-n) - \beta_n(v)\,n],
\end{aligned}$$

with membrane capacitance $C_{\mathrm{m}} = 1\ \mu\mathrm{F/cm^2}$; maximal conductances $g_{\mathrm{L}} = 0.1\ \mu\mathrm{S/cm^2}$, $g_{\mathrm{Na}} = 35\ \mu\mathrm{S/cm^2}$, $g_{\mathrm{K}} = 9\ \mu\mathrm{S/cm^2}$; reversal potentials $E_{\mathrm{L}} = -65$ mV, $E_{\mathrm{Na}} = 55$ mV, $E_{\mathrm{K}} = -90$ mV; and the following functions:

$$\begin{aligned}
I_{\mathrm{gate}} &= g_{\mathrm{Na}} m_\infty(v)^3 h(E_{\mathrm{Na}} - v) + g_{\mathrm{K}} n^4 (E_{\mathrm{K}} - v),\\
m_\infty(v) &= \frac{\frac{v+35}{\exp[-0.1\,(v+35)]-1}}{\frac{v+35}{\exp[-0.1\,(v+35)]-1} - 40\,e^{-(v+60)/18}},\\
\alpha_h(v) &= 0.07\,\exp[-(v+58)/20],\\
\beta_h(v) &= \frac{1}{1+\exp[-0.1\,(v+28)]},\\
\alpha_n(v) &= -0.01\,\frac{v+34}{\exp[-0.1\,(v+34)]-1},\\
\beta_n(v) &= 0.125\,\exp[-(v+44)/80].
\end{aligned}$$

APPENDIX B: PRC SYMMETRY

The PRC asymmetry at the SNL bifurcation is a direct consequence of the broken symmetry in the dynamics at the SNL bifurcation. This section gives more detail on the relationship between dynamics and PRC, both intuitively and with a mathematical argument. We will describe first how the dynamics at the SNIC bifurcation leads to a symmetric PRC and then show that these conditions are not met at the SNL bifurcation, predicting an asymmetric PRC at an SNL bifurcation. While the arguments are presented with a small SNL bifurcation in mind, they hold in a similar way for a big SNL bifurcation.

As introduced in the main text, the orbit at a SNIC bifurcation follows the semistable manifold of the saddle-node fixed point, which corresponds to the central manifold of a fold bifurcation. The zero eigenvalue of the Jacobian J at the saddle node on the semistable manifold eliminates the linear term. The leading second-order term results in a parabolic normal form. For dynamics centered around $x = 0$, stimulated with input s, the dynamics is

$$\dot{x} = s + x^2, \tag{B1}$$

where all variables are chosen unitless for convenience.

The dynamics is symmetric around the saddle-node fixed point; i.e., the orbit has corresponding velocities at the approach and exit of the saddle node. The orbit flip at the SNL bifurcation breaks this symmetry in the dynamics, and, as we will show, also in the PRC.

From a mathematical perspective, the normal form allows for a calculation of the PRC. We, however, will use the normal form to directly analyze PRC symmetry. For the SNIC bifurcation, the reflection symmetry of the PRC can be inferred from the symmetry of the dynamics: If $x(t)$ is a solution of the dynamical system given by Eq. (B1), then the same holds for $-x(-t)$; $x(t)$ is hence point symmetric in time, $x(t) = -x(-t)$. Derivation of the right-hand side of Eq. (B1) by x results in a Jacobian linear in x, which is hence point symmetric in x, $J(x) = -J(-x)$. Inserting both into the adjoint equation [Eq. (3)] directly leads to a PRC reflection symmetric in time, $Z_{\mathrm{SNIC}}(t) = Z_{\mathrm{SNIC}}(-t)$. In contrast, the asymmetric dynamics at the SNL bifurcation lead to an asymmetric PRC.

Intuitively, on an orbit that connects to a saddle-node fixed point, the dynamics becomes arbitrary slow at the fixed point. The limit cycle shows the slowest dynamics in the same region

in state space, in proximity to the ghost of the former saddle node. A perturbation that propels the dynamics over the ghost of the saddle node will therefore maximally advance the next spike. The maximum of the PRC is at the phase value that corresponds to the saddle node. For a SNIC bifurcation, the PRC maximum lies at $\phi = 0.5$ because the symmetric dynamics of a SNIC take equal time for the approach (from $\phi = 0$ to $\phi = 0.5$) and the exit (from $\phi = 0.5$ to $\phi = 1$) of the saddle node. In comparison, the PRC maximum is shifted towards the left at the SNL bifurcation, because the accelerated entry along the strongly stable manifold advances the saddle node to earlier phases. The shift of the maximum away from the center destroys the symmetric shape of the PRC.

The symmetry breaking generalizes beyond the SNL bifurcation: A saddle homoclinic orbit shows an asymmetric PRC [33] if the saddle has different stabilities along stable and unstable manifold and, hence, nonsymmetric dynamics. In summary, we showed that the symmetry breaking in the PRC is an immediate consequence of the symmetry breaking in the dynamics that occurs as orbit flip at the SNL bifurcation. Hence, the observed symmetry breaking in the PRC is a general property of the SNL bifurcation.

APPENDIX C: MATHEMATICAL ARGUMENT FOR THE GENERIC OCCURRENCE OF THE SNL BIFURCATION IN PLANAR MODELS

We show in the following that, with a variation of a time-scale parameter, such as capacitance, in a broad set of planar conductance-based models, a SNIC bifurcation is always enclosed by two SNL bifurcations and that a decrease in capacitance passes the big SNL bifurcation and only afterwards reaches the BT point. Beyond the BT point, a Hopf bifurcation destabilizes the resting state before the fold bifurcation occurs.

To this aim, we prove that the general structure of the bifurcation diagram (Fig. 6) holds for any planar neuron model that conforms with our assumptions stated below.

1. Model definition

We consider a generic class of type I planar conductance-based neuron models. The single gating variable, n, commonly models the opening and closing of a restorative current originating, say, from the potassium ion channel. The dynamics is given by

$$\begin{pmatrix} \dot{v} \\ \dot{n} \end{pmatrix} = F(v,n) = \begin{pmatrix} \frac{1}{C_\mathrm{m}}(I_\mathrm{DC} - I_\mathrm{ion}) \\ \frac{n_\infty(v)-n}{\tau_n(v)} \end{pmatrix}, \tag{C1}$$

with $I_\mathrm{ion}(v,n) = g_\mathrm{L}(v - v_\mathrm{L}) + g_\mathrm{Na}\, m_\infty(v)(v - v_\mathrm{Na}) + g_\mathrm{K}\, n\, (v - v_\mathrm{K})$; compare Eq. (A1).

We chose the model such that it fulfills the following assumptions.

(A1) The firing onset of the model occurs, for some capacitance value C_SNIC and a specific input current $I_\mathrm{DC} = I_\mathrm{SN1}$ (the *threshold* current), at a nondegenerated SNIC bifurcation.

(A2) We demand that at the capacitance C_SNIC the subthreshold dynamics for $I_\mathrm{DC} < I_\mathrm{SN1}$ relax to a single stable fixed point, the *resting state*. We furthermore assume that with an increase in input current, the limit-cycle dynamics eventually terminates in a bifurcation denoted *excitation block*, after which the dynamics relaxes again to a stable fixed point. This assumption prevents diverging dynamics.

(A3) The nullcline of the voltage has an inverted N shape.

(A4) We require that $n_\infty(v)$ from Eq. (C1) is an increasing, positive, bounded, twice differentiable function that becomes sufficiently flat in the limit $v \to \pm\infty$, $\lim_{v\to\pm\infty} v\, \partial_v n_\infty(v) = 0$. This assumption allows us to use results from Ref. [27].

All of these assumptions are fulfilled in common neuron models with type I excitability.

2. Construction of the bifurcation diagram

The following proof establishes an ordering in a sequence of limit-cycle bifurcations, whereby a SNIC is enclosed by two SNL bifurcations. The ordering is established by analyzing the relaxation limit as an anchoring point. We thereby capitalize on recent results from the relaxation limit, $C_\mathrm{m} \to 0$. As we will show, the ordering that arises in this limit along I_DC implies the same ordering along C_m, mainly because limit-cycle bifurcation branches cannot cross in planar systems.

The limit-cycle bifurcation branches that we consider lie in the region with $I_\mathrm{DC} \leqslant I_\mathrm{SN1}$, because, for neuronal firing, the limit-cycle creation has to happen before (i.e., at lower I_DC) or at the fold bifurcation at which the resting state is eliminated. C_SNIC separates the region $I_\mathrm{DC} \leqslant I_\mathrm{SN1}$ into a lower and an upper subregion. Since the occurrence of limit-cycle bifurcations at C_SNIC is prevented by the requirement (A2) that stable dynamics are given by a unique fixed point, all limit-cycle bifurcation branches lie either in one or the other subregion. In the proof, we start with the lower subregion and then consider the upper one.

3. The lower part of the bifurcation diagram, $C_\mathrm{m} < C_\mathrm{SNIC}$

Observation 0: Vertical fold bifurcation branches—Fixed point location depends on I_DC, but not on C_m. The nullclines of Eq. (C1) are given by $I_\mathrm{DC} - I_\mathrm{ion}(v,n) = 0$ and $n = n_\infty(v)$. The nullclines are independent of C_m, and therefore also the location of the fixed points, because the fixed points sit at intersections of the nullclines. Hence, the location of the fold bifurcations is also independent of C_m, which ensures that the fold branches [marked with SN in Fig. 6(a)] are vertical in a bifurcation diagram of C_m versus I_DC.

Based on the inverted N shape of the voltage nullcline and the monotonous shape of the gating nullcline, we can infer the existence of one to three fixed points. For the following discussion, we name these fixed points; a visualization of our nomenclature is shown in Fig. 6(c). The number and location of the fixed points is set by the input current I_DC, which shifts the voltage nullcline up or down in the state space. For low, i.e., subthreshold I_DC, the model has a single, stable fixed point, P_rest. With an increase in I_DC, the knee of the voltage nullcline approaches the gating nullcline from below and results in a fold bifurcation at some $I_\mathrm{DC} = I_\mathrm{SN0}$. The fold bifurcation creates a saddle, P_saddle, and a node, P_block. Our assumptions ensure that P_block is unstable because (A2) requires that P_rest is the only stable fixed point at $C_\mathrm{m} = C_\mathrm{SNIC}$. Increasing the input current further leads to a second fold bifurcation at some $I_\mathrm{DC} = I_\mathrm{SN1}$.

This fold bifurcation annihilates P_{rest} and P_{saddle}. Beyond the bifurcation, P_{block} remains as the only surviving fixed point.

The saddle fixed point P_{saddle} exists only between I_{SN0} and I_{SN1}. The association of HOM bifurcations with saddles directly constrains their bifurcation branches to the region $I_{\text{SN0}} \leqslant I_{\text{DC}} \leqslant I_{\text{SN1}}$. In an analogous way, Hopf bifurcation branches are constrained by the existence of the associated focus fixed point: The Hopf branch that destabilizes the resting state P_{rest} is restricted to input currents below I_{SN1}, and the other Hopf branch that changes the stability of P_{block} is restricted input currents above I_{SN0}. Further constraints will be developed throughout the following arguments.

Observation 1: Starting points for the branches of big HOM and neighboring Hopf bifurcation—Anchoring the bifurcation diagram in the limit $C_m \to 0$ yields $I_{\text{big HOM}} < I_{\text{Hopf}}$. In the limit $C_{\text{m}} \to 0$, the conductance-based model is transformed into a relaxation oscillator with voltage as the fast variable, as sketched in Fig. 6(c) [82]. For this limit, de Maesschalck and Wechselberger have identified the full bifurcation structure for generic planar neuron models [42]. Their Theorem 2 demonstrates for sufficiently small C_{m} that an increase in I_{DC} results for model neurons such as ours in a generic sequence of bifurcations. Relevant for our consideration is the occurrence of a big HOM bifurcation at input $I_{\text{big HOM}}$ and a subcritical Hopf bifurcation that destabilizes P_{rest} at I_{Hopf}. Their full bifurcation structure ensures furthermore that neither the big HOM branch nor the Hopf branch returns to the limit $C_{\text{m}} \to 0$, which is important to ensure the existence of a codimension-two bifurcation at the other end. They state an ordering of the bifurcation currents, $I_{\text{big HOM}} < I_{\text{Hopf}} < I_{\text{SN1}}$, which will be used in the following to infer the same ordering at finite values of C_{m}.

Lemma 1: HOM branches cannot "bend backwards"—A variation in C_m generically breaks homoclinic orbits to hyperbolic fixed points. In order to constrain the location of HOM bifurcations in subsequent paragraphs, we want to show that the tracing of a HOM branch leads us always in one direction along the input current (increasing or decreasing input). Equivalently, we can show that a HOM branch cannot "bend backwards" along the input current dimension. This is the case if we show that HOM branches cannot have "vertical parts": A HOM branch cannot align with a parameter variation exclusively in C_{m}, because, as we show with this lemma, a variation in C_{m} generically breaks the homoclinic orbit.

Homoclinic orbits arise when the trajectory of the unstable direction of a fixed point connects to its stable direction, i.e., stable and unstable manifold overlap. A parameter variation can separate stable and unstable manifolds from each other, allowing for the definition of a distance. This distance is measured by the so-called separation function, sep [Fig. 1(b)]. For parameter values that lie on the HOM branch, the separation function is zero, $\text{sep}(C_{\text{HOM}}) = 0$, and becomes nonzero, $\text{sep}(C_{\text{m}}) \neq 0$, if a variation in the parameter breaks the homoclinic orbit, i.e., leaves the HOM branch. This is analogous to a nonzero value of the partial derivative of the separation function, which is known as the *Melnikov integral*, M [for a derivation in planar systems, see, for example, Ref. [83], leading to Eq. (6.12), which we use in Eq. (C2)].

A variation in C_{m} breaks the homoclinic orbit if the corresponding Melnikov integral evaluated on the homoclinic orbit is nonzero [24]. The Melnikov integral with respect to C_{m} for a homoclinic orbit with flow $h(t)$ is

$$M = \int_{-\infty}^{\infty} K(t) F(h(t)) \frac{\partial F(h(t))}{\partial C_{\text{m}}} dt = -\int_{-\infty}^{\infty} K(t) \frac{[I_{\text{DC}} - I_{\text{ion}}(h(t))]^2}{C_{\text{m}}^3} dt, \tag{C2}$$

where $K(t) = \exp[-\int_0^t \text{div} F(h(s)) ds]$. For our system, the Melnikov integral is strictly positive, $0 < M$, because (i) $K(t)$ is, as an exponential function, strictly positive, $\forall\, t:\ 0 < K(t)$, and (ii), because we implicitly assume the existence of a homoclinic orbit, the difference of ionic and injected currents cannot be zero at all times; hence, $\exists t:\ [I_{\text{DC}} - I_{\text{ion}}(h(t))]^2 > 0$. With that, the capacitance breaks the homoclinic orbit, and thus tracing a HOM branch along one direction results either in continuously increasing or decreasing input current values on the branch. This lemma is used in the following Observation 2 in order to pursue the big HOM branch starting in the limit $C_{\text{m}} \to 0$ (see Observation 1).

Observation 2: The big HOM branch eventually approaches the fold bifurcation at I_{SN1}. Based on the directionality of the big HOM branch derived in the literature, we will show in this observation that the big HOM branch eventually approaches the fold bifurcation branch at which the resting state collides with the saddle. The point of contact corresponds to an SNL bifurcation, as we will show in subsequent paragraphs.

The statement of Theorem 2 by de Maesschalck and Wechselberger states for sufficiently small C_{m}, in addition to the ordering used in Observation 1, that the big HOM branch departs from its starting point to the right, i.e., in the direction of increasing input current [42]. This directionality of the big HOM branch generalizes to larger values of C_{m}, because Lemma 1 prevents "backward bends" of HOM branches. Given that the big HOM branch does not return to the limit $C_{\text{m}} \to 0$ (Observation 1), the big HOM branch eventually has to approach the fold bifurcation at I_{SN1}. The next lemma ensures that the connection point is an SNL point.

Lemma 2: A HOM branch and the fold branch at I_{SN1} connect in an SNL bifurcation—A HOM branch is stable when it connects to a nondegenerated fold bifurcation involving a stable node. An SNL bifurcation involves a stable homoclinic orbit that transitions between a HOM bifurcation and a SNIC bifurcation. The homoclinic orbit of the HOM branch is stable if the associated saddle quantity is negative (the sum of the two eigenvalues of the associated fixed point). At the connection point with the fold branch, the homoclinic orbit is associated with a saddle-node fixed point arising from the collision of a stable node and a saddle. It has one zero eigenvalue (prerequisite for the fold bifurcation) and one negative eigenvalue (the former stable node sets the stability of the strongly stable manifold). The sum evaluates to a negative saddle quantity, ensuring a stable homoclinic orbit, and hence an SNL bifurcation.

Lemma 3: The bifurcation sequence in the lower part of the bifurcation diagram—For $I_{\text{DC}} = I_{\text{SN1}}$, increasing C_m from zero passes first a BT point, then an SNL point, before a nondegenerated SNIC bifurcation occurs, $C_{\text{BT1}} < C_{\text{big SNL}} < C_{\text{SNIC}}$. Combining Observation 2 and Lemma 2, we conclude that the big HOM branch connects to the fold bifurcation

branch at I_{SN1} with a stable homoclinic orbit, i.e., in an SNL bifurcation. This big SNL bifurcation happens at some point $(I_{SN1}, C_{big\,SNL})$, with $C_{big\,SNL} < C_{SNIC}$ because the big HOM branch cannot pass the capacitance value of C_{SNIC} as (A2) prohibits stable limit-cycle bifurcations for $I_{DC} < I_{SN1}$. From Observation 1, we know for $C_m \to 0$ that a Hopf branch starts at I_{Hopf} and that this branch does not return to the limit $C_m \to 0$. Because limit-cycle bifurcation branches cannot cross each other in a planar system, the Hopf branch can furthermore not cross the big HOM branch. Instead, it connects to the fold bifurcation branch in a BT bifurcation at some point (I_{SN1}, C_{BT1}). The ordering $I_{big\,HOM} < I_{Hopf}$ from Observation 1 immediately implies an ordering in C_m, i.e., $C_{BT1} < C_{big\,SNL}$. In summary, we have shown in this lemma that $C_{BT1} < C_{big\,SNL} < C_{SNIC}$.

These arguments have proven the bifurcation sequence in the lower part of the bifurcation diagram arising from the limit $C_m \to 0$. In the following, we use the unfolding of a second BT point to show the upper part of the bifurcation diagram.

4. The upper part of the bifurcation diagram, $C_m > C_{SNIC}$

Observation 3: The bifurcation diagram contains exactly two BT points. Kirst *et al.* identified the BT point for a generic class of conductance-based neuron models (including our model group) at a capacitance value that can be calculated from the input current at which the fold bifurcation occurs (Ref. [27], Supplemental Material). With the twofold bifurcation branches occurring in our model group at input currents I_{SN0} and I_{SN1}, we find one unique BT point on each fold branch. Lemma 3 identified one of them at the BT point (I_{SN1}, C_{BT1}), and the second BT bifurcation occurs at some point (I_{SN0}, C_{BT0}). From the BT point at (I_{SN0}, C_{BT0}) arises by normal form theory a Hopf bifurcation branch and a branch of a small HOM bifurcation. Both depart in the direction of increasing input I_{DC}, which will be used as before to constrain their location.

Observation 4: The second BT point lies in the upper part of the bifurcation diagram—The BT point at (I_{SN0}, C_{BT0}) *occurs at* $C_{BT0} > C_{SNIC}$. We restrict the region accessible to the Hopf branch that arises from the BT point at (I_{SN0}, C_{BT0}): A limit cycle bifurcation branch cannot cross other limit cycle bifurcation branches (in a planar system), and hence the Hopf branch cannot pass the SNIC bifurcation line between (I_{SN1}, C_{SNIC}) and $(I_{SN1}, C_{big\,SNL})$ or the big HOM branch. Furthermore, (A2) demands that no stable fixed point exists for $I_{DC} < I_{SN1}$ for $C_m = C_{SNIC}$, effectively preventing the Hopf branch to pass this line. The Hopf branch lies, hence, either entirely within or outside of the region bounded by these lines.

We show that the Hopf branch lies outside of this region by identifying this branch with the excitation block occurring at $C_m = C_{SNIC}$: (A2) demands that the excitation block at some $I_{DC} > I_{SN1}$, i.e., outside of the identified region. Around the excitation block, P_{block} is stabilized by a Hopf bifurcation. This Hopf bifurcation affects P_{block} and hence belongs to the same branch of Hopf bifurcations that arises at the BT point at (I_{SN0}, C_{BT0}), because this is where P_{block} is created. With that, the Hopf branch must lie outside the region denoted above and correspondingly also the BT point at its end. We hence conclude $C_{BT0} > C_{SNIC}$.

Lemma 4: The small SNL bifurcation—A second SNL bifurcation occurs at some $C_{small\,SNL} > C_{SNIC}$. The branch of the small HOM bifurcation that arises from the BT point at (I_{SN0}, C_{BT0}) (see Observation 3) continues by Lemma 1 in the direction of increasing input I_{DC}. Hence, we find some $C_m = C_{small\,SNL}$ for which the small HOM branch connects to the fold bifurcation at I_{SN1}. At the connection point, the HOM branch must be stable by Lemma 2. We identify the point $(I_{SN1}, C_{small\,SNL})$ as small SNL bifurcation.

For the overall proof, it remains to show the ordering $C_{small\,SNL} > C_{SNIC}$. For that, we observe that a limit cycle exists between the small HOM and the Hopf branch arising from the BT point and contrast this with the limit cycle arising from the SNIC bifurcation. As the Hopf bifurcation has to terminate the limit cycle of the SNIC bifurcation at C_{SNIC} [following (A2)], it cannot terminate the limit cycle arising from the small HOM bifurcation at this capacitance value. This leaves only the possibility for the SNL point to occur at some $C_{small\,SNL} > C_{SNIC}$.

In summary, we have shown that $C_{BT1} < C_{big\,SNL} < C_{SNIC} < C_{small\,SNL}$. This generic bifurcation structure occurs with the membrane capacitance C_m as bifurcation parameter at $I_{DC} = I_{SN1}$. For a model starting at a SNIC bifurcation, a variation in the capacitance will thus pass an SNL bifurcation before a BT point is reached.

[1] L. L. Gollo and M. Breakspear, Philos. Trans. R. Soc. London, Ser. B **369**, 20130532 (2014).

[2] P. Villegas, P. Moretti, and M. A. Muñoz, Sci. Rep. **4**, 5990 (2014).

[3] Y. D. Sato and K. Aihara, Neural Comput. **26**, 2395 (2014).

[4] A. L. Barth and J. F. A. Poulet, Trends Neurosci. **35**, 345 (2012).

[5] F. C. Hoppensteadt and E. M. Izhikevich, *Weakly Connected Neural Networks* (Springer Science & Business Media, Berlin, 1997).

[6] W. Gerstner and W. M. Kistler, *Spiking Neuron Models: Single Neurons, Populations, Plasticity* (Cambridge University Press, Cambridge, UK, 2002).

[7] P. Dayan and L. F. Abbott, *Theoretical Neuroscience: Computational and Mathematical Modeling of Neural Systems* (Massachusetts Institute of Technology Press, Cambridge, MA, 2001).

[8] R. D. Traub, R. K. Wong, R. Miles, and H. Michelson, J. Neurophysiol. **66**, 635 (1991).

[9] X.-J. Wang and G. Buzsáki, J. Neurosci. **16**, 6402 (1996).

[10] A. L. Hodgkin, J. Physiol. **107**, 165 (1948).

[11] G. B. Ermentrout and N. Kopell, SIAM J. Appl. Math. **46**, 233 (1986).

[12] J. Rinzel and G. B. Ermentrout, Analysis of neural excitability and oscillations, in *Methods in Neuronal Modeling*, 2nd ed., edited by C. Koch and I. Segev (MIT Press, Cambridge, MA, 1998), pp. 251–291.

[13] P. Arhem, G. Klement, and C. Blomberg, Biophys. J. **90**, 4392 (2006).

[14] K. M. Stiefel, B. S. Gutkin, and T. J. Sejnowski, J. Comput. Neurosci. **26**, 289 (2009).

[15] S. A. Prescott, S. Ratté, Y. D. Koninck, and T. J. Sejnowski, J. Neurophysiol. **100**, 3030 (2008).

[16] E. Phoka, H. Cuntz, A. Roth, and M. Häusser, PLoS Comput. Biol. **6**, e1000768 (2010).

[17] M. J. E. Richardson, N. Brunel, and V. Hakim, J. Neurophysiol. **89**, 2538 (2003).

[18] S. Schreiber, I. Samengo, and A. V. M. Herz, J. Neurophysiol. **101**, 2239 (2009).

[19] S. Schreiber, I. Erchova, U. Heinemann, and A. V. M. Herz, J. Neurophysiol. **92**, 408 (2004).

[20] E. Izhikevich, Int. J. Bifurcation Chaos **10**, 1171 (2000).

[21] S. Schecter, SIAM J. Math. Anal. **18**, 1142 (1987).

[22] The SNL bifurcation [21] is also known as *saddle-node homoclinic orbit*, *saddle-node noncentral homoclinic*, *saddle-node separatrix-loop* bifurcation [23], or *orbit flip* bifurcation [24].

[23] E. M. Izhikevich, *Dynamical Systems in Neuroscience* (MIT Press, Cambridge, MA, 2007).

[24] A. J. Homburg and B. Sandstede, in *Handbook of Dynamical Systems III*, edited by H. W. Broer, F. Takens, and B. Hasselblatt (Elsevier, Amsterdam, 2010).

[25] P. Jiruska, M. de Curtis, J. G. R. Jefferys, C. A. Schevon, S. J. Schiff, and K. Schindler, J. Physiol. **591**, 787 (2013).

[26] S. J. Schiff, Philos. Trans. R. Soc. London, Ser. A **368**, 2269 (2010).

[27] C. Kirst, J. Ammer, F. Felmy, A. Herz, and M. Stemmler, bioRxiv (2015), doi:10.1101/022475.

[28] U. Pereira, P. Coullet, and E. Tirapegui, Entropy **17**, 7859 (2015).

[29] A. A. Lazar, IEEE Trans. Inf. Theory **56**, 821 (2010).

[30] A. A. Lazar and Y. B. Slutskiy, Neural Comp. **26**, 264 (2014).

[31] Y. A. Kuznetsov, *Elements of Applied Bifurcation Theory* (Springer Science & Business Media, Berlin, 2013).

[32] B. Ermentrout, Neural Comput. **8**, 979 (1996).

[33] E. Brown, J. Moehlis, and P. Holmes, Neural Comput. **16**, 673 (2004).

[34] K. M. Shaw, Y.-M. Park, H. J. Chiel, and P. J. Thomas, SIAM J. Appl. Dyn. Syst. **11**, 350 (2012).

[35] A. Pikovsky, M. Rosenblum, and J. Kurths, *Synchronization: A Universal Concept in Nonlinear Sciences* (Cambridge University Press, Cambridge, UK, 2003).

[36] Y. Kuramoto, *Chemical Oscillations, Waves, and Turbulence* (Springer Science & Business Media, Berlin, 1984).

[37] G. B. Ermentrout and D. H. Terman, *Mathematical Foundations of Neuroscience* (Springer Science & Business Media, Berlin, 2010).

[38] H. Daido, Prog. Theor. Phys. **88**, 1213 (1992).

[39] H. Daido, Phys. D (Amsterdam, Neth.) **91**, 24 (1996).

[40] J.-H. Schleimer and M. Stemmler, Phys. Rev. Lett. **103**, 248105 (2009).

[41] A. Franci, G. Drion, V. Seutin, and R. Sepulchre, PLoS Comput. Biol. **9**, e1003040 (2013).

[42] P. De Maesschalck and M. Wechselberger, J. Math. Neurosci. **5**, 16 (2015).

[43] S. Blankenburg, W. Wu, B. Lindner, and S. Schreiber, J. Comput. Neurosci. **39**, 349 (2015).

[44] C. C. Chow and J. A. White, Biophys. J. **71**, 3013 (1996).

[45] S. Hong, B. Agüera y Arcas, and A. L. Fairhall, Neural Comput. **19**, 3133 (2007).

[46] A. L. Hodgkin and A. F. Huxley, J. Physiol. **117**, 500 (1952).

[47] The bifurcation structure of the HH model arises in our model when the twofold bifurcations collide in a cusp bifurcation. This can be achieved by parameters that affect the shape of the nullclines, but is not possible with input and capacitance as bifurcation parameters as used here.

[48] The normal form used to calculate PRCs for the generalized Hopf bifurcation in Ref. [33] assumes a circular symmetric fold of limit cycles bifurcation. This holds locally around the subcritical Hopf bifurcation, but is unrealistic for full-blown pulselike spikes, for which a separation of time scales is required in the dynamics.

[49] Y. Tsubo, J.-n. Teramae, and T. Fukai, Phys. Rev. Lett. **99**, 228101 (2007).

[50] A. Abouzeid and B. Ermentrout, Phys. Rev. E **84**, 061914 (2011).

[51] J. Hesse and S. Schreiber, Curr. Biol. **25**, R324 (2015).

[52] K. Bozek, Y. Wei, Z. Yan, X. Liu, J. Xiong, M. Sugimoto, M. Tomita, S. Pbo, C. C. Sherwood, P. R. Hof, J. J. Ely, Y. Li, D. Steinhauser, L. Willmitzer, P. Giavalisco, and P. Khaitovich, Neuron **85**, 695 (2015).

[53] G. Eyal, M. B. Verhoog, G. Testa-Silva, Y. Deitcher, J. C. Lodder, R. Benavides-Piccione, J. Morales, J. DeFelipe, C. P. de Kock, H. D. Mansvelder *et al.*, eLife **5**, e16553 (2016).

[54] T. H. Rumbell, D. Dragulji, A. Yadav, P. R. Hof, J. I. Luebke, and C. M. Weaver, J. Comput. Neurosci. **41**, 65 (2016).

[55] G. Hadjilambreva, E. Mix, A. Rolfs, J. Müller, and U. Strauss, J. Neurophysiol. **93**, 843 (2005).

[56] C. P. Billimoria, R. A. DiCaprio, J. T. Birmingham, L. F. Abbott, and E. Marder, J. Neurosci. **26**, 5910 (2006).

[57] K. M. Stiefel, B. S. Gutkin, and T. J. Sejnowski, PLoS ONE **3**, e3947 (2008).

[58] T. Netoff, M. A. Schwemmer, and T. J. Lewis, *Phase Response Curves in Neuroscience* (Springer, New York, 2012), pp. 95–130.

[59] S. Wang, M. M. Musharoff, C. C. Canavier, and S. Gasparini, J. Neurophysiol. **109**, 2757 (2013).

[60] B. S. Gutkin, G. B. Ermentrout, and A. D. Reyes, J. Neurophysiol. **94**, 1623 (2005).

[61] G. B. Ermentrout, B. Beverlin, II, T. Troyer, and T. I. Netoff, J. Comput. Neurosci. **31**, 185 (2011).

[62] The deposition of energy by infrared laser pulses leads to a fast increase in the membrane capacitance [63,64] changing the capacitive current $I_{\mathrm{cap}} = \frac{dC_{\mathrm{m}}v}{dt} = \dot{C}_{\mathrm{m}}v + C_{\mathrm{m}}\dot{v}$. Given the time course of energy dissipation, the fast transient capacitance increase, sufficient to excite the neuron [64], is followed by a time interval of increased C_{m}. Our study applies to neuronal properties beyond the initial transient.

[63] J. Wells, C. Kao, K. Mariappan, J. Albea, E. D. Jansen, P. Konrad, and A. Mahadevan-Jansen, Opt. Lett. **30**, 504 (2005).

[64] M. G. Shapiro, K. Homma, S. Villarreal, C.-P. Richter, and F. Bezanilla, Nat. Commun. **3**, 736 (2012).

[65] Z. Levnajić, Sci. Rep. **2**, 967 (2012).

[66] Actually, in some theories, single-cell characteristics fade into the background, while network features determine the macroscopic states [2,67,68]. Moreover, it has been concluded that cell heterogeneity in deterministic parameters can be approximated by white noise [69,70]. This, however, is due only to the fact that the varied parameters were ineffective in altering the neurons' computational and synchronization properties. For neurons close to an SNL point these results will not hold.

[67] D. J. Amit and N. Brunel, Network **8**, 373 (1997).
[68] N. Brunel and V. Hakim, Neural Comput. **11**, 1621 (1999).
[69] A. K. Alijani and M. J. E. Richardson, Phys. Rev. E **84**, 011919 (2011).
[70] J. F. Mejias and A. Longtin, Phys. Rev. Lett. **108**, 228102 (2012).
[71] D. Witthaut and M. Timme, New J. Phys. **14**, 083036 (2012).
[72] S. A. Marvel, S. H. Strogatz, and J. M. Kleinberg, Phys. Rev. Lett. **103**, 198701 (2009).
[73] M. C. Eguia and G. B. Mindlin, Phys. Rev. E **60**, 1551 (1999).
[74] J. F. Martinez Avila, H. L. D. de S. Cavalcante, and J. R. Rios Leite, Phys. Rev. Lett. **93**, 144101 (2004).
[75] Y. Ekşioğlu, Ö. E. Müstecaplıoğlu, and K. Güven, Phys. Rev. A **87**, 023823 (2013).
[76] R. Labouvie, B. Santra, S. Heun, and H. Ott, Phys. Rev. Lett. **116**, 235302 (2016).
[77] N. Shimizu, T. Morooka, and M. Morisue, Jpn. J. Appl. Phys. **34**, 5588 (1995).
[78] M. Romanelli, A. Thorette, M. Brunel, T. Erneux, and M. Vallet, Phys. Rev. A **94**, 043820 (2016).
[79] F. W. Schneider and A. F. Münster, J. Phys. Chem. **95**, 2130 (1991).
[80] V. Balakotaiah, S. M. S. Dommeti, and N. Gupta, Chaos **9**, 13 (1999).
[81] E. J. Doedel and B. E. Oldeman, *AUTO-07P: Continuation and Bifurcation Software for Ordinary Differential Equations* (Concordia University, Montreal, Quebec, Canada, 2009).
[82] E. M. Izhikevich and F. C. Hoppensteadt, SIAM J. Appl. Math. **63**, 1935 (2003).
[83] C. Chicone, *Ordinary Differential Equations With Applications* (Springer Science & Business Media, Berlin, 2006).

Part III.

Discussion

6. Outline

The publications of Part II investigate different aspects of neuronal information processing. Both studies show that cellular parameters have a considerable impact on neurons, either by determining neuronal morphology, or by setting neuronal dynamics, potentially, to a transition point highly influential on neuronal function.

The first publication investigates signal transmission from dendrite to axon under energetic constraints. Depending on the soma size and other basic parameters, neurons can increase their signal transmission and thereby decrease their energy consumption by externalizing their soma. This may explain the divergent evolution of the soma location in mammals and insects, as considered in the next chapter (Chapter 7). If the soma is relatively large, an externalization of the soma can enhance signal transmission between dendrite and axon. This allows for spike initiation in response to a number of synaptic inputs that is smaller compared to a morphology with a central soma, and which hence consumes proportionally less energy. This result predicts measurable differences between unipolar and multipolar cells, which can indeed be qualitatively found in experimental data.

The second publication focuses on the signal transformation into a spike, identifying a regime that is particular interesting for flexible information encoding. Spike generation changes qualitatively around the saddle-node-loop bifurcation, and, with it, various aspects of neuronal coding. The analysis considers signal processing in a neuron with constant mean firing rate, whose response to input can be captured by its phase-response curve, *i.e.*, a *spike-timing code* [47]. In the second publication, it is shown that the changes in phase-response curve at the saddle-node-loop bifurcation can drastically enhance synchronization. As detailed in Sec. 8.3, the phase-response curve also informs about the filtering properties of the neurons and other measures quantifying neuronal coding [143]. The second publication also demonstrates that the saddle-node-loop bifurcation occurs in generic two-dimensional conductance-based neuron model with so-called type-I dynamics (in the sense of a saddle-node on invariant cycle bifurcation at spike onset), and that it can be reached with any parameter that affects the relative speed of voltage and gating. While the publication mainly considers the membrane capacitance, temperature has similar effects (see Sec. 3.5.1), which has potentially important implications for pathologies, as discussed in Chapter 10.

Neuronal processing in health and disease fundamentally depends on ion channels and their characteristics [93]. This thesis, in addition, highlights the importance of morphological and so-called *passive* parameters such as leak conductance, capacitance, or axial resistance. In contrast to ion channels, whose characteristics can vary greatly between phyla[1], the parameters considered in this thesis are shared by all bilaterian

[1] In fact, the number of ion channel isoforms has increased throughout evolution and correlates better with increased complexity of an organism than other properties of single neurons [113].

animals since more than 555 million years ago[2]. While passive parameters can be significantly different between neurons (see Table I in the Supplementary Information of the first publication), they are fundamental to any neuron[3], and for parameters such as leak and capacitance, the impact on neuronal dynamics is well established and easily described in models (Sec. 3.2). The focus on passive parameters hence allows to investigate signal processing on a fundamental level, emphasizing the similarities between neurons more than their differences.

The following chapters expand on the results of the publications (Chapters 7 - 10), and summarize modeling assumptions (Chapter 11). Chapter 7 proposes a potential evolutionary path that could explain the development of unipolar and multipolar morphologies based on two hypotheses. First, the functional polarization and other potential advantages of central or externalized somata are reviewed, and the size of the soma, one essential parameter in the soma-to-neurite ratio, is discussed. The discussion culminates in the formulation of a hypothesis on the distribution of organelles in unipolar and multipolar neurons, which could explain the different soma-to-neurite ratios observed in nature. Together with the dependence of the soma location on the soma-to-neurite ratio, this entails a consistent picture for the divergent evolution of the soma location. The picture is furthermore discriminated from alternative explanations resting on the advantages of ganglionic arrangements by a second hypothesis, which delimits ganglion size.

The second project of this thesis is discussed in the following chapters. Chapter 8 provides more background on bifurcations, with further results supporting the generality of the saddle-node-loop bifurcation, and a discussion of its implications. As an outlook, phase-response curves at other bifurcations and beyond spike onset are considered. In Chapter 9, the temperature is discussed as bifurcation parameter for the saddle-node-loop bifurcation, in alternative to the membrane capacitance used in the second publication, and experimental results are presented. The temperature as bifurcation parameter is particularly interesting with respect to febrile seizures, and as medical application of the results of the second publication, Sec. 10 illustrates the potential of the saddle-node-loop bifurcation as unifying mechanism for seizure induction.

[2]Many aspects of the nervous system can also be found in even older *phyla* such as jellyfish.

[3]Membrane leak and capacitance are indeed fundamental to every living cell even beyond the nervous system.

7. Evolution and functional consequences of the soma location

Depending on the soma size (and other parameters), neurons can increase signal transmission between axon and dendrite by an externalization of their soma. The associated decrease in energy consumption could be evolutionary favorable. The results of the first publication challenge the believe of Santiago Ramón y Cajal that the difference in soma location is only of minor importance, due to the functional similarity he observed for retinal amacrine cells that are unipolar or multipolar, and dorsal root ganglion cells that are bipolar in fish and unipolar in mammals [128]. The results of the first publication, in contrast, predict that it is the soma-to-stem ratio of these neurons that advocates different soma locations for optimal signal transmission, at minimal energetic costs. The soma-to-neurite ratio is given by the size of the soma in comparison with the diameter of the stem neurite, weighted by axial and membrane resistance. Experimental data fit the resulting prediction qualitatively. The externalization of the soma is especially effective in optimizing signal transmission with an increased axial resistance along the stem neurite. Hence, one prediction of the first publication is that, for neurons with externalized soma, the stem neurite has a higher axial resistance than the low value that is typically reported in the literature for the dendritic or axonal tree of these cells (Sec. 7.5.3).

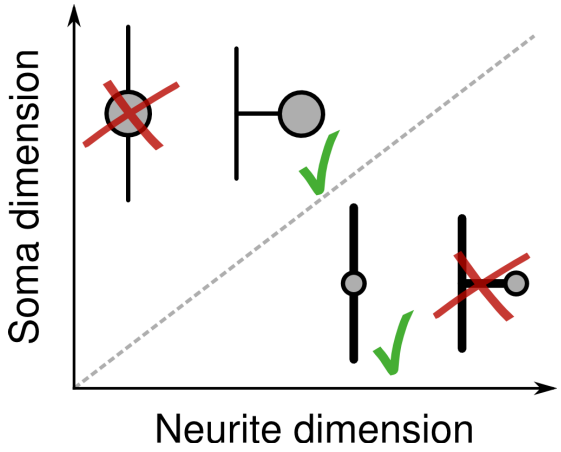

Figure 7.1.: Following the results of the first publication, whether unipolar and multipolar morphologies are favorable for energy-efficient signaling depends on the soma and neurite size.

In the following, the results of the first publication will be put into a broader context. The discussion leads to two hypotheses, one that speculates on the evolutionary development of different soma locations more in detail, and another that rejects certain advantages of ganglionic arrangements (commonly used to explain unipolar mor-

phologies) by suggesting an upper bound on the ganglion size. Before this, main assumptions of the study, functional polarization and the existence of a dedicated spike initiation zone in the beginning of the axon, are considered in biological neurons. The discussion then contrasts energy-efficient signaling with other potential advantages of central or externalized somata. Next, the conclusion of the first publication, that the divergent evolution of the soma location may result from different soma-to-neurite ratios, is taken one step further by the development of a potential explanation for the broad range of soma-to-neurite ratios observed in nature. Finally, unipolar neurons are considered in their ganglionic arrangement, which was repeatedly related to their morphology (compare Sec. 2.3.2). A maximal ganglion size is derived based on volume minimization.

7.1. Functional polarization

The hypothesis from the first publication, that soma location optimizes signal transmission, implicitly relies on the assumption that the signal has to be transmitted from dendrites to the axon, either through a central soma, or directly from dendrite to axon for an externalized soma. This assumption requires that one process can be identified as the *axon* that predominantly transfers information to other cells, while the other branches predominantly collect information as *dendrites*. A preference for unidirectional information flow in neurons has already been hypothesized by Ramón y Cajal at the end of the 19th century [128], and is one of the central assumptions for the analysis in this study. Especially for more complex animals such as mammals or insects, many neurons in the central nervous system abide to this form of *functional polarization*.

7.1.1. Neuronal polarity of unipolar cells

Examples for neurites with simultaneously occurring pre- and postsynaptic terminals can be found for both vertebrates and higher invertebrates, but neuronal polarity is in general less strictly established in invertebrates than in vertebrates [48]. Yet, even with pre- and postsynaptic terminals on the same branch, the proportion of input to output is in most cases different enough to distinguish dendritic and axonal structures [106]. Especially for insects, increasing evidence suggests that dendritic and axonal structures are homologue to vertebrate structures, for example based on the microtubule orientation[1] [137, 157], and the complexity of the dendritic tree of certain insect neurons is comparable to that of vertebrate neurons [101].

7.1.2. Spike initiation zone

In the first publication, the signal transmission is evaluated between dendrite and the initial part of the axon. In vertebrates, this location is a major spike initiation zone,

[1] A hallmark of neuronal polarization on the level of neurite ultrastructure is the orientation of microtubules. Microtubule orientation is to a large part set by function. For example, the removal of an axon in both mammals and insects leads to the transformation of a dendrite into an axon, with a full reversal of microtubule polarity [135]. Moreover, a lack of strict microtubule polarization is observed in neuronal cultures of vertebrates as well as invertebrates, probably due to the missing functional input [135].

it is called *axon initial segment* and can be recognized by specific molecular markers. A recent study found evidence for a specialized axon initial segment also in fly [167]. More in general, for both unipolar and multipolar neurons, spike initiation zones have been reported mostly right after the multipolar soma or the unipolar dendritic tree (*Aplysia* [159], gastropods [49]). The functional relevance of a dedicated spike initiation is best illustrates by recent experiments that show a shift in the location of this structure. Both vertebrates and invertebrates can shift their spike initiation zone in an activity-dependent manner (unipolar neuron [109], multipolar neurons [57, 95]). The distance by which the spike initiation zone moves further up into the axon effectively decreases the excitability of the neuron[2].

If already a small shift in spike initiation zone can influence spike initiation considerably, the different distances between dendrite and axon depending on the soma location is likely to be even more influential (the direct communication between dendrite and axon for an externalized soma, compared to the increased distance between dendrite and axon due to a central soma).

7.2. Output control

The output of a neuron that is generated at the spike initiation site is in general a nonlinear function of its past inputs (and potentially noise). While both central and externalized soma locations allow to regulate neuronal output, they do so differently, as discussed below. With a central soma, the regulation depends mainly on active conductances, while the morphology with an externalized soma can control spike initiation also by passive parameters.

7.2.1. Signal regulation in central somata

The membrane voltage of a central soma directly influences spike initiation in the axon initial segment, and hence provides the means to control neuronal output. A central soma can effectively separate different parts of the neuron, because its large somatic surface provides a considerable current sink (sometimes called a large capacitive and resistive load). For example, a central soma can ensure a certain independence of different proximal dendritic branches by clamping the background voltage at a rather low level [8]. Moreover, it can separate axonal and dendritic activity, on one hand as a noise filter, on the other hand as a region with low-probability spike transmission: The filtering of noise arises from the capacitive load of a (large) central soma, which acts as a *low pass filter* (a filter that passes low frequencies and suppresses high frequencies). The somatic dampening of high frequencies may be useful to filter synaptic noise, both from dendritic and somatic synapses. On the other hand, a central soma can control excitability and even block spikes, and thereby provides a region with a low *safety factor*, as this was called in the older literature [19]). With that, it may hinder dendritic spikes to invade the axon, or, *vice versa*, it may also prevent the spread of axonal activity into the dendrite, so called *backpropagating action potentials* (bAPs) [19]. Due to its privileged location, a central soma can directly regulate neuronal output, and may hence provide

[2]Excitability is used here in the sense of current threshold.

an attractive target for synaptic input, which is for vertebrate central neurons typically inhibitory [33].

7.2.2. Signal regulation in externalized somata

In order to understand signal regulation in neurons with externalized soma, it is helpful to categorize neurons by the length of their stem neurite with respect to signal transmission. The latter is given by the *electrotonic length*, the ratio of the spatial length, L, divided by the *length constant*[3], λ, *i.e.*, $\frac{L}{\lambda} = 2L\sqrt{\frac{R_\mathrm{a}}{R_\mathrm{m}d}}$. An electrotonically short neurite transmits signals with less attenuation than an electrotonically long neurite. With an electrotonically short stem neurite, the externalized soma is hardly shielded from dendritic and axonal trees, and hence acts in all practical purposes similar to a central soma. The following discussion, and the first publication, only consider neurons with an electrotonically long stem neurite when talking about unipolar neurons or an externalized soma. In the simulations, an electrotonic length of the stem neurite of at least 0.1 was required to distinguish central and externalized somata. Only for such neurons, the signal, at least partly, bypasses the externalized soma.

Some animals do show unipolar neurons with electrotonically short stem neurites. Spike initiation in such neurons has been reported to be influenced by somatic hyperpolarization [99]. In *gastropoda*, neurons may show an excitable, externalized soma that is spatially and electrotonically close to the spike initiation zone, as reviewed by Gillette [49]. The externalized soma can, in this case, act with respect to its capacitive and resistive load similar a central, excitable soma. However, compared to a central soma, the propagation of the somatic action potential along the stem neurite delays the somatic action potential compared to the axonal action potential. Neurons with excitable, externalized neurons seem to control the delay introduced by the stem neurite: The stem neurite grows in concert with the ganglion, which may preserve the synchrony between soma and axon [49] when the electrotonic length is fixed by a coordinated growth of length and diameter (as is mentioned in Sec. 7.6). Especially with a long stem neurite, the delayed arrival of the somatic spike may lead to conflicting signals from axon and soma [49]. The stem neurite may hence induce disadvantageous signal reflections, which are not known in mammals [15].

The neurons mainly considered in this thesis are unipolar neurons with an electrotonically long stem neurite, which are found, for example, in insects and cephalopods [49]. These neurons typically have an inexcitable soma that is electrotonically separated from dendritic and axonal trees. Especially for a large soma, a passive membrane is probably energetically favorable, saving on the inclusion of energy-expensive ion channels in the somatic surface. This suggests that in particular large somata should be passive and show long stem neurites.

For unipolar neurons with long stem neurite, signal processing is more influenced by the T-junction (at which the stem neurite connects to the axon), than by the externalized soma itself. Similar to a central soma, the T-junction of the stem neurite can serve as

[3]The length constant for a neurite of diameter d is given as $\lambda = \sqrt{\frac{R_\mathrm{m}}{R_\mathrm{a}}\frac{d}{4}}$, with axial resistance R_a and membrane resistance R_m. It corresponds to the distance over which an input signal decays to $1/\mathrm{e}$, and thereby provides a measure of the passive signal spread along a neurite.

low pass filter, *e.g.*, in the frog dorsal root ganglion neuron [102]. Moreover, unipolar neuron can control their threshold by the coupling of axon initial segment and soma via the passive properties of the stem neurite (by changing internal resistances or dimensions). Passive properties can control excitability without the costs associated with an increase in the number of ion channels[4] (with energetic costs on the level of ion channel synthesis and gating activity which requires the reestablishment of ion concentration by ion pumps).

An electrotonically long stem neurite provides a shielding between somatic and axonal membrane potential that may be useful for ionic balancing. The shielding allows the resting potential in the soma to be higher than the resting potential in the processes. A higher resting potential in the soma compared to the neurites might save energy because less drastic concentration gradients have to be established by somatic ion pumps[5]. A somatic membrane potential closer to zero may also be useful for the uptake of negatively charged substances, which have to be taken up against the barrier provided by the potential difference. Indeed, a preliminary literature review suggests that while somatic recordings often report membrane potentials around -50 mV, neurite recordings tend to lie around -70 mV, for example in Drosophila neurons, the reported resting potentials vary between -25 mV to -70 mV [55]. More experimental results are required to allow for a thorough comparison of the resting potential in the soma and in the neurites of unipolar cells.

An interesting example with respect to the previous discussion are unipolar dorsal root ganglion cells. As described above, neurons with an electrotonically long stem neurite should have passive somata, whereas, with an electrotonically short stem neurite, active somata that boost the arriving signal may be more advantageous. The externalized somata of dorsal root ganglion cells can either be passive or active, and the length of their stem neurite seems to increase throughout evolution. A passive soma with a short stem neurite has been suggested as potential mechanism to control signal transmission by clamping the axonal voltage (allowing for spike initiation only when the soma is depolarized) [40]. A long stem neurite, in contrast, increase the electrical isolation between soma and axon, and hence decreases the somatic clamping of the axon [30]. This has been suggested as the evolutionary pressure for the increase of the stem neurite length of dorsal root ganglion cells [30]. In mammals, the stem neurite is commonly elongated by curling around the soma, and this curling increases from frog over chicken to mammals [107]. A long stem neurite effectively isolates the soma from the axon, such that somatic signaling cannot interfere with axonal signals. An active soma, in contrast, can directly influence signaling. Active conductances are typically distributed over soma and stem neurite, and, upon depolarization, the resulting currents may contribute to the signal in the axon [30]. The function of active conductances in the soma (and stem neurite) is unclear. It may be an evolutionary

[4] Multipolar neurons with a central soma can adapt their threshold by energetically costly, additional ion channels in the soma or the axon initial segment, or by morphological changes in the dendritic tree.

[5] The resting potential is a weighted average of the reversal potentials of different ions, each of which is a function of the ion concentration ($v_k = \frac{RT}{zF} \ln\left(\frac{[k]_{\text{out}}}{[k]_{\text{in}}}\right)$ is the reversal potential for ion k, with intra-/extracellular concentrations $[k]_{\text{in/out}}$, gas constant R, Faraday constant F, absolute temperature T and ionic valence z) [45]. Estimates of the energy spend at rest on the maintenance of the resting potential in the whole neuron vary between 11% and 20% of the overall energy spend on neuronal signaling [62, 148].

left-over from the times of bipolar dorsal root ganglion cells, as they are found in fish. If it is experimentally possible to obtain electrophysiological and morphological data from the same cell, it would be interesting to test whether active somata show in general shorter stem neurites than passive somata.

7.3. Spatial proximity

The somata of unipolar and multipolar cells influence signal processing in different ways. While a central soma is close to the spike initiation zone, an externalized soma is often located in proximity of the surrounding hemolymph, facilitating hormonal communication.

7.3.1. Support of axon initial segment by a central soma

Adjacent localization of central soma and axon initial segment allows the soma to support the spike generation zone in the restoration of ionic concentrations after spiking. The central soma could either provide ATP to fuel the ion pumps in the spike initiation zone, or act as drainage for sodium molecules such that the sodium load of the axon initial segment is reduced. In the latter case, the combination of thin axon and thick soma produces an asymmetric structure that facilitates unidirectional diffusion from axon to soma (acting similar to periodic asymmetric structures known as *drift ratchets* [84]). Somatic support may be especially relevant for spike initiation zones in thin processes as common in vertebrates, which contain disproportionally small densities of energy-supplying mitochondria compared to larger processes [122].

7.3.2. Hormonal communication

Functional advantages of the separation of somata and neurites in insects may be related to neuro-secretion. While vertebrates commonly show specialized non-neuronal glands for hormonal communication, such glands are considerably less common in invertebrates [33]. This suggests that neuro-secretory cells are particularly important in invertebrates, where often a clear distinction between non-secretory and neuro-secretory cells is difficult because also many typical neurons with chemical synapses can non-synaptically emit neuromodulators [33]. The large number of neuro-secretory cells in invertebrates is widely distributed, probably to affect in an effective way the relatively large volume of the hemolymph (which can be 20-30% of the body volume compared to a blood volume of 5-8% typical for vertebrates) [33]. Neuro-secretion is energetically costly and requires cellular machinery, which is probably easier to provide in large, externalized somata than in small, central somata. Externalized somata distributed on the surface of ganglia led themselves for neuro-secretion on a local level, as common in invertebrates [33]. The somata in the environment of such local neuro-secretion provide a well-defined target for regulation, while in a situation where somata are intermingled with various processes, potentially from distant brain areas, the latter may be activated simultaneously with the local somata. In summary, neuro-secretory cells are more prevailing in invertebrates compared to vertebrates, and may profit from a superficial arrangement in the ganglia. As neuro-secretory

cells require more somatic machinery, neuro-secretion may be one of the evolutionary pressures for large somata in invertebrates.

7.3.3. Support of somatic synapses

The large volume of a central soma could not only provide energy for the spike initiation, but also for postsynaptic terminals. Synapses are commonly found on central somata, and the large volume-to-surface ratio may allow for a higher synaptic density on the soma than on a dendritic process. High input densities may be especially relevant in vertebrates with their high amount of recurrent connections. The environment of central somata preferentially receives input from inhibitory neurons [33], somatic surface and proximal dendrites are densely populated with inhibitory postsynaptic terminals. Because inhibitory interneurons can show high firing rates, it is likely to observe numerous inhibitory post-synaptic potentials. Synaptic activation implies high energetic costs on the postsynaptic side, which may explain the predominance of somatic inhibitory inputs, because the soma is probably the location in a neurons with the highest buffer capacities for short and strong energy demands.

7.4. Organelle exclusion hypothesis

The divergent evolution of the soma location seems to provide alternative solutions to the same problem: How to transmit signals efficiently from the dendrite to the axon. Both solutions bear slightly different advantages, as discussed above. Which neuronal morphology is observed depends on the soma-to-neurite ratio, as suggested by the analysis in the first publication. This raises the question of the causes for the divergent evolution of the soma-to-neurite ratio. In this section, I will present the hypothesis that the difference in soma-to-neurite ratio might be explained by the ultrastructural organization of the neurons. Starting with the idea that soma size underlies evolutionary constraints (*e.g.*, signal transmission), the main hypothesis is that neurons with a large amount of somatic organelles require a larger soma, and may hence be better off with an externalized soma.

7.4.1. Increased soma size through evolution

The size of the soma is correlated with the size of the neuron, which increases with body size and complexity of the nervous system throughout evolution[6] [119]. The correlation in size probably originates from the need of the soma to satisfy the increased demand of support and maintenance of a large neuron.

Soma size correlates with neurites

As the soma is responsible for the maintenance of the cell, a correlation between the size of the soma, and the extent and dimensions of the axonal and dendritic branches can be expected. In several studies, the soma diameter could be correlated with the

[6] Also during development, the neuron increases with body size [61, 128], and in some cases the soma diameter even relates linearly to the body length [72].

axon diameter [28, 66], more precisely, the soma volume correlates positively with the diameter of the axon [119]. Furthermore, the soma diameter correlates with the dendritic innervation field for both vertebrates and higher invertebrates [119] and weakly with the sum of proximal dendrite diameters [169]. The total somatic-dendritic membrane surface area of geniculate cells, and the surface area of their somata, grows about square-root like [9]. In accordance to the correlation between soma size and the dimensions of their neurites, giant neurons contain more nucleic acids, proteins and DNA (analyzed for *gastropoda* [49]).

Soma size determined by DNA

The soma contains the nucleus with the DNA, and its size is hence bounded below by the nucleus size [119]. More in general, it was claimed that the cell size is determined by the DNA content and the transcriptional activity, see Pena et al. [121]. As the DNA content is fixed in a neuron (or any other cell), the soma size seems to mainly depend on transcriptional activity, which has been correlated for frog motor neurons [121]. Transcription rate is also positively correlated with the activity of the innervation of the neuron [121]. This may be the direct link responsible for the correlation between soma and axon dimensions, because the axon diameter has been reported to be linear to the typical mean firing rate (experimental measurements from nine different neurons by Perge et al. [122]). The relation between size and transcriptional activity forms the bases for the organelle exclusion hypothesis presented in this section.

Soma size in bipolar cells

The lower bound on soma size given by the nucleus is for example accomplished by bipolar cells. The soma of these cells appears to be just large enough to accommodate the nucleus. For example, only a thin rim of somatic cytoplasm surrounds the nucleus in cortical bipolar cells [123]. The soma is slightly elongated, it looks like a flexible tube in which the nucleus was squeezed. The soma is relatively small, only the largest bipolar neurons reach 30 nm. At least for peripheral cells, the bipolar shape was explained by their clear functional polarity (one end receiving, the other one sending, and no feedback needed) [154]. In view of the first publication, the straight signal transmission executed by these neurons (relaying information without recurrent input) is indeed a cause of their bipolar morphology, but only an indirect one: Information transmission as observed in these cells, without more complicated forms of processing, such as complex dendritic calculations, probably requires less somatic support and maintenance. These cells hence tolerate a small soma, for which then the bipolar shape, facilitating signal transmission, is advantageous. Bipolar cells may represent an example where the morphology (a soma so small that it hardly fits the nucleus) is optimizing signal transmission (essential for peripheral neurons), supporting the relevance of soma size as an evolutionary constraint.

7.4.2. Externalized somata support large cells

Externalized somata seem to support larger neurons size than central somata. Many invertebrates show so called *giant neurons*, whose thick axons allow for an increased

conduction speed [63]. Giant neurons are considerably less frequent in vertebrates[7], probably because of the abundance of myelination[8], which also increases conduction speed. Moreover, one of the largest cell types in the mammalian nervous system are dorsal root ganglion cells, which have an externalized soma.

The following arguments show that, in large cells, the relative size of neurites and soma can lead to a large soma-to-neurite ratio that, as shown in the first publication, favors externalization. When neurons become larger, it seems reasonable to assume some form of correlated growth between soma and stem neurite, because proteins important for the maintenance of axonal and dendritic trees are synthesized in the soma, and must subsequently be transported through the stem neurite. This transportation, independent of whether the transport is active or passive, is probably bounded by the cross section of the stem neurite, which is proportional to the square of the stem neurite diameter, d^2_{stem}. The somatic protein synthesis is probably bounded by the soma volume, which is proportional to the cube of the soma diameter, d^3_{soma}. A proportional growth between soma volume and stem neurite cross section seems reasonable in order to allow for a balanced protein synthesis and dispersion, which suggests the relation $d^3_{\text{soma}} \propto d^2_{\text{stem}}$ throughout the evolutionary increase in neuron size. This allows for an assessment of the development of the soma-to-neurite ratio, $R \propto d^2_{\text{soma}}/d_{\text{stem}}$:

$$d^3_{\text{soma}} \propto d^2_{\text{stem}} \;\rightarrow\; R \propto d^{1/2}_{\text{soma}},$$

which suggests that an increase in neuron size leads to an increase in soma-to-neurite ratio with the square root of the soma diameter. This makes an externalization of the soma more and more favorable with an evolutionary increase in neuron size.

7.4.3. Why large somata?

Various aspects of neuronal anatomy and physiology have been related to a trade-off between energy and information [149]. Also the size of neurons may arise from such a trade-off because, at least in single-compartment models, larger models have the lowest energy-efficiency (but also a higher information rate) compared to smaller models [149]. This led the authors to suggest a *Law of Diminishing Returns* that reduces coding capacity, neuronal size and channel density to the possible minimum [149]. Externalization of the soma may relax the constraints on energy consumption such that large specialized neurons can develop. Driving forces for large neurons may include the requirements of a large soma surface, volume minimization and spike initiation at multiple locations, as discussed in the following.

Soma surface for substance uptake

The membrane surface per neuronal volume has to be large enough to allow for the exchange of nutrients and gases [128]. This may explain repeatedly reported somatic invaginations in arthropods [59, 166] and dorsal root ganglion cells [30]. Those invaginations increase the somatic surface above the value estimated from the soma

[7] Examples for large vertebrate neurons are Mauthner cells in fish and reptiles.

[8] Myelination developed (probably independent) in vertebrates, annelids, and *crustacea* [63], and also in insects examples for enhance signal transmission by wrapping of axons is known.

diameter. Microvilli or perikaryal projections in dorsal root ganglion cells, for example, can increase the soma surface by up to 40%, as reviewed by Pannese [119]. When the somatic surface has to be enlarged in neurons with central soma, an increase in soma diameter is preferable over invaginations, because the latter increase the capacitive and resistive load without decreasing the axial resistance, which an increase in soma diameter would provide. Invaginations in vertebrate neurons would only be expected due to spatial constraint, and no corresponding reports are found in the literature. For unipolar neurons with sufficiently long stem neurite, the signal transmission is not hindered by invaginations on the soma surface, and they hence provide an efficient way to increase the surface-to-volume ratio at minimal spatial costs.

Volume minimization

One large neuron instead of multiple smaller ones can use space more effectively as part of the cellular machinery is only needed once. Large somata are, for example, economically advantageous when several axons can share one soma [65]. The DNA, which sets the lower bound of the soma size, is in this case only required once. As the somatic volume grows correlated to the axon diameter [119], the soma diameter grows slower than the axonal diameter, and hence the somatic surface area per axon decreases for multiple axons. Multiple axons are, for example, found in locust [65] and invertebrate motor neurons that commonly innervate distinct areas (*e.g.*, bilateral stimulation of muscle tissue [61]), in contrast to the typical vertebrate motor neuron.

Multiple spike initiation sites

Computations of different axonal branches can be independent, and thereby more variable, if the neuron lacks a unique, central integration zone. Such an integration zone is for example given by a central soma [103]. An externalized soma, in contrast, could facilitate parallel computations as the dendritic signal is directly transmitted to the axon. Independent computations are furthermore facilitated by multiple spike initiation sites, which are relatively common in invertebrates. Independent spikes are known to occur for different axonal branches of locust [65] or *Aplysia* neurons, as well as for crustacean heart, crayfish [159], and cricket neurons [117]. With multiple spike initiation sites, a higher degree of integration is reached in a single cell, such that complex computations need fewer cells. In neurons with multiple spike initiation zones, compartments can interact with each other via spikes, as reviewed by Bucher and Goaillard [15]. In general, the literature may even suggest that invertebrate neurons are marked by a higher degree of specialization compared to vertebrate neurons.

7.4.4. Divergent evolution of unipolar and multipolar neurons

The common ancestors of higher invertebrates and vertebrates [139, 140] probably had multipolar neurons. The increase in soma size with evolution suggests that the neurons had large somata relative to their neurites, in particular compared to peripheral bipolar neurons (Sec. 7.4.1).

Further increase in the soma size during evolution may have hindered signal transmission because of the large capacitive and resistive load. I suggest that higher inverte-

brates and vertebrates found different solutions to cope with those large somata: While higher invertebrates externalized their whole soma, vertebrates externalized somatic machinery into the proximal dendrites. This allows for a smaller soma at the cost of thicker proximal dendrites, which leads to a lower soma-to-neurite ratio.

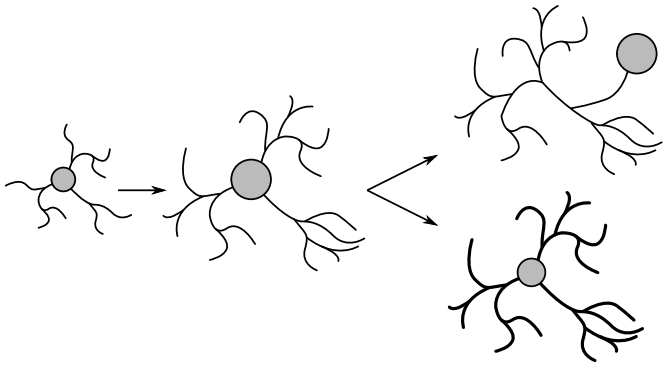

Figure 7.2.: **Two solutions to the same problem.** When evolution scales up the size of neurons, the resulting large soma in the signaling path is a problem. While higher invertebrates reacted with an externalization of the whole soma, vertebrates may have relocated part of the somatic machinery into proximal dendrites, such that the size of the soma could be decreased.

An example for the externalization of somatic machinery is the rough endoplasmic reticulum. In higher invertebrates, it is restricted to the soma [136], whereas in vertebrates, it is also found in proximal dendrites [120], as also reviewed by Sánchez-Soriano et al. [157]. The endoplasmic reticulum synthesizes proteins [172], and regulates metabolism [120] and excitability of the neuron [172]. As a large rough endoplasmic reticulum is especially prominent in secretory cells [120], and neuro-secretion is ubiquitous in invertebrates (Sec. 7.3.2), it is possible that invertebrates in general tend to have a larger rough endoplasmic reticulum than vertebrates. A large rough endoplasmic reticulum might simply not fit into proximal dendrites, which could explain why invertebrates left the rough endoplasmic reticulum in the soma, and externalized the soma instead.

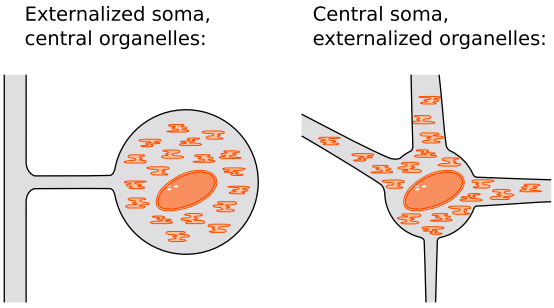

Figure 7.3.: Hypothetical organelle distribution in unipolar and multipolar cells.

7.5. Predictions of the organelle exclusion hypothesis

7.5.1. Relative nucleus volume

The DNA of a neuron, constant over the lifetime of the cell, is contained in the nucleus. The machinery required for protein synthesis surrounds the nucleus and increases the soma size. Considering the volume ratio of soma and nucleus for unipolar and multipolar neurons, my hypothesis predicts a larger ratio for unipolar neurons (because of additional somatic machinery), and a ratio closer to one for multipolar neurons. Indeed, unipolar invertebrate motor neurons have typically a quite large soma with lots of cytoplasm [61]. A quantitative consideration of this ratio could be analyzed in future research. Estimates for the ratio of the soma-to-nucleus volume could in particular be extracted from electron microscopy data that is used for three-dimensional reconstructions of neurons.

7.5.2. Mitochondria distribution

Mitochondria are small organelles that produce ATP and thereby satisfy a large proportion of the energetic requirements of eukaryotic cells [1]. Mitochondria are in general distributed all over the neuron, and are observed both in the soma and the neurite[9] [166]. Mitochondria are particularly important for structures that transmit signals, for example, activity in unipolar dorsal root ganglion cells increases the energy consumption of the neurites, but not of the somata[10] [83]. For multipolar neurons, where the central soma also participates in signaling, activity should increase energy consumption both in the neurites and the soma.

For both unipolar and multipolar neurons, mitochondria are required in and around the soma to supply energy for protein synthesis. If the somatic machinery in unipolar neurons is indeed confined to the soma proper, as suggested by the organelle exclusion hypothesis, this may be reflected in a higher number of mitochondria in the soma compared to the neurites. In this case, the ratio of the mitochondria number of soma and neurites is expected to be larger for unipolar neurons.

The localization of mitochondria in regions with high ATP consumption has the advantage that ATP is synthesized and consumed at the same spot, such that ATP is not transported through the neuron. On the other hand, this requires that nutrients consumed by the mitochondria are transported to this location. In vertebrates, this is at least partly accomplished by astrocytes which provides nutrients to the neuron at different locations. In invertebrates, nutrients are mainly taken up by the soma [61, 157] (compare Sec. 2.3.2), which requires a subsequent nutrient transportation along the neurites. If the transportation of ATP is easier than the transportation of nutrients, it also seems reasonable to locate a high density of mitochondria in regions with easy access to nutrients, such as the soma in the case of unipolar neurons. From this perspective, a higher proportion of mitochondria in the soma compared to the

[9] In some cells, mitochondria can move through the cytoplasm, in other cells they are located permanently in regions with high ATP consumption [1].

[10] Indeed, the soma is not essential for signal transmission at all, as dorsal root ganglion cells transmit signals even when their somata are mostly degenerated after blocking blood supply [61].

neurites in invertebrates could support the organelle exclusion hypothesis, but it could also result from an easy access to nutrients.

While the energy consumption related to protein synthesis may be concentrated in unipolar neurons in the externalized soma, the overall energy consumption of a central soma may still be higher due to its active conductances and synaptic inputs. Hence, a fair comparison of energy consumption between unipolar and multipolar neurons may in general be difficult to ensure. Yet, as energy is considered an important evolutionary pressure [98, 114], I believe the mitochondria distribution to be an interesting starting point for the investigation for neuronal signaling.

7.5.3. Axial resistance in organelle-dense neurites

The axial resistance models the resistance that an ion in the cytoplasm is subjected to. Impediments such as organelles and the endoplasmic reticulum increase the axial resistance [29]. Externalization of cellular components into the dendrites may hence implicate a higher axial resistance in the dendrites of vertebrates compared to higher invertebrates. Indeed, higher axial resistances are reported for vertebrate than for higher invertebrate neurons ($24 - 150\Omega cm$ in higher invertebrates, once $70\Omega cm$ and otherwise $200 - 390\Omega cm$ in vertebrates, see the first publication, Supplementary Information, Table I). For invertebrates, on the other hand, an increase in the axial resistance of the stem neurite may be advantageous for signal transmission, see the first publication. This may be achieved by a tighter packing of the stem neurite compared to dendritic and axonal trees. A large density of molecular structures in the stem neurite could furthermore explain how the thin stem neurite can transport sufficient proteins for the support of the thicker axonal and dendritic trees.

7.6. Wiring optimization in ganglionic structures

While the previous sections discuss aspects of different soma locations with respect to the individual neuron, this section draws conclusions with respect to the network arrangement of neurons. The arrangement of unipolar neurons in ganglia, with a central neuropil and a superficial soma layer, was used to explain their morphology (see Sec. 2.3.1). Yet, the advantages of a superficial arrangement of somata, such as facilitated access to the surrounding hemolymph, deteriorates when the number of neurons is so large that several layers of somata have to be stacked one over the other. Based on efficiency arguments, as used in the first publication, an upper bound on the ganglion size is derived in this section. Following the size considerations inspired by the first publication, I first review the ordering of somata of different sizes within a ganglion. Using the electrotonic length (one of the decisive parameters in the first publication), I then derive a maximal ganglion size based on arguments of volume minimization. Both observations on the ganglionic arrangement of unipolar neurons are based on an efficient use of space, which poses an additional constraint besides energy efficiency.

7.6.1. Spatial ordering in the ganglionic soma layer

Typically, unipolar neurons are arranged in a ganglionic structure, with the neurites intermingled in a central neuropil, surrounded by a dense layer consisting of externalized somata (and glia cells, see Sec. 2.3.2). The somata are arranged in sheets with the largest the furthest out, smaller ones at the inside, and some very small neurons may also be found in the neuropil, *e.g.*, in cephalopods [11].

This ordering has three conceivable advantages. The first advantage is related to optimal stacking. Arguably, the ordering facilitates the passage of stem neurites through the soma layer. The small size of the more central (inner) somata may allow for a relatively straight passage of the stem neurites of more superficial (outer) neurons, minimizing the length of the stem neurite. The second advantage is a comparable electrotonic lengths for all stem neurites, with similar functional implications. Outer somata have longer stem neurites than inner somata. Outer somata furthermore have thicker stem neurites, because their larger soma volume allows for a larger amount of somatically synthesized proteins, which demands for a thicker stem neurite with higher throughput (Sec. 7.4.2). The thicker and longer stem neurites of outer somata and the shorter and thinner stem neurites from inner somata may have a similar electrotonic length, because a constant electrotonic length requires that the spatial length of the stem neurite increases with the square root of its diameter, see Sec. 7.4.2. Furthermore, the third advantage is that the ordering puts the larger cells, which probably consume more energy, in closer contact with the surrounding nutrients.

7.6.2. Upper bound on ganglion size

The separation of neuronal somata from the neuropil, as typical for unipolar neurons, is thought to save tissue volume, see Sec. 2.3.1. When neuronal somata are located inside the neuropil, neurites have to circle around the somata (Fig. 7.4A). This, besides others, elongates the neurites, for which the negative consequences, such as an increase in signal transmission delay, have been summarized by Rivera-Alba et al. [133]. Whether a ganglion-like structure with separated soma layer, or somata embedded within the neuropil minimizes tissue volume depends on the relative size of soma and connecting neurite (the stem neurite in the case of unipolar cells). Under the assumption that tissue minimization is indeed evolutionary favorable[11], one can derive an upper bound for the size of a ganglionic structure, because, with a sufficiently large number of soma sheets, the length of the stem neurites required to reach the neuropil implies a larger volume than is saved by an separation of the somata and the neuropil, see Fig. 7.4. Hence, the advantage for volume minimization of a separated soma layer depends not only on neuronal morphology, but also on the number of neurons.

The constraint of minimal tissue volume allows for an educated guess on the maximal number of soma sheets. Tissue volume is reduced when the neuropil is void of somata, as then a dendritic or axonal neurite does not need to circumvent somata (Fig. 7.4). Yet, the exclusion of somata from the neuropil requires a stem neurite which connects the

[11] Minimization of volume (or wiring length) is in the literature common regarded as an evolutionary pressure, see Sec. 2.3.1. Yet, I am not aware of empirical evidence for this claim. While it makes sense that neuronal systems should not be larger than they need to be, to me it seems to be of only minor importance compared to other evolutionary pressures such as an increase in complexity.

soma with the dendritic and axonal trees. Each additional sheet of somata increases the distance between somata and neuropil, and hence lengthens the stem neurite by at least one soma diameter. This increases the required volume with each additional soma sheet. The exclusion of somata from the neuropil hence saves volume as long as the volume decrease due to straight dendrites is larger than the volume increase due to longer stem neurites.

The minimization of volume can be bounded in the simple model depicted in Fig. 7.4. For a soma intermingled within the neuropil, the volume is increased by the difference between the volume of the straight dendrite, and the encircling dendrite. In any neuropil, this would affect several dendrites (and axons). Yet, the largest volume saving occurs for the thickest dendrite because the change in length between straight and circling is the same for thick and thin dendrites, such that the volume saving is larger for thicker dendrites. For simplicity, all dendrites but a single, thick dendrite are hence ignored. The volume saved in this case is compared with the minimal volume of the stem neurite required to locate the soma on top of the some layer consisting of n sheets of somata. This comparison allows to predict under which condition the exclusion of somata from the neuropil saves tissue volume.

For a soma with diameter s within the neuropil that is encircled by a dendrite of diameter d, the dendrite volume required for wrapping around the soma is $V_{\text{around}} = \pi/4d^2(\pi/2s)$, while a straight passage without soma in the way amounts to $V_{\text{direct}} = \pi/4d^2s$. An exclusion of the soma from the neuropil is useful as long as the difference of both is larger than the stem neurite volume required to exclude the soma. The diameter d of the thickest part of a dendrite is often related to the stem neurite diameter, and a value of $0.5d$ is supported by data, as shown in the first publication, Supplemental Information. For an estimate of the volume decrease, the stem neurite diameter is denoted as $p * d$, where p is the ratio between stem neurite diameter and neurite diameter. An exclusion of the soma will save tissue volume only if the minimal volume required by the stem neurite is smaller than the decrease in volume due to the straight dendrite,

$$\begin{aligned} V_{\text{stem}} &< V_{\text{around}} - V_{\text{direct}} \\ \pi/4(pd)^2\,(n-1)s &< \pi/4d^2s(\pi/2-1) \\ p^2(n-1) &< \pi/2-1 \approx 0.57 \end{aligned}$$

where n is the number of stacked somata in the soma layer, see Fig. 7.4. Choosing $p = 0.5$ as in the first publication, we find $n < 3.3$ as condition for volume-minimizing soma exclusion. This simple estimate predicts that, from three layers of somata on, additional somata should rather be located inside the neuropil, instead of adding them as an additional sheet of somata on the surface of the ganglion. This estimate is conservative, because the stem neurite will be longer than estimated as it often passes also part of the neuropil, and as it may also need to encircle somata when passing underlying sheets. Note that this educated guess compares a dendrite which typically participates in signal transmission with the stem neurite which is typically only partly depolarized by the signal. Partial depolarization is probably energetically

less costly than full depolarization of a dendrite, such that exclusion of somata may be energetically favorable even when increasing tissue volume.

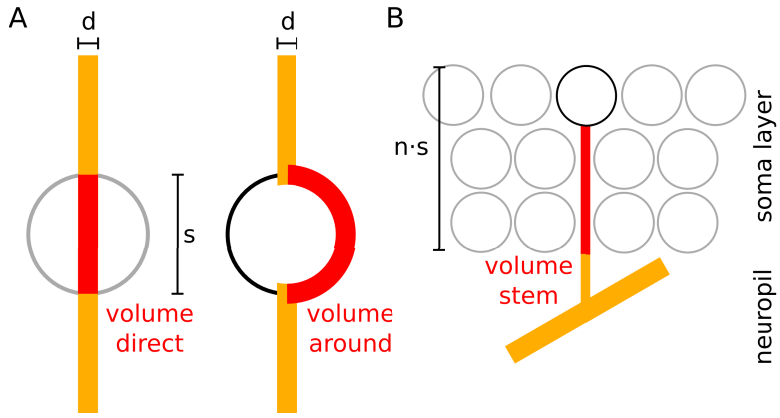

Figure 7.4.: A: Neurites have to circle around the soma if the soma is located inside the neuropil (right), which requires more volume than if the neurite can pass through the space taken up by the soma (left). B: A stem neurite connects soma and neuropil. An exclusion of the somata from the neuropil reduces the overall volume of the ganglion if the volume reduction illustrated in A is larger than the volume of the stem neurite.

The prediction of maximal three soma layers per ganglion demands for a quantitative analysis of the soma layer number for different animals. While this is left for future research, many species considered in the first publication show indeed only a small number of soma layers.

As a side note, it seems that a living example for an upper bound on the number of soma sheets is provided by the octopus. The octopus has mostly unipolar neurons. While many neurons are arranged in ganglia as known from other invertebrates, its neurons are partly arrange in layers rather than spherical ganglia [61, 115]. In the light of the hypothesis of this section, the disintegration of spherical ganglia in the octopus could result from its large number of neurons, too large for a pure ganglionic arrangement. Moreover, in the highly developed optical lobe of octopus, multipolar neurons can also be found besides the typically unipolar shape [61, 115]. Maybe this could be explained by one of the advantages of a multipolar neuron discussed in Sec. 7.2, such as a facilitation of recurrent connections. While I consider it as unlikely that intelligence is constrained by neuronal morphology or arrangement, as there is general agreement that intelligence rather arises from the connection pattern of neurons, it is nevertheless interesting that brain activity in octopuses shows oscillations in the field potential, similar to vertebrates and in contrast to most other invertebrates [16], and that the large brain of the octopus allows it to compete on a cognitive level with vertebrates of the sea [82]. In summary, the octopus is one example that shows increased neuron number and a deviation of the ganglionic arrangement. The question whether this relation is indeed causal, as suggested by the hypothesis above, is left for future research.

7.7. Recapitulation

The first project of this thesis shows that signal transmission can be optimized by a central or externalized soma[12]. In addition, further advantages of unipolar and multipolar morphologies were discussed, with an emphasis on signal processing and the spatial environment of the soma. The discussion portrays (energy-)efficient signal transmission as a mayor driving force for the divergent evolution of neurons with central or externalized soma. As detailed above, I hypothesize that the divergent evolution arises from different solutions to the problem that a large central soma poses for signal transmission: While invertebrates externalized the large soma that evolved to support complex neurons, vertebrates retained the central soma location, but externalized part of the somatic machinery into proximal dendrites.

[12] Energetic or other advantages may also have driven the development of unipolar neurons in vertebrates (*e.g.*, spinal dorsal root ganglion cells), and multipolar neurons in invertebrates (*e.g.*, octopus gravity receptor system [25]).

8. The saddle-node-loop bifurcation

The saddle-node-loop bifurcation was identified in the second publication as a fundamental transition in conductance-based neurons models. This chapter provides aspects on the generality and relevance of the saddle-node-loop bifurcation that extend beyond the second publication. The saddle-node-loop bifurcation can be reached by various bifurcation parameters. One of them is the membrane capacitance, whose biological relevance is discussed below (Sec. 8.1). Similar to what is observed at a small saddle-node-loop bifurcation, a reduction in limit cycle period and an increased asymmetry in the phase-response curve emerge in the one-dimensional model identified in Sec. 8.2 (a quadratic integrate-and-fire model with variable reset). The changes in phase-response curve at a small saddle-node-loop bifurcation have drastic consequences not only for synchronization (as shown in the second publication), but also for other aspects of neuronal processing discussed in Sec. 8.3. With these functional implications, the saddle-node-loop bifurcation may provide an energetically favorable coding regime described in Sec. 8.4. Because the discussed implications are largely based on the shape of the phase-response curve, phase-response curves are then discussed beyond the saddle-node-loop bifurcation, both for higher firing rates and at other spike onset bifurcations (Sec. 8.5.2). This chapter is based on joint work with Jan-Hendrik Schleimer (equal contribution to Secs. 8.2, 8.3, 8.5), and builds upon work from Schleimer [142].

8.1. The membrane capacitance as biological parameter

In the second publication, the membrane capacitance was used as bifurcation parameter. Yet, capacitance can only have biological relevance as bifurcation parameter, if it can be adapted in real neurons. In the literature, the membrane capacitance is often treated as a parameter that is fixed by the biophysical properties of the bilipid membrane of the cell, and hence universal between species and neuron types. Indeed, the membrane capacitance of cortical pyramidal neurons, spinal cord neurons, and hippocampal neurons in rat show very similar values around $0.9\mu\mathrm{F/cm}^2$ [46]. On the other hand, recent reports show reduced capacitance in human neurons [10, 41]. This may be due to the lipid composition of the cell membrane [41].

Changes in membrane composition are for example known to occur in invertebrates in response to changes in temperature [106]. The ratio of saturated and unsaturated fatty acids has been shown to affect spiking, in a way that can stabilize neuronal dynamics against changes in temperature [106]. One could even speculate that the ratio of different fatty acids changes the capacitance in a way that directly counteracts the change in temperature, such that an increase in temperature results in a membrane composition that decreases the membrane capacitance. This could be tested experimentally.

8.2. Quadratic integrate-and-fire neurons as model of the small saddle-node-loop bifurcation

As was shown in the second publication, conductance-based models show specific changes in limit cycle period and phase-response curve around a small saddle-node-loop bifurcation. As shown in this section, both characteristics also appear in a simple quadratic integrate-and-fire (qIF) model with variable reset. The existence of such a simple model supports the ubiquitousness of the saddle-node-loop bifurcation proposed in the second publication. The model furthermore allows to investigate the effect of saddle-node-loop bifurcations in networks with reasonable computational resources, compared to numerically involved network simulations of conductance-based neuron models.

The model consists of a single variable x with the dynamics $\dot{x} = I + x^2$ with reset to $x = x_{\text{reset}}$ for $x \to \infty$, see for example Izhikevich [79]. This *reset model* allows for an analytical expression for the phase-response curve derived in the following.

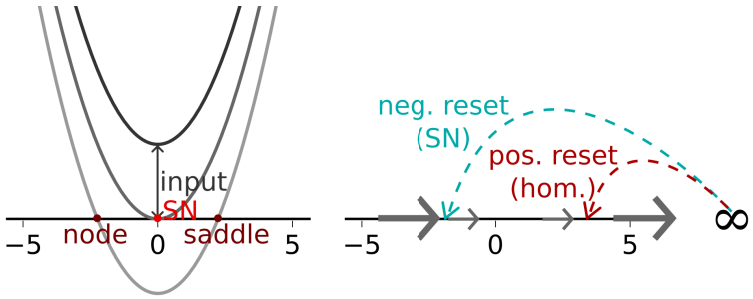

Figure 8.1.: For the quadratic integrate-and-fire model with variable reset, a shift in the reset value from negative to positive values passes by the saddle-node-loop.

For a one dimensional model, an analytical expression of the trajectory allows to directly state the phase-response curve [14, 36]. For a generalized integrate-and-fire model given by $\dot{x} = f(x)$ with x between reset and threshold value, the phase-response curve is given as $Z = 1/f(x_0)$, where $x_0(t)$ is a solution of the system [14].

The reset model shows two fixed points for negative input, $I < 0$, which are destroyed in a saddle-node bifurcation at $I = 0$. In the following, small positive inputs are considered, *i.e.*, inputs nearby threshold. For $I > 0$, the trajectory of the system is given as $x(t) = -\sqrt{I}\cot(\frac{t-T}{I})$, with $T = \frac{1}{I}\operatorname{arccot}(x_{\text{reset}}/\sqrt{I})$ (with the image of arccot $\in [0, \pi)$), where t is restricted to $t \in [0, T]$. With this, the phase-response curve of the reset model evaluates to

$$Z(\theta) = \frac{1}{2IT}(1 - \cos(2\sqrt{I}T(\theta - 1))), \tag{8.1}$$

with $\theta \in [0, 1)$.

In the limit $x_{\text{reset}} \to -\infty$, this phase-response curve recovers the symmetrical $(1 - \cos)$ shape typically observed at saddle-node on invariant cycle bifurcations [35]. With increasing reset value, the phase-response curve becomes increasingly asymmetric, until it finally resembles for positive reset values the exponential decay expected for saddle-homoclinic orbit bifurcations [14]. A reset value of $x_{\text{reset}} = 0$ can be identified

with the saddle-node-loop bifurcation. The analytical phase-response curve is then half of the phase-response curve at a saddle-node on invariant cycle bifurcation, as expected from the consideration in the second publication.

The phase-response curve allows to assess the synchronization ability of neurons coupled with δ-synapses, as introduced in Sec. 3.4.1. The entrainment range is given by the odd part of the phase-response curve. The entrainment range of the reset model can be matched with that of a conductance based neuron model[1] (the two-dimensional sodium-potassium model as stated in Izhikevich [79], and the relative time scale of voltage and gating dynamics was changed, in alternative to the capacitance, by adding a prefactor to the gating kinetics, mimicking a temperature dependence in the gating rates of ion channel conductances in the form of Eq. 3.4). When the entrainment range of both models is aligned by the (putative) saddle-node-loop bifurcation, the bifurcation parameters of both models can be scaled in a way that the entrainment range fits qualitatively around the saddle-node-loop bifurcation, see Fig. 8.2.

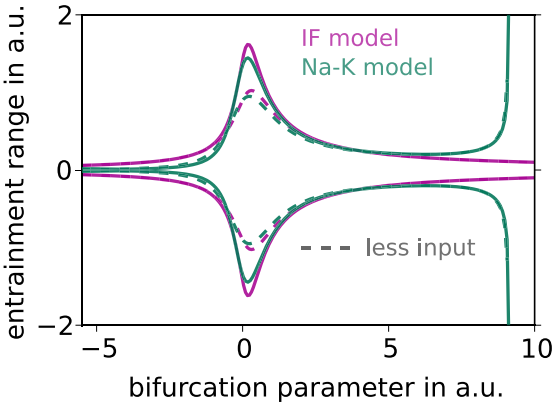

Figure 8.2.: Entrainment range assuming δ-synapse-coupling versus the bifurcation parameter for the conductance-based model (Na-K (sodium-potassium) model from Izhikevich [79]), and for the reset model (IF model).

While the reset model nicely reproduces phase-response curves around the small saddle-node-loop bifurcation, the following arguments show that one-dimensional models are probably not sufficient to capture a big saddle-node-loop bifurcation. The symmetry of the phase-response curve changes at the big (small, respectively) saddle-node-loop bifurcation by a shift to the right (left, respectively), compare the second publication. A similar shift of the phase-response curve maximum can be observed can be observed in models in which the threshold acts as a parameter in addition to the reset value, $\dot{x} = I + x^2$ with reset to $x = x_{\text{reset}}$ for $x = x_{\text{threshold}}$. The phase-response curve maximum shifts to the right for $-x_{\text{reset}} > x_{\text{threshold}}$, and to the left for $-x_{\text{reset}} < x_{\text{threshold}}$. A starting point for a simple model with a big saddle-node-loop bifurcation may be a model with a negative reset value, in which the threshold value decreases from a large positive value to the reset value, with the saddle-node-loop equivalent for a threshold value of zero. In this model, a non-degenerated saddle-node

[1]The entrainment range observed here is qualitatively similar to the entrainment range observed in higher-dimensional neuron models, see Fig. 10.1 (adapted Traub-Miles model [165]) and Fig. 5b (adapted Wang-Buzsaki model with the capacitance as bifurcation parameter).

on invariant cycle bifurcation would be observed for threshold and reset values with equal magnitude but different signs. However, the dynamics at a big saddle-node-loop bifurcation suggests that a one-dimensional model is in general insufficient: The limit cycle dynamics at a big saddle-node-loop bifurcation are slow at two different phases, because, both on the exit and on the approach to the saddle-node fixed point, the trajectory runs parallel to the semi-stable manifold[2], compare Fig. 3a in the second publication. A second slowing down in the dynamics can probably only be captured by a model with at least two dimensions.

8.3. Coding properties at the saddle-node-loop bifurcation

The saddle-node-loop bifurcation is not only interesting for synchronization, but also for spike-based coding in general. The following discussion demonstrates the impact of the small saddle-node-loop bifurcation on various measures that can be derived from the phase-response curve. Considered below is the locking to an external signal, filter properties, and the rate of information transmission. A more detailed discussion on the consequences of saddle-node-loop bifurcations for neuronal coding is provided in the preprint Hesse et al. [68].

8.3.1. Locking to external inputs

The entrainment range quantified in the second publication is related to the ability of neurons to synchronize within a population of identical, weakly coupled oscillators [96]. A population of identical neurons can also appear synchronized due to common input, even without coupling within the population (*stochastic synchronization*, see Marella and Ermentrout [104], Pikovsky et al. [124]). Starting from random conditions, an uncoupled population with white-noise input synchronizes over time. The corresponding relaxation time constant is related to the stability of the state with zero phase lag between two oscillators entrained by the same stimulus, *i.e.*, the state where both spike simultaneously. The stability of the phase fixed point corresponding to this state is given by its Lyapunov exponent, whose inverse gives the relaxation time constant. The Lyapunov exponent, λ, can be calculated based on the derivative of the phase-response curve $Z(\varphi)$ [52, 160],

$$\lambda = -\sigma^2 \int_0^1 \left(\frac{\mathrm{d}Z(\varphi)}{\mathrm{d}\varphi} \right)^2 \mathrm{d}\varphi, \tag{8.2}$$

here σ^2 is the correlation of the common input ν, $\langle \nu(0)\nu(\Delta t)\rangle = \sigma^2\delta(\Delta t)$. The steeper slopes of the phase-response curve at the saddle-node-loop bifurcations leads to larger Lyapunov exponents in their proximity (Fig. 8.3b).

[2]The orbit flip at the big saddle-node-loop bifurcation brings the limit cycle off the semi-stable manifold (along the approach of the saddle-node fixed point), but only off by a tiny bit, and it still runs in parallel for a large part of the limit cycle orbit before it approaches the saddle-node fixed point along the strongly stable manifold.

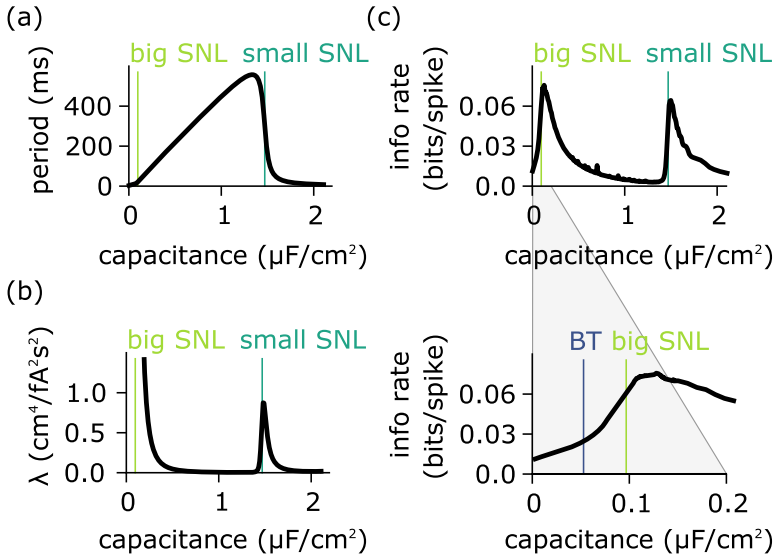

Figure 8.3.: Coding properties for the Wang-Buzsaki model with input $I_{DC} \approx 0.16\ \mu A/cm^2$ (about 2% above limit cycle onset). (a) Limit cycle period. (b) Magnitude of the Lyapunov exponent, $|\lambda|$, of the locking state to a time-varying white noise stimulus. (c) Lower bound on the mutual information rate (denoted info rate), with zoom below. Note the maxima in proximity of both SNL bifurcations. Numerical continuation of phase-response curves and limit cycles with AUTO-07P [31].

8.3.2. Information transmission

The amount and kind of information that a neuron can possibly transmit can be evaluated based on the rate of information transmission, and the linear filtering properties. Considering the neuron as an information filter, its output strength depends not only on its input strength, but also on the frequency of its input. This dependence is captured by the first-order relation between input and output, the *linear response filter* (Fig. 8.4). The linear response filter is the Laplace transform of the transfer function, which can be calculated based on the phase-response curve [143]. Evaluating the linear response function at different bifurcations, saddle-node-loop bifurcations facilitate the transmission of higher frequencies compared to the saddle-node on invariant cycle bifurcation (Fig. 8.4c).

Filter properties also determine the total amount of information that can be transmitted. In a time-continuous system, the rate at which information on the input can be gained by observing the output (or vice versa) is quantified by the *mutual information rate*. This rate can be bounded below using the phase-response curve, under the assumption of band-limited white noise as input [22, 143]. Intuitively, the lower bound on the mutual information rate results from a summation of the transmission rate over each frequency. With that, the facilitation of high frequency transmission around the saddle-node-loop bifurcation explains the increase in the lower bound observed in proximity of the saddle-node-loop bifurcation (Fig. 8.3c).

Information rate, high frequency transmission, and locking to an external signal (as measured by the Lyapunov exponent) all increase in proximity of the saddle-node-loop bifurcations (Fig. 8.3). This observation is explained both by a reduction of the limit

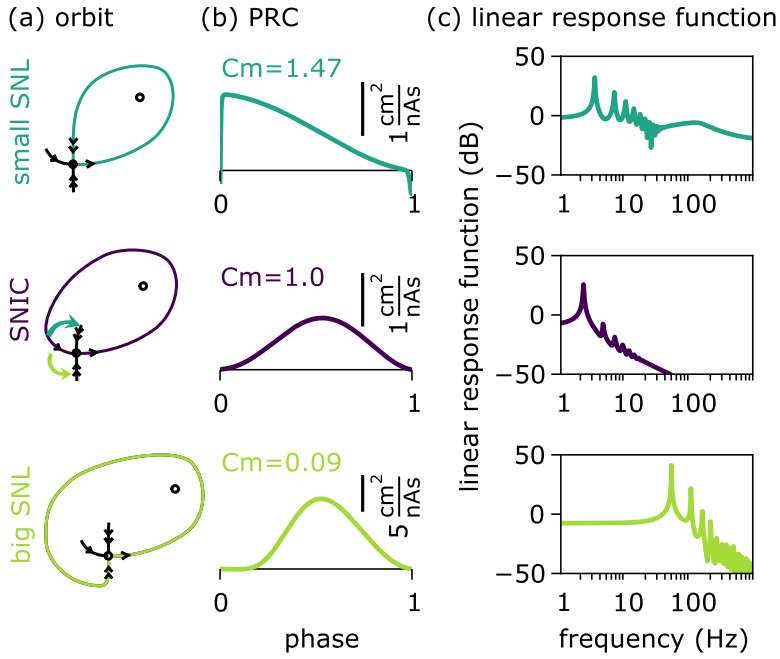

Figure 8.4.: Filter properties at small saddle-node-loop, saddle-node on invariant cycle and big saddle-node-loop bifurcation for the Wang-Buzsaki model with input $I_{DC} \approx 0.16$ µA/cm^2 (about 2% above limit cycle onset). Membrane capacitance reported in panel (b), units in μF/cm^2. (a) Sketch of the homoclinic orbit to the saddle-node fixed point. (b) Phase-response curve for a perturbation with a current input. (c) Linear response function calculated based on the phase-response curve. Filters at the saddle-node-loop bifurcations show a larger frequency range than the filter at the saddle-node on invariant cycle bifurcation.

cycle period and by the changes in phase-response curve shape. Because the limit cycle period scales the phase-response curve (the faster the spiking, the more robust is the system to perturbations, and hence the smaller is the phase-response curve), the change in period (Fig. 8.3a) contributes in particular to the peak at the small saddle-node-loop bifurcation. Furthermore, the increase in the measures is related to the changes in the phase-response curve. In the theoretical limit, the phase-response curve is symmetric and composed of a single Fourier mode (the first cosine mode) at the saddle-node on invariant cycle bifurcation. The phase-response curve gets asymmetric components at the saddle-node-loop bifurcations, and the number of nonzero Fourier modes increases considerably, each of which contributes also to the derivative of the phase-response curve relevant for stochastic synchronization. As these properties occur generically at saddle-node-loop bifurcations (see the second publication), the derived coding properties may also be of interest in other information-processing systems.

8.4. Energy-efficient information processing

The functional implications summarized in the last section suggest that information processing around the saddle-node-loop bifurcation may be interesting for neurons. As any biological implementation of a dynamical regime requires energy in a real nervous

system, this section discusses bifurcations from the perspective of energy consumption. Two aspects are worth mentioning, the extreme sensitivity to parameter variations, and the energetic costs of different spike generation mechanisms.

Compared to other bifurcations that were considered in the second publication, the saddle-node-loop bifurcation induces the stronger change in coding properties. Hence, minimal changes in parameters show the maximal effect. It would be interesting to compare the energy required for changing the synchronization either with a bifurcation parameter of the saddle-node-loop bifurcation, or with a change in the synaptic coupling strength, which can also affect the entrainment range of δ-coupled oscillators [124]. Potentially, the saddle-node-loop bifurcation allows to change coding properties at minimal expenses.

The functional implications of the saddle-node-loop bifurcation result from the associated change in spike onset bifurcation. While energy consumption has been considered for spike initiation in different models [148], it has so far not been related to the spike onset bifurcation. As illustrated below, it may be possible to relate dynamical characteristics of the limit cycle on one hand, with the associated energy consumption on the other hand. The energetic costs, in addition to the functional implications, may also constrain a neuron's dynamical state.

Already within one group of neuron models with the same spike onset bifurcation, energetic costs depend largely on the parameters of the model. For example, the number of ion channels is proportional to the sodium ion flow, and hence scales the energetic costs[3]. Particularly, the overlap of potassium and sodium currents is considered as energetically wasteful, because although ions flow, the net current is zero when potassium and sodium ions flow simultaneously.

Both features of energy consumption are, potentially generically, affected by the spike onset bifurcation (at least at spike onset where normal form theory holds). Here, a spike onset at either a saddle-node on invariant cycle or a saddle-homoclinic orbit bifurcation is considered[4]. Both bifurcations result in different dynamics around the fixed point from which the limit cycle detaches, with quadratic dynamics at a saddle-node on invariant cycle bifurcation and linear dynamics at a saddle-homoclinic orbit bifurcation. The linear dynamics are faster, and hence may allow generically for a clearer separation between the sodium and potassium flow, because the difference in ion channel time constants (considerably faster sodium gating) is only visible when the dynamics are faster than the slower potassium kinetics. Furthermore, the limit cycle resulting from a small saddle-homoclinic orbit bifurcation reaches smaller maximal voltage values than the saddle-node on invariant cycle bifurcation, at least in two-dimensional models. This results from the continuous limit cycle deformation visible around the saddle-node-loop bifurcation, compare Fig. 3.2. Smaller maximal voltages, combined with the smaller afterhyperpolarization introduced in Sec. 3.3.2, suggest that at least the small saddle-homoclinic orbit bifurcation results in limit cycles with particular little sodium flow.

[3] Sodium ion flow reduces the concentration gradient between in- and outside of the cell, which is reestablished by energy-consuming ion pumps, see Sec. 1.4.

[4] The two bifurcations between which the saddle-node-loop bifurcation switches.

8.5. Phase response beyond spike onset

Strictly speaking, the analysis of the second publication with regard to the phase-response curve shape is mainly valid in a small environment of the spike onset bifurcation under consideration. This section considers how the phase-response curve is reshaped when the mean input is further increased, and concludes that besides the spike onset bifurcation, also the excitation block may be relevant for a classification of neuronal dynamics.

8.5.1. Spiking from onset to excitation block

While the generic phase-response curves considered so far only occur at limit cycle bifurcations (Sec. 3.3.2), phase-response curves can be measured all along the limit cycle branch. In typical neuron models, spiking starts at one bifurcation, *e.g.*, a saddle-node on invariant cycle bifurcation, and spiking stops at another bifurcation, the excitation block, *e.g.* a supercritical Hopf bifurcation. When following the limit cycle from spike onset to excitation block (without further bifurcations on the limit cycle branch), it is transformed in a topological isomorphic manner, visible as a continuous deformation of its shape. Assuming that the dynamical system is sufficiently differentiable [175], this directly implies continuous (*i.e.*, topological isomorphic) transformations of the phase-response curve shape.

In the example mentioned above, the phase-response curve at spike onset will have the $(1 - \cos)$ shape typical for saddle-node on invariant cycle bifurcations. At the excitation block, the phase-response curve will have the sine shape typical for supercritical Hopf bifurcations. In between, for input values between spike onset and excitation block, numerical continuation shows that the phase-response curve shape corresponds to some interpolation between both stereotypical phase-response curves. Starting at spike onset, the phase-response curve will gain an negative component for early phases. This negative component will increase in size, until its amplitude equals the amplitude of the positive component at the excitation block, resulting in a perfect sine shape. While a continuous transformation of the phase-response curve can be expected along any well-behaving branch of stable limit cycles, it remains so far unclear whether such continuous transformations are also to be expected when the limit cycle changes stability, as happens at the fold of limit cycles bifurcation discussed below.

8.5.2. Spike onset at subcritical Hopf bifurcations

In order to compare the saddle-node-loop bifurcation with other potential spike onset mechanisms, this paragraph takes up the discussion of the subcritical Hopf bifurcation in the second publication. The phase response has been derived for various bifurcations that occur as spike onset or excitation block in neuron models [14]. So far missing is the phase response in models in which spiking is initiated by a subcritical Hopf bifurcation, for example in the original Hodgkin-Huxley model [73] or other so called type-II models. The subcritical Hopf bifurcation in these cases has to be distinguished from supercritical Hopf bifurcations, for which the phase-response curve is a well-known sine curve [14]. The supercritical Hopf bifurcation is hardly relevant as onset

for spiking, because, at the bifurcation, limit cycles have an infinitely small amplitude, in contrast to the all-or-nothing spikes typically observed in neurons.

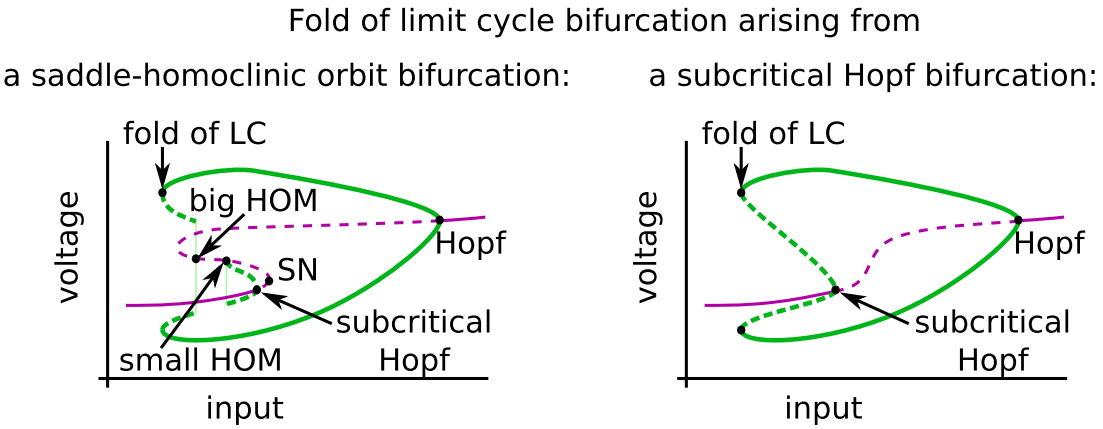

Figure 8.5.: Sketch of the relation between membrane voltage and input when the fixed point loses stability at a subcritical Hopf bifurcation. The unstable branch of the fold of limit cycles bifurcation either ends in a saddle-homoclinic orbit bifurcation (left) or directly in the Hopf bifurcation (right), as in the original Hodgkin-Huxley model [73]. Fixed point voltage in violet, limit cycle (LC) maximal and minimal voltage in green. Straight lines denote linearly stable dynamics, dashed lines linear unstable dynamics.

When the resting state is destabilized by a subcritical Hopf bifurcation, the arising limit cycle (also with infinitely small amplitude) is unstable. Neuron models that allow for repetitive spiking show a stable limit cycle, on which the dynamics falls once the resting state looses stability. This stable limit cycle is not directly related to the subcritical Hopf bifurcation, and its phase-response curve can hence not be derived from this bifurcation. Instead, the phase-response curve should be derived from the bifurcation that creates the stable limit cycle. In conductance-based neuron models, the stable limit cycle typically arises from a fold of limit cycles bifurcation (as in the original Hodgkin-Huxley model [73]) or from a saddle homoclinic orbit bifurcation, compare Fig. 8.5. In the latter case, the saddle-homoclinic orbit bifurcation must be a *big* saddle-homoclinic orbit bifurcation, whose limit cycle encircles all three fixed points (rest, saddle, and unstable node). With an increase in input, the unstable limit cycle that is required for the subcritical Hopf bifurcation arises from a small saddle homoclinic orbit bifurcation, and eventually disappears in the subcritical Hopf bifurcation. Note that in this case, the stable and unstable limit cycle have no connection at all, and the properties of the saddle homoclinic orbit bifurcation alone will decide on the phase-response curve at the creation of the limit cycle. In alternative to the sequence of big and small saddle-homoclinic orbit bifurcation, a fold of limit cycles bifurcation can directly connect the unstable limit cycle created at the subcritical Hopf bifurcation with the stable limit cycle corresponding to repetitive spiking. Note that this fold of limit cycles bifurcation does not imply radially symmetric limit cycles as assumed by Brown et al. [14], because radial symmetry would imply equal depolarization and hyperpolarization around the stable fixed point, while biological neurons show considerably larger positive excursions in the voltage dynamics. The fold of limit cycles bifurcation that occurs before the subcritical Hopf bifurcation results in a bistability of

stable limit cycle and stable fixed point[5]. The continuous limit cycle branch from the subcritical Hopf bifurcation to the fold of limit cycles bifurcation may allow the former to influence the phase-response curve at the stable branch of the latter, for example by retaining a biphasic phase-response curve for which perturbations can advance or delay the next spike.

An analytical derivation of the exact phase-response curve shape at a fold of limit cycles bifurcation remains an open challenge that is further pursued in the lab. A precise statement of this phase-response curve could ameliorate the confusion on phase-response curves related to either sub- and supercritical Hopf bifurcations as sometimes apparent in the literature. Many models with subcritical Hopf bifurcations show a negative component in the early phase of the phase-response curve, which is, in analogy to the phase-response curve at the supercritical Hopf bifurcation, often related to the subcritical Hopf bifurcation. However, this connection was, to the best of my knowledge, never properly established. As stated above, the dynamics falls on a stable limit cycle once the subcritical Hopf bifurcation occurs. This limit cycle is already at a certain distance from its creation bifurcation, because of the bistability of limit cycle and resting state just before the subcritical Hopf bifurcation. The limit cycle observed at the subcritical Hopf bifurcation is thus intermittent between limit cycle onset and limit cycle destruction. Hence, the phase-response curve measured for the stable limit cycle at the subcritical Hopf bifurcation is a combination of the canonical phase-response curves at the excitation block on one hand, and the limit cycle creation bifurcation on the other hand (*i.e.*, a fold of limit cycles or big saddle-homoclinic orbit bifurcation). If the excitation block is a supercritical Hopf bifurcation as common in neuron models, this might explain the biphasic phase-response curve observed at the subcritical Hopf bifurcation. Alternatively, the excitation block might also be sequence of a subcritical Hopf bifurcation that stabilizes the unstable node, and a fold of limit cycles bifurcation, that eliminates the stable limit cycle. A model that is particularly interesting for the phase-response curve shape is one, in which the limit cycle generation, in addition, happens at a fold of limit cycles bifurcation. In this case, the limit cycle branch starts and ends at the same bifurcation type, which might lead to less deformations of the phase-response curve than observed in common neuron models with different bifurcations. If it turns out that the excitation block bifurcation is indeed influencing neuronal dynamics in a reasonable spiking regime, as suggested in this section, neurons with a finite firing rate may be better classified by both the spike onset and spike termination bifurcation (*i.e.*, excitation block).

[5]This bistability is also found in the fundamental bifurcation structure of conductance-based neuron models by Kirst et al. [90], as long as the subcritical Hopf bifurcation is non-degenerated.

9. Temperature as a control parameter in biological systems

While direct consequences from the second publication were discussed in the last chapter, the following two chapters present the implications of a saddle-node-loop bifurcation when the bifurcation parameter is interpreted as temperature. The omnipresence of temperature variation in organisms (compare Sec. 3.6), makes this bifurcation parameter particularly versatile, and allows even for a discussion of the saddle-node-loop bifurcation in a medical context, as potential trigger mechanism for temperature-induced seizures, as described in the introduction (Sec. 3.6.1). The search for temperature-induced changes in synchronization originally motivated the study of the saddle-node-loop bifurcation, and a publication on the subject is in preparation.

This chapter presents preliminary data which suggest that hallmarks of a saddle-node-loop bifurcation can be observed with an increase in temperature. This is used in the following chapter to suggest that the saddle-node-loop bifurcation may be relevant for temperature-induced pathologies.

As summarized in the introduction (Sec. 3.5.2), temperature is a parameter that influences the nervous system, and indeed the whole organism, in many aspects. While endotherm animals spend a considerable amount of their energy on keeping the body temperature more or less constant, the body temperature of ectotherm animals adapts to the surrounding temperature. In ectotherm animals, the nervous system has to remain functional over a particular large temperature range (*e.g.*, day and night, or summer and winter). But already the small changes in temperature observed in endotherm animals can drastically alter neuronal dynamics, compare Sec. 3.6. The temperature dependence of neuronal dynamics will be considered in this chapter, with a particular emphasize on temperature as a bifurcation parameter of the saddle-node-loop bifurcation.

9.1. Regulation of temperature-dependence

Before considering changes in temperature as a bifurcation parameter, this paragraph shortly reviews that neurons have also means to counter such changes. Such a counter (temperature-compensation) is essential when neuronal function has to be ensured over a certain range of temperatures.

While neurons can show a drastic temperature dependence in their dynamics (Sec. 3.5), in some cases it is useful to minimize the effect of temperature to remain functional. This can be achieved by a well-chosen set of ion channels that counter each others temperature dependence, allowing them to remain functional even when temperature differences of 10°C occur, compare Roemschied et al. [134]. In addition, both vertebrates and invertebrates use temperature-activated ion channels (*e.g.*, TRP channels) for thermo-regulation [176]. (Partial) temperature-compensation shows that the scaling of

ion channel gating in response to temperature, as implemented in the models, is just part of the story. As discussed later (Sec. 10.4.1), temperature compensation may be seen in the experimental data.

9.2. Temperature-induced bifurcations

In direct analogy to the capacitance (Sec. 3.5.1), temperature can be used as bifurcation parameter for the saddle-node-loop bifurcation. As mentioned in the introduction (Sec. 3.5.1), the saddle-node-loop bifurcation can be reached by an adaptation of the relative time scale of the voltage and gating dynamics. In the second publication, this is done by a change in the membrane capacitance, which adapts the voltage time scale. In alternative, the relative time scale can be changed by an adaptation in the time scale of the gating kinetics. This can be achieved by a change in temperature, whose main effect is on the speed of active ion channel gating (Sec. 3.5.2). Both perspectives can be transferred into each other by a simple rescaling of the time variable (for details see Sec. 3.5.1).

The temperature as bifurcation parameter will be particularly relevant for potential medical implications of the second project. As discussed in the next chapter (Chapter 10), the increase in synchronization at the small saddle-node-loop bifurcation can serve as a mechanism for seizure induction, when the seizure is induced by an increase in temperature, as is the case for fever cramps and certain forms of epileptic seizures (Sec. 3.6.1). In analogy to the capacitance, an increase in temperature induces in models a small saddle-node-loop bifurcation marked by an increasingly asymmetric phase-response curve, and hence enhanced synchronization. The entrainment range against different temperatures (implemented as a scaling of the ion channel kinetics) is plotted in Fig. 8.2 for a two-dimensional sodium-potassium model (the bifurcation parameter on the x-axis is described in the main text), in Fig. 10.1 for the Traub-Miles model, and in Fig. 10.2 for other models.

9.3. Experimental evidence for a saddle-node-loop bifurcation in hippocampal cells

In addition to the theoretical work presented in the second publication, the project on saddle-node-loop bifurcations also has an experimental part in collaboration with the Schmitz lab at the Charité. Together with Nikolaus Maier and Jan-Hendrik Schleimer[1], phase-response curves were measured at two different temperatures. The experiments tested whether an increase in phase-response curve asymmetry as found in models can be observed in hippocampal cells when the temperature is increased. This would suggest an approach of a (small) saddle-node-loop bifurcation with temperature.

[1] J.H., J.-H.S. and N.M. devised the experiment. N.M. performed the experiments (slice preparation, patch clamping), and J.H. and J.-H.S. performed the phase-response curve recordings in successfully patched neurons. J.H. programmed and performed the data analysis. J.H., J.-H.S. and N.M., together with Susanne Schreiber and Dietmar Schmitz, discussed the results.

9.3.1. Methods

Whole-cell patch-clamp recordings were done in slices from CA1 hippocampal pyramidal cells (mice between age 22 and 30 days post-natal). Synaptic activity was blocked with the $GABA_A$ receptor antagonist SR95531 (gabazine) and glutamate receptor blockers (CNQX and d-APV)[2]. Recordings were done using a Multiclamp 700A amplifier (Axon Instruments, Union City, CA, USA), and the recorded data was analyzed using Spyke Viewer [126] extended with additional plug-ins for phase-response curve measurements. Phase-response curves were measured at low (around 32°C) and high (around 40°C) temperatures. Neurons were stimulated with a step current adapted to obtain repetitive spiking with a firing rate around 10 Hz, and an additional noise current with zero mean. The noise current represented an Ornstein-Uhlenbeck process with a time constant of 4 ms, meant to simulate typical synaptic time-scales. The membrane voltage was recorded and spikes were identified based on a voltage threshold. The variations in spiking induced by the noise current were used to estimate the phase-response curves.

In theory, it is possible to estimate phase-response curves from the deviations in the mean firing rate due to the perturbations that the injected noise causes. While the theory is based on infinitesimal perturbations in a deterministic, noise-free system, the estimation of phase-response curves in more realistic, noisy systems is extremely sensitive to the amplitude of the noise. Four methods for the reconstruction of the phase-response curve were compared, one based on spike triggered averages [39], one based on weighted spike triggered averages [118] and two based on the minimization of spike-time prediction errors, adapted from Torben-Nielsen et al. [164] and Hong et al. [76]. The appropriate amount of noise current (to perturb the spiking without deviating too much from the mean firing rate that represents the limit cycle dynamics) is difficult to adjust as it is different for every neuron (and may even change within one recording session). Thus, the estimated phase-response curves do not only depend on the temperature but also on the noise amplitude.

The experimental results were compared to simulations running on Brian2 [54, 156]. The phase-response curves were estimated in the simulations in the same way as for the experimentally measured pyramidal cells, via an adaptation of the so-called STEP method based on a minimization of spike-time prediction errors [164]. Simulations used a simplified version of a model originally fitted to CA3 hippocampal pyramidal cells, the Traub-Miles model [165], with a temperature-dependence on the gating rates (Eq. 3.4 with $\phi = Q_{10}^{\Delta T/10}$ and Q_{10} between three and four). The model shows a saddle-node on invariant cycle bifurcation at spike onset with the original parameters, and reaches a saddle-node-loop bifurcation with an increase in temperature (Fig. 9.1, Fig. 10.1).

9.3.2. Preliminary results

The estimation of phase-response curves from spike data requires around one thousand spikes. Data of sufficient quality was obtained for 18 cells. In only half of those, the

[2] The synaptic blockers turned out to be temperature dependent; in order to block synaptic activity also at higher temperatures, the blocker concentration was doubled to 2 μM gabazine, 40 μM CNQX and 60 μM d-APV.

estimated phase-response curves suggest a comparable dynamical regime at low and high temperatures (*e.g.*, comparable noise amplitudes). The measured phase-response curves of five cells demonstrate a shift of the maximum to earlier phases when the temperature is increased, increasing asymmetry as expected with an approach to the saddle-node-loop point (Fig. 9.1). The remaining cells showed similar phase-response curves at low and high temperature, suggesting that the dynamics for those cells are at both temperatures far from the saddle-node-loop point. An adaptation of the noise amplitude and the temperature in the model allows to capture the phase-response curve changes observed in the experiment (Fig. 9.1). A model close to the saddle-node-loop point shows a similar shift in phase-response curve as observed in a subset of hippocampal pyramidal cells.

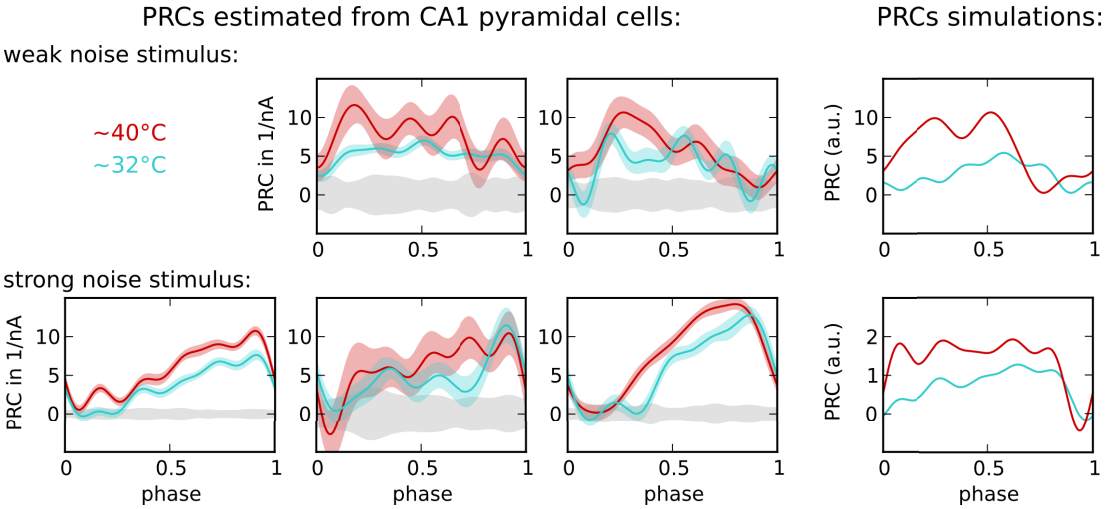

Figure 9.1.: phase-response curves as measured in simulations and experiments. phase-response curves were estimated based an adaptation of the so-called STEP method which uses spike-time prediction error minimization [164].

The cells compatible with an approach of the saddle-node-loop point could be taken as a hint that the saddle-node-loop bifurcation can be close to the dynamical state of biological neurons. In this case, the saddle-node-loop bifurcation could indeed be relevant for seizure induction under physiological conditions.

10. The saddle-node-loop bifurcation as seizure onset

The transfer of theoretical results into a medical context is a particular challenge for future research [17, 50]. While this transfer requires extreme care to prevent over-simplification and -generalization, theoretical ideas may provide useful inspirations for medical interventions. This chapter investigates the potential of the saddle-node-loop bifurcation as putative mechanism for seizure induction. In particular for febrile seizures, so far unconnected observations may be united in the framework provided by the saddle-node-loop bifurcation.

10.1. Temperature-induced seizures and saddle-node-loop bifurcations

Around the transition at the saddle-node-loop bifurcation, synchronization can be altered drastically in response to only infinitesimal changes in system parameters. Changes in synchronization are also observed at the initiation of (epileptic) seizures, which are often accompanied by a sudden increase in neuronal activity and synchronization [110]. This invites the speculation that the approach of saddle-node-loop bifurcations, and the resulting increase in synchronization ability of single neurons, could be involved in seizure initiation. The saddle-node-loop bifurcation is particular attractive as potential seizure onset, because it entails more drastic changes in the entrainment range than other spike onset bifurcations, such as the Bogdanov-Takens bifurcation (Fig. 5b in the second publication). To induce a seizure-prone regime, it would probably be sufficient for a subset of neurons to approach the saddle-node-loop bifurcation. The resulting facilitation of synchronization could act as a seed for seizure dynamics.

Because bifurcations are in general difficult to pinpoint in experimental systems, it will be demanding to test this hypothesis experimentally. The saddle-node-loop bifurcation should hence be rather taken as a potential seizure mechanism that opens up new perspectives on seizure induction. The multi-causality of seizure induction is well documented in the literature, and the saddle-node-loop bifurcation is but one of these causes, if at all. As the saddle-node-loop bifurcation is a mechanism acting on the level of the dynamics, and not on the level of the biophysical implementation, it could be the underlying mechanism of epilepsy conditions that are induced by different parameters, as long as all of them can act as bifurcation parameter for the saddle-node-loop bifurcation (see also Sec. 10.3).

The following sections suggest that the saddle-node-loop bifurcation hypothesis could indeed be applicable for one seizure condition, febrile seizures (Sec. 3.6.1). Febrile seizures occur during a period of high fever in about 5% of young children,

inducing muscle cramps and, potentially, loss of consciousness [32]. The causes for why fever triggers seizures has been identified as a key question [26]. One answer may be the saddle-node-loop bifurcation and its potential role in the induction of febrile seizures. The discussion relies on two bold assumptions: Seizures are induced when synchronization becomes more probable, and synchronization probability of the network can be inferred from single cell characteristics via the phase-response curve (this is based upon the mathematical theory of weakly coupled networks). While the results of the project are by far not sufficient to claim direct relevance in a medical context, the theoretical and experimental observations discussed in this chapter support the saddle-node-loop point as relevant for febrile seizures, and hence warrants further research in this direction.

10.2. Experimental observations

If the saddle-node-loop point is related to febrile seizures, the rise in temperature during a fever must be sufficient to approach the critical saddle-node-loop bifurcation temperature, which enhances the synchronization in the network. This presupposes that at least some neurons are already at normal body temperature close to a saddle-node-loop bifurcation. Two observations suggest that this could indeed be the case, at least for rat. Healthy rats reliably get seizures when the brain temperature is increased to 42°C [58, 92, 105], and a temperature increase above 38°C induces epileptiform activity in CA1 hippocampal slices from young rats [158]. In humans, certain patients that are particular prone to febrile seizures (and often develop epilepsy in their later life) also get seizures in response to hot water, and a lowering of the ambient temperature is recommended as treatment, as reviewed by Cross [26]. These observations show that temperature alone can induce seizures, which may be explained by neurons whose dynamics are close to an saddle-node-loop bifurcation.

Febrile seizures are thought to involve mainly the hippocampus [3], in particular CA1 and CA3 [81]. Compatibly, the experiments reported in Sec. 9.3 test neurons from hippocampus CA1 *in vitro* for the change in phase-response curve asymmetry expected at saddle-node-loop bifurcations. In a subset of neurons, the experimentally measured phase-response curves show a temperature dependence that fits phase-response curves predicted *in silico*. Whether these transitions are indeed responsible for the enhanced synchronization observed with an increase in temperature (as described above) could be tested by an experimental design that allows to balance heating and some other bifurcation parameter of the saddle-node-loop bifurcation. This way, the approach of the saddle-node-loop bifurcation by an increase in temperature could be countered by a variation in some other parameter such as pH level[1] (see Sec. 10.3). If this can prevent synchronization of the network, this could be taken as further evidence that the saddle-node-loop bifurcation underlies the transition to a synchronized network state.

[1] As counter bifurcation parameter to temperature, the pH level has the advantage that it is relatively easy changed in an experimental setting, and it is, as was tested for the experiments described in Sec. 9.3, not affected by the temperature in a slice experiment. Yet, its disadvantage is that pH affects neurons in many ways beyond the changes in ion channels that were implemented in the model, such that its effect on the neuron is not well controlled.

In general, an experimental result cannot proof a bifurcation itself, but only its hallmarks, such as an asymmetric phase-response curve in the case of a saddle-node-loop bifurcation. While the experiment described in Sec. 9.3 provides a first hint for the saddle-node-loop bifurcation hypothesis, proper evidence demands for further accumulation of experimentally observed hallmarks of a saddle-node-loop bifurcation with an increase in temperature.

10.3. Shift in seizure temperature in response to pH or genetic ion channel mutations

Febrile seizures can have many causes, including temperature, inflammatory cytokines, mutated GABA receptors, or alkalosis, as reviewed by [26, 32]. The saddle-node-loop bifurcation may provide a framework to understand these dependencies. This is shown in the following at the example of the facilitation of febrile seizures under either increased pH or genetic mutations of sodium ion channels. The effect of both physiological changes on the sodium ion channels shifts the system closer to the saddle-node-loop point, thereby lowering the critical saddle-node-loop bifurcation temperature at which seizures would be expected to occur.

For both alterations, sodium ion channel mutations or pH increase, the models analyzed in the next sections are based on experimental results. While the considered alterations affect a biological neuron in potentially complex ways, the models focus on the implementation of the qualitatively strongest effects on neuronal dynamics. That these simplest models already show a reduction in critical temperature, and hence enhanced likelihood of seizures, highlights the explicatory potential of the saddle-node-loop bifurcation as unifying seizure initiation mechanism.

10.3.1. Increased pH shifts the saddle-node-loop bifurcation with respect to temperature

Normal febrile seizures have been related to alkalosis (Higher than normal pH levels in the blood) [146, 147]. In models, as shown below, higher pH affects the sodium channels in a way that also reduces the critical temperature for seizure initiation (Fig. 10.1). This suggests that lower temperatures are sufficient to observe increased synchronization under alkalosis – temperatures low enough to be potentially reached during a fever.

Children with febrile seizures have a blood pH about 0.15 ± 0.05 higher than children with high fever but without febrile seizure [147]. On the level of ion channels, one of the main effects of pH is a shift in the sodium activation curve to lower voltages [163]. Implementation of a pH-induced sodium activation shift in an adapted Traub-Miles model lowers the critical temperature of the saddle-node-loop point (Fig. 10.1). A decrease in the critical temperature would bring such neurons closer to the saddle-node-loop point, and thus increase the probability of synchronization. The saddle-node-loop bifurcation hypothesis could hence reconcile the reported effects of temperature and pH for the induction of febrile seizures. While one or the other is sufficient to induce seizures, febrile seizures are particularly likely to occur if the combined effect of temperature and pH lowers the critical temperature to physiologically accessible fever temperatures.

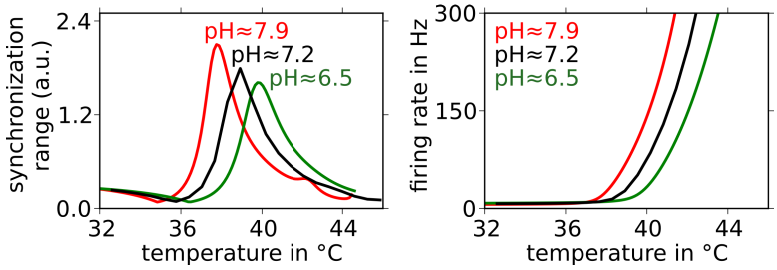

Figure 10.1.: An shift in pH changes the critical saddle-node-loop bifurcation temperature (adapted Traub-Miles model [165], with the pH change implemented as a shift in the sodium activation curve [163]). Synchronization range in arbitrary units (a.u.) refers to the entrainment range of two δ-coupled oscillators as used in the second publication.

10.3.2. Febrile seizure mutations shift the saddle-node-loop bifurcation with respect to temperature

Patients with multiple febrile seizures are prone to develop epilepsy later in life. For a small subgroup of these patients, the unusually high rate of febrile seizures has been linked to genetic mutations that affect ion channels, see Cross [26] for an overview. The implementation of the effect of some of these mutations in conductance-based neuron models suggests that different mutations reduce the critical saddle-node-loop bifurcation temperature, which potentially facilitates seizure occurrence.

This hypothesis can be tested based on conductance-based neuron models that mimic the effect of mutations. The implemented model is based a model by Barela et al. [7] (ModelDB accession number 87585 [108]) and Spampanato et al. [152]. The model without mutations (control model) contains fast and slow sodium currents as well as a delayed rectifier potassium current. This model was modified by one of three mutations (T875M, R1648H, R859C). R859C affects the fast sodium activation curve (shift to higher voltages) and the time constant of the slow gating variable (shift to lower voltages)[2], R1648H decreases the time constant of the sodium inactivation gating variable, and T875M mainly decreases the time constant of the slow sodium gating variable and shifts the activation curve of the slow gating variable to lower voltages.

In control and mutation models, the phase-response curve and the resulting entrainment range (odd part of the phase-response curve, see Sec. 3.4.1) was measured. The entrainment range of the models with mutations increases at lower temperatures, as expected from a decrease of the critical temperature at which the saddle-node-loop bifurcation occurs (Fig. 10.2). Thus, in a similar manner as an increase in pH, also these mutations render neurons particularly prone to reach the saddle-node-loop point with an increase in temperature. In line with the saddle-node-loop bifurcation hypothesis, a higher probability of febrile seizures is exactly what would be expected when neurons have a lowered critical saddle-node-loop bifurcation temperature.

A mouse model for SMEI mutations (one of the strong forms of febrile seizures) seems to be in general more susceptible to other seizure inducers besides temperature, for example certain drugs, as mentioned in Oakley et al. [116]. This fits the hypothesis

[2]The effect of the mutation R859C was implemented as a mean of the control model, and the reported mutation values, because, for the full mutation model, limit cycle dynamics were not stable enough to allow for the analysis of phase-response curves.

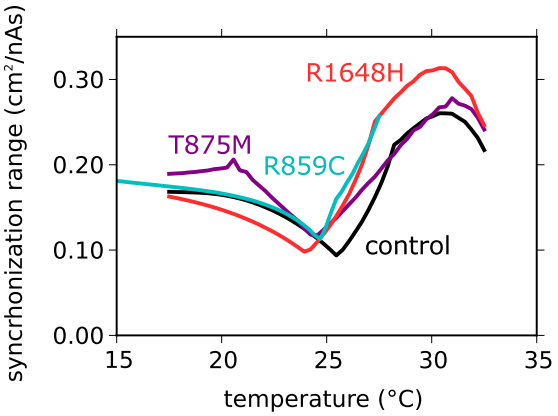

Figure 10.2.: Mutations related to enhanced febrile seizure susceptibility [152] affect ion channels in ways that decreases the critical temperature at which the saddle-node-loop bifurcation occurs.

that a susceptibility for febrile seizures arises from neurons whose dynamical state lies in the proximity of a seizure-prone state, potentially resulting from a saddle-node-loop bifurcation.

10.4. Medical applications

In summary, this chapter proposes that fever triggers seizures in response to an approach of the saddle-node-loop bifurcation, for which the temperature change during a fever, and the pH level are possible bifurcation parameters. While the previous sections have collected support for the saddle-node-loop bifurcation hypothesis from experiments and models, this section shortly discusses the implications of the hypothesis for the design and evaluation of medical interventions.

10.4.1. Seizure induction by absolute temperature or temperature increase?

With febrile seizures caused by an increase in body temperature, the seizure initiation could either depend on the absolute brain temperature, or it could depend on its rate of increase [26]. For example, in rat hippocampal slices, epileptiform activity with increasing temperature is only observed if the temperature change is quite fast, which may prevent some otherwise counteracting, temperature-induced regulations [158]. As shown in the following, the saddle-node-loop bifurcation hypothesis provides an explanation for the potential occurrence of both possibilities.

The dependence of febrile seizures on either absolute temperature or change in temperature may be based on different degrees of temperature-compensation in neurons[3].

[3]Different degrees of temperature compensation could for example be observed in the recordings used to analyze phase-response curves experimentally (Sec. 9.3). The input current required for a firing rate of 10 Hz for some neurons was the same at low and high temperatures, for others the input had to be increased at high temperatures (around 40°C). While some neurons continued to spike at 40°C qualitatively in the same way as at lower temperatures, others changed behavior, and showed intermittent spiking with spike clusters or bursting. Sometimes neuron even retained the altered

Without temperature compensation, neurons have a well-defined saddle-node-loop bifurcation temperature that is reached independent of whether the temperature is increased slowly or fast. Such neurons are likely to induce seizures in response to the absolute temperature. On the other hand, with temperature compensation, the location of the saddle-node-loop bifurcation may be shifted by the compensation, ensuring a larger distance to this critical regime. In response to a slow increase in temperature, the temperature compensation may have sufficient time to prevent an approach of the saddle-node-loop bifurcation. This may not be possible when the temperature changes faster than the compensation mechanisms can react. In this case, seizures are only induced with a fast increase in temperature (too fast to fully activate temperature-compensating mechanisms). The full development of temperature compensation could be one potential explanation why febrile seizures do not occur in older children above five years.

10.4.2. Brain heating

The observation that an increase in temperature can enhance synchronization lends itself to a new perspective on long-duration epileptic seizures (*status epilepticus*): One can suppose that the high levels of neuronal activity heat the brain tissue in the initial part of the seizure above the normal temperature [91]. This heating may result in temperature-induced synchronization, which acts as a kind of positive feedback for the seizure activity. A prime candidate for temperature-induced synchronization, strengthening seizure activity over a long period of time, are neurons that are brought closer to a saddle-node-loop bifurcation by the increase in temperature. On the other hand, the prevention of seizures by cooling of brain tissue [44] may result from an increase in the distance to the saddle-node-loop bifurcation.

The saddle-node-loop bifurcation hypothesis should also be considered when using deep-brain stimulations, for which a concurrent increase is local brain temperature was reported [34]. This has again the potential to bring neurons closer to the saddle-node-loop bifurcation, which may lead to a seizure.

10.4.3. Distance measure for anti-epileptic drugs

As discussed above, the distance to the saddle-node-loop bifurcation may be decisive for the likelihood of seizures. A pathological closeness to the saddle-node-loop bifurcation could be countered by targeted medical interventions. What is still missing is a sound, parameter-independent distance measure that could be used to compare the effect of different drugs.

The distance to the saddle-node-loop bifurcation could provide an interesting, intermediate measure for drug development. For example, a drug that reduces the leak

behavior after cooling back to lower temperatures, which suggests that the increase in temperature (or some other internal process) induced some more fundamental change in the system than a simple scaling in gating rates as assumed in models. Note, however, that is difficult to distinguish temperature effects from effects that result from the recording duration and the concurrent degradation of the cell. Yet, at least in some cases, the observations suggest that temperature-compensation in a subset of neurons allows them to remain in the same functional regime over the temperature range used in the experiments while other neurons responded more strongly to temperature changes, showing little temperature-compensation.

conductance, which is one of the bifurcation parameters of the saddle-node-loop bifurcation [90], could be a potential candidate for drug development. Speculatively, seizure induction at a saddle-node-loop bifurcation would have the advantage that drugs would not need to counter the biologically relevant parameter (such as the increase in temperature during febrile seizures), but could act on any bifurcation parameter affecting the closeness to the saddle-node-loop bifurcation (such as the pH, *e.g.*, lowing blood pH by respiratory control reduces febrile seizures [147]). Indeed, a rather unintuitive combination of drugs may turn out to be most effective in increasing the distance to the saddle-node-loop bifurcation, and hence establishing a safety margin against seizure induction.

10.5. Recapitulation

In this chapter, the potential application of the saddle-node-loop bifurcation in a medical context was discussed. In a biological system, the increase in synchronization when neurons reach a saddle-node-loop bifurcation could manifest itself as a seizure, with devastating consequences for the patient. The discussion has focused on febrile seizures, showing that the dependence of febrile seizures on pH levels and genetic mutations can be reproduced in conductance-based neuron models. Furthermore, experimental results in response to an increase in temperature were summarized with respect to seizure induction, and the saddle-node-loop bifurcation. Both fit the saddle-node-loop bifurcation hypothesis for the induction of febrile seizures, which may, in analogy, also be relevant for hot water epilepsy. Beyond temperature as bifurcation parameter, the saddle-node-loop bifurcation may also be relevant for other epilepsy types.

11. Reflections on neuronal modeling

While the previous chapters have focused on the functional and evolutionary implications of the two core publications of this thesis, this chapter discusses major assumptions underlying their analyses. For both projects, the subject was first considered in models with a certain amount of biological realism, in (multi-compartmental) conductance-based neuron models, and then it was shown that the essential features can already be observed in simpler models (passive single compartmental models and a quadratic integrate-and-fire neuron, respectively). The simpler models allow for an analytical evaluation, and support the mathematical generality of the claims in this thesis.

In many biological neurons, signal processing is considerably more sophisticated than in the simple picture used in this thesis, the passive signal transmission between dendrite and axon, and spike generation at the axon initial segment. Active conductances are for example also found in the cell body and in particular in the dendritic tree, with considerable computational power [27]. Furthermore, synaptic connections commonly target the soma besides the dendrites, and signals can also be exchanged via gap junctions, *i.e.*, electrical synapses that allow for a direct, typically bidirectional ion flow between two neurons [45]. In contrast to models of higher complexity that include these and other details, the advantage of a simplifying approach as used in this thesis is a clearer separation of cause and effect and hence a more general understanding. The phenomenon under consideration can in both studies be analyzed by mathematical simple models that allow for an analytical treatment.

This thesis mainly considers neurons that show functional polarization, *i.e.*, cells with distinguishable input and output branches, compare Sec. 7.1. In the second publication, this focus arises indirectly from the choice of a single-compartment model (*point neuron*), because it produces one output from the summation of all inputs, which implicitly assumes at least a dedicated axon. In the first publication, the focus on functional polarization (arising from the consideration of signal transmission from dendrite to axon) can be relaxed to not fully polarized cells, as long as a large part of the information is still routed through the (central) soma or the T-junction. This thesis does not consider neurons in which computations are mostly done on a local level within single branches.

In the first publication, the current threshold, and its passive counterpart, signal attenuation, was measured in order to assess energy-efficiency as previously discussed. The publication investigates passive signal propagation between dendrite and axon, with either a central or an externalized soma. In order to measure the current threshold, the models were augmented by active conductances in the axon initial segment, and the minimal step current amplitude sufficient to induce spiking was recorded. This kind of excitability measure is widely used for an experimental characterization of neurons, for example with different drugs or mutations. Yet, not for every neuron

a current threshold is well-defined [79], and the activation threshold measured with step currents (or ramps) provides little evidence on other aspects of signal processing beyond simple thresholding of input. For example, all natural neurons are faced with various sources of noise that influences their signaling [42]. To evaluate noise in the context of unipolar and multipolar neurons of the first publication, the Supplemental Information includes models with a noise source in the axon initial segment, where the spike was initiated (simulating *channel noise* from stochastic channel opening and closing). The signal-to-noise ratio measured in the axon initial segment in this specific model increases when signal attenuation decreases ([67], Supplemental Information, inset in Fig. 2c). This shows that efficient signal transmission from the dendrite to the axon is also relevant to overcome noise in the axon initial segment. In particular, it shows that enhanced signal transmission from dendrite to axon is not only explained by an increased input resistance of the axon, as the axonal input resistance would boost signal and noise equally.

The prediction of the synchronization in the second publication assumes weak inputs, as it relies on the theory of weakly coupled networks [78]. Small connection strength are for example not relevant for communication with graded potentials. Yet, in practice, the restrictions on weak input are not too restrictive [142], in particular in the dynamical regime with saddle-node on invariant cycle bifurcations as spike onset, as well as for big and small saddle-node-loop bifurcation. This can be seen from the limit cycle stability shown in the second publication, Fig. 5. The analysis focuses on δ-coupled neurons, which is easily relaxed to synaptic coupling with sufficiently fast time constants. Slower synapses and in particular synapses with temperature-dependence have to be considered in future research.

The active models in this thesis mostly implement simple, voltage-gated ion channels. This ignores many adapting processes common in neurons, such as firing rate adaptation or changes in ion concentration gradients due to overstrained ion pumps. Both modifications alter the firing rate at constant input and would hence complicate the consideration of a constant mean firing rate required for the analysis of phase-response curves in the second publication. Moreover, any kind of temperature-adaptation (apart from faster ion channel gating) goes beyond the scope of this thesis, although such adaptations were observed in the experiments (Sec. 10.4.1), and have been reported in the hippocampus due to temperature-dependent TRP channels [151]. The analysis is furthermore restricted to deterministic models without stochastic ion channel gating and other noise sources. This is a major simplification, because stochasticity is, besides non-linearity, the second source of the richness in neuronal dynamics.

12. Conclusion

In this thesis, the influence of single cell properties on neuronal processing is investigated. It is shown that neuronal morphology and biophysical parameters affect information transmission in substantial ways. The analysis can hence be seen as compatible with the old neuroscience claim that *form follows function*. This claim underlies the identification of neuronal cell classes based on morphological characteristics. The results of this thesis suggest furthermore that whether differences in parameters imply functional differences (or not) depends fundamentally on the dynamical state of the neuron, and its closeness to codimension-two bifurcations. This is particularly relevant for recent results showing that functional heterogeneity is one potential basis for synchronization codes in the electro-sensory system [173].

The influence of basic parameters such as morphology or passive properties on neuronal function has been established in various studies: The membrane time constant (product of membrane capacitance and resistance) and morphology influence the temporal aspects of voltage dynamics [12, 79], the velocity of spike propagation depends on leak and axial resistance, as well as on the amount of myeline, which is dynamically regulated [6, 80], the location of the axon initial segment influences excitability [57, 95, 109], and the addition of a dendritic tree can change the spike generation mechanism of a neuron[1] [51, 89]. This thesis considers two additional effects: The dependence of signal transmission on the soma location, and the capacitance as bifurcation parameter for saddle-node-loop bifurcations.

The results of the first project suggest that different soma locations (central versus externalized) observed in the animal kingdom may be explained by an evolutionary development that optimizes signal transmission depending on the soma-to-neurite ratio [67]. In turn, different soma-to-neurite ratios may have developed because neurons, facing the disadvantage of a large central soma, externalized either the soma, or somatic organelles (Sec. 7.4). Both adaptations are likely to lower the energetic costs of signal transmission. The study illustrates that a restriction of the analysis to morphological parameters can greatly obscure the picture. Neuronal function depends intrinsically on the interplay between morphology and biophysics. In the first publication, the relevant parameter to distinguish neurons with central or externalized soma is the soma-to-neurite ratio, which depends not only on morphology (soma and neurite diameter), but also on electrophysiological parameters (axial and membrane resistance). The consideration of both allowed for the large parameter space considered in the simulations to be collapsed on a single dimension, and to recognize a pattern in the collected data. A comprehensive assessment of neuronal function requires also in general the simultaneous consideration of morphology and electrophysiological properties (including passive parameters).

[1] The change from type-II to type-I dynamics probably results from the current sink that the dendrite provides, which acts similar to a change in leak conductance.

This thesis also illustrates that, in order to obtain an appropriate characterization of a neuron's dynamics, the measurement has to be chosen with the functional state of the neuron in mind: For a decision-making neuron, such as the escape-inducing neuron in locust, the current threshold may be appropriate, as it reflects the behavioral threshold. For a sensory neuron that selects a particular frequency band from its input, the transfer function which characterizes its filtering properties may be appropriate. And for a neuron that spikes continuously and is perturbed by small inputs (*mean-driven* regime [145]), *e.g.*, olfactory neurons [13, 77], the phase-response curve may be suited to survey neuronal function. Detailed experimental measurements of neuronal dynamics beyond classical electrophysiology may pave the way for a more fundamental understanding of various nervous systems.

The second project illustrates the relevance of a transition in spike onset mechanism at a saddle-node-loop bifurcation, and proves that, starting with spike onset at a saddle-node on invariant cycle bifurcation, this bifurcation occurs ubiquitously in two-dimensional conductance-based neurons models. The saddle-node-loop bifurcation acts as a major switch in neuronal dynamics. Changes in spike onset bifurcations are especially interesting when considering the robustness of neurons to parameter variations. Robust encoding, for example, is facilitated if neurons remain in one dynamical regime independent of particular parameter values. In this case, the system must ensure a large distance to any co-dimension two bifurcation, which would switch the spike onset bifurcation. On the other hand, the saddle-node-loop bifurcation provides a particularly interesting coding regime for sensory neurons, which may profit from faster locking to impending stimuli and enhanced reliability. Furthermore, due to the anti-synchronization observed with excitatory coupling, the saddle-node-loop bifurcation results in the emergence of a frustrated network state, which has been suggested as relevant regime for cortical neurons [53]. The detailed investigation of coding and network properties around the saddle-node-loop bifurcation is ongoing research in the *Computational Neurophysiology Group* led by S. Schreiber.

The saddle-node-loop bifurcation considered in the second part of the thesis may not only be relevant for neuronal processing in health, but may also offer potential explanations for pathologies, as exemplified in Chapter 10 for febrile seizures and other temperature-induced seizures. The causes of febrile seizures are still an open question as temperature influences basically all biological processes, from gene expression and protein synthesis over transportation rates to electrical signaling. This multitude of effects poses a serious challenge for the investigation of temperature effects. This thesis faces the challenge by strong simplifications that model brain dynamics with coupled oscillators. While this approach is clearly too simple, it provides, so I hope, a good starting point for a more thorough understanding of febrile seizures. In particular, the saddle-node-loop bifurcation hypothesis has the potential to unite three observations on febrile seizures: (i) Febrile seizures occur with an increase in brain temperature. (ii) Febrile seizures occur in particular when the blood pH level is high (assuming that this also affects the pH around the neuron). (iii) Certain ion channel mutations favor febrile seizures. All of these parameters (temperature, pH, channel mutations) can tune neuronal dynamics to a saddle-node-loop bifurcation, where synchrony is facilitated.

Much work in this thesis is comparative in nature. Contrasting morphologies present in different animal clades, or different spike onset mechanisms found in various neu-

ronal types, it sheds new light on their functional implications and ultimate reasons for their existence. The generalization of the insights gained first from numerical continuation or simulations, followed by abstract mathematical arguments, ensures that the conclusions hold beyond the chosen model parameters, lending the work, under the stated assumptions, scope and applicability also to other systems. I hope that this thesis, with its consideration of basic neuronal building blocks and their influence on neuronal signaling, takes us one step further in the exploration of the principles underlying the function of the nervous system.

Bibliography

1. B. Alberts, A. Johnson, J. Lewis, M. Raff, K. Roberts, and P. Walter. *Molecular Biology of the Cell*. Garland Science, New York, 5th edition edition, 2008.

2. R. Andrade, R. C. Foehring, and A. V. Tzingounis. The calcium-activated slow AHP: cutting through the Gordian knot. *Frontiers in Cellular Neuroscience*, 6, October 2012.

3. N. Ateş, O. Akman, and A. Karson. The effects of the immature rat model of febrile seizures on the occurrence of later generalized tonic–clonic and absence epilepsy. *Developmental Brain Research*, 154(1):137–140, January 2005.

4. D. Attwell and S. B. Laughlin. An energy budget for signaling in the grey matter of the brain. *Journal of cerebral blood flow and metabolism: official journal of the International Society of Cerebral Blood Flow and Metabolism*, 21(10):1133–1145, October 2001.

5. M. A. Baker. Brain Cooling in Endotherms in Heat and Exercise. *Annual Review of Physiology*, 44(1):85–85, 1982.

6. M. Baraban, S. Mensch, and D. A. Lyons. Adaptive myelination from fish to man. *Brain Research*, 1641(Pt A):149–161, June 2016.

7. A. J. Barela, S. P. Waddy, J. G. Lickfett, J. Hunter, A. Anido, S. L. Helmers, A. L. Goldin, and A. Escayg. An Epilepsy Mutation in the Sodium Channel SCN1a That Decreases Channel Excitability. *Journal of Neuroscience*, 26(10):2714–2723, August 2006.

8. B. F. Behabadi and B. W. Mel. Mechanisms underlying subunit independence in pyramidal neuron dendrites. *Proceedings of the National Academy of Sciences*, 111(1):498–503, January 2014.

9. S. A. Bloomfield, J. E. Hamos, and S. M. Sherman. Passive cable properties and morphological correlates of neurones in the lateral geniculate nucleus of the cat. *The Journal of Physiology*, 383(1):653–692, February 1987.

10. K. Bozek, Y. Wei, Z. Yan, X. Liu, J. Xiong, M. Sugimoto, M. Tomita, S. Pääbo, C. C. Sherwood, P. R. Hof, J. J. Ely, Y. Li, D. Steinhauser, L. Willmitzer, P. Giavalisco, and P. Khaitovich. Organization and Evolution of Brain Lipidome Revealed by Large-Scale Analysis of Human, Chimpanzee, Macaque, and Mouse Tissues. *Neuron*, 85(4):695–702, February 2015.

11. O. Breidbach and W. Kutsch. *The Nervous Systems of Invertebrates: An Evolutionary and Comparative Approach*. Experientia Supplementum (Book 72). Birkhäuser, Basel, 1995. ISBN 978-3-7643-5076-5.

12. R. Brette. Sharpness of Spike Initiation in Neurons Explained by Compartmentalization. *PLOS Comput Biol*, 9(12):e1003338, December 2013.

13. C. D. Brody and J. J. Hopfield. Simple Networks for Spike-Timing-Based Computation, with Application to Olfactory Processing. *Neuron*, 37(5):843–852, March 2003.

14. E. Brown, J. Moehlis, and P. Holmes. On the Phase Reduction and Response Dynamics of Neural Oscillator Populations. *Neural Computation*, 16(4):673–715, April 2004.

15. D. Bucher and J.-M. Goaillard. Beyond faithful conduction: Short-term dynamics, neuromodulation, and long-term regulation of spike propagation in the axon. *Progress in Neurobiology*, 94(4):307–346, September 2011.

16. T. H. Bullock and E. Başar. Comparison of ongoing compound field potentials in the brains of invertebrates and vertebrates. *Brain Research Reviews*, 13(1): 57–75, January 1988.

17. J. Bélair, L. Glass, U. a. d. Heiden, and J. Milton. Dynamical disease: Identification, temporal aspects and treatment strategies of human illness. *Chaos: An Interdisciplinary Journal of Nonlinear Science*, 5(1):1–7, March 1995.

18. Q. Cai and Z.-H. Sheng. Molecular Motors and Synaptic Assembly. *The Neuroscientist : a review journal bringing neurobiology, neurology and psychiatry*, 15(1): 78–89, February 2009.

19. R. L. Calabrese and D. Kennedy. Multiple sites of spike initiation in a single dendritic system. *Brain Research*, 82(2):316–321, December 1974.

20. C. N. Carlo and C. F. Stevens. Structural uniformity of neocortex, revisited. *Proceedings of the National Academy of Sciences*, 110(4):1488–1493, January 2013.

21. B. C. Carter and B. P. Bean. Sodium Entry during Action Potentials of Mammalian Neurons: Incomplete Inactivation and Reduced Metabolic Efficiency in Fast-Spiking Neurons. *Neuron*, 64(6):898–909, December 2009.

22. M. J. Chacron, B. Lindner, and A. Longtin. Noise Shaping by Interval Correlations Increases Information Transfer. *Physical Review Letters*, 92(8):080601, February 2004.

23. J. A. Coles. Glial cells: invertebrate. In L. R. Squire, editor, *Encyclopedia of Neuroscience*, pages 749–759. Elsevier, Amsterdam, 2009. ISBN 978-0-08-045046-9.

24. L. L. Colgin. Rhythms of the hippocampal network. *Nature Reviews Neuroscience*, 17(4):239–249, April 2016.

25. W. F. Colmers. Neuronal and synaptic organization in the gravity receptor system of the statocyst of Octopus vulgaris. *Cell and Tissue Research*, 185(4): 491–503, December 1977.

26. J. H. Cross. Fever and fever-related epilepsies. *Epilepsia*, 53:3–8, September 2012.

27. H. Cuntz, M. W. H. Remme, and B. Torben-Nielsen. *The Computing Dendrite: From Structure to Function*. Springer New York, November 2013. ISBN 978-1-4614-8093-8.

28. W. J. Davis. Functional significance of motorneuron size and soma position in swimmeret system of the lobster. *Journal of Neurophysiology*, 34(2):274–288, March 1971.

29. E. D. De Schutter. *Computational Neuroscience: Realistic Modeling for Experimentalists*. CRC Press, Boca Raton, November 2000. ISBN 978-1-4200-3929-0.

30. M. Devor. Unexplained peculiarities of the dorsal root ganglion. *Pain*, 82, Supplement 1(0):S27–S35, August 1999.

31. E. Doedel and B. Oldeman. Auto-07p: Continuation and bifurcation software for ordinary differential equations. Technical report, Concordia University, Montreal, Quebec, Canada, 2009.

32. C. M. Dubé, A. L. Brewster, C. Richichi, Q. Zha, and T. Z. Baram. Fever, febrile seizures and epilepsy. *Trends in neurosciences*, 30(10):490–496, October 2007.

33. J. Dudel, R. Menzel, and R. F. Schmidt. *Neurowissenschaft: Vom Molekül zur Kognition*. Springer, Berlin, 2001. ISBN 9783540413356.

34. M. M. Elwassif, Q. Kong, M. Vazquez, and M. Bikson. Bio-heat transfer model of deep brain stimulation-induced temperature changes. *Journal of Neural Engineering*, 3(4):306, 2006.

35. B. Ermentrout. Type I Membranes, Phase Resetting Curves, and Synchrony. *Neural Computation*, 8(5):979–1001, July 1996.

36. G. B. Ermentrout. n:m Phase-locking of weakly coupled oscillators. *Journal of Mathematical Biology*, 12(3):327–342, August 1981.

37. G. B. Ermentrout and N. Kopell. Parabolic bursting in an excitable system coupled with a slow oscillation. *SIAM Journal on Applied Mathematics*, 46(2): 233–253, 1986.

38. G. B. Ermentrout and D. H. Terman. *Mathematical Foundations of Neuroscience*. Springer Science & Business Media, Berlin, July 2010. ISBN 978-0-387-87708-2.

39. G. B. Ermentrout, R. F. Galán, and N. N. Urban. Relating Neural Dynamics to Neural Coding. *Physical Review Letters*, 99(24), December 2007.

40. C. G. Evans, B. C. Ludwar, and E. C. Cropper. Mechanoafferent Neuron With An Inexcitable Somatic Region: Consequences for the Regulation of Spike Propagation and Afferent Transmission. *Journal of Neurophysiology*, 97(4):3126–3130, April 2007.

41. G. Eyal, M. B. Verhoog, G. Testa-Silva, Y. Deitcher, J. C. Lodder, R. Benavides-Piccione, J. Morales, J. DeFelipe, C. P. d. Kock, H. D. Mansvelder, and I. Segev. Unique membrane properties and enhanced signal processing in human neocortical neurons. *eLife*, 5:e16553, October 2016.

42. A. A. Faisal, L. P. J. Selen, and D. M. Wolpert. Noise in the nervous system. *Nature Reviews Neuroscience*, 9(4):292–303, April 2008.

43. M. R. Freeman and J. Doherty. Glial cell biology in Drosophila and vertebrates. *Trends in Neurosciences*, 29(2):82–90, February 2006.

44. M. Fujii, H. Fujioka, T. Oku, N. Tanaka, H. Imoto, Y. Maruta, S. Nomura, K. Kajiwara, T. Saito, T. Yamakawa, T. Yamakawa, and M. Suzuki. Application of Focal Cerebral Cooling for the Treatment of Intractable Epilepsy. *Neurologia medico-chirurgica*, 50(9):839–844, 2010.

45. G. Galizia and P.-M. Lledo. *Neurosciences - From Molecule to Behavior: a university textbook*. Springer Science & Business Media, Berlin, July 2013. ISBN 978-3-642-10769-6.

46. L. J. Gentet, G. J. Stuart, and J. D. Clements. Direct measurement of specific membrane capacitance in neurons. *Biophysical Journal*, 79(1):314–320, July 2000.

47. W. Gerstner, A. K. Kreiter, H. Markram, and A. V. M. Herz. Neural codes: Firing rates and beyond. *Proceedings of the National Academy of Sciences*, 94(24): 12740–12741, November 1997.

48. C. N. G. Giachello, P. G. Montarolo, and M. Ghirardi. Synaptic Functions of Invertebrate Varicosities: What Molecular Mechanisms Lie Beneath. *Neural Plasticity*, 2012:1–14, 2012.

49. R. Gillette. On the Significance of Neuronal Giantism in Gastropods. *The Biological Bulletin*, 180(2):234–240, April 1991.

50. L. Glass. Dynamical disease: Challenges for nonlinear dynamics and medicine. *Chaos: An Interdisciplinary Journal of Nonlinear Science*, 25(9):097603, September 2015.

51. J. A. Goldberg, C. A. Deister, and C. J. Wilson. Response Properties and Synchronization of Rhythmically Firing Dendritic Neurons. *Journal of Neurophysiology*, 97(1):208–219, January 2007.

52. D. S. Goldobin and A. Pikovsky. Antireliability of noise-driven neurons. *Physical Review E*, 73(6):061906, June 2006.

53. L. L. Gollo and M. Breakspear. The frustrated brain: from dynamics on motifs to communities and networks. *Philosophical Transactions of the Royal Society B: Biological Sciences*, 369(1653):20130532–20130532, September 2014.

54. D. F. M. Goodman and R. Brette. The Brian simulator. *Frontiers in Neuroscience*, 3, 2009.

55. N. W. Gouwens and R. I. Wilson. Signal Propagation in Drosophila Central Neurons. *The Journal of Neuroscience*, 29(19):6239–6249, May 2009.

56. C. M. Gray and W. Singer. Stimulus-specific neuronal oscillations in orientation columns of cat visual cortex. *Proceedings of the National Academy of Sciences of the United States of America*, 86(5):1698–1702, March 1989.

57. M. S. Grubb and J. Burrone. Activity-dependent relocation of the axon initial segment fine-tunes neuronal excitability. *Nature*, 465(7301):1070–1074, June 2010.

58. G. Gulec and B. Noyan. Do recurrent febrile convulsions decrease the threshold for pilocarpine-induced seizures?: Effects of nitric oxide1. *Developmental Brain Research*, 126(2):223–228, February 2001.

59. G. F. Gwilliam and M. Burrows. Electrical Characteristics of the Membrane Of An Identified Insect Motor Neurone. *The Journal of Experimental Biology*, 86(1): 49–61, June 1980.

60. D. Hansel, G. Mato, and C. Meunier. Synchrony in excitatory neural networks. *Neural Computation*, 7(2):307–337, March 1995.

61. B. Hanström. *Vergleichende Anatomie des Nervensystems der wirbellosen Tiere unter Berücksichtigung seiner Funktion*. Springer, Berlin, 1928.

62. J. J. Harris, R. Jolivet, and D. Attwell. Synaptic Energy Use and Supply. *Neuron*, 75(5):762–777, September 2012.

63. D. K. Hartline and D. R. Colman. Rapid Conduction and the Evolution of Giant Axons and Myelinated Fibers. *Current Biology*, 17(1):R29–R35, January 2007.

64. A. Hasenstaub, S. Otte, E. Callaway, and T. J. Sejnowski. Metabolic cost as a unifying principle governing neuronal biophysics. *Proceedings of the National Academy of Sciences of the United States of America*, 107(27):12329–12334, July 2010.

65. W. J. Heitler and C. S. Goodman. Multiple Sites of Spike Initiation in a Bifurcating Locust Neurone. *The Journal of Experimental Biology*, 76(1):63–84, October 1978.

66. E. Henneman, G. Somjen, and D. O. Carpenter. Functional Significance of Cell Size in Spinal Motoneurons. *Journal of Neurophysiology*, 28(3):560–580, May 1965.

67. J. Hesse and S. Schreiber. Externalization of neuronal somata as an evolutionary strategy for energy economization. *Current Biology*, 25(8):R324–R325, April 2015.

68. J. Hesse, J.-H. Schleimer, and S. Schreiber. Qualitative changes in spike-based neural coding and synchronization at the saddle-node loop bifurcation. *arXiv:1606.07398 [q-bio]*, June 2016.

69. J. Hesse, J.-H. Schleimer, and S. Schreiber. Qualitative changes in phase-response curve and synchronization at the saddle-node loop bifurcation. *Physical Review E*, 95(5):052203, May 2017. Reprinted from Physical Review E 95(5), Hesse, Schleimer and Schreiber, Qualitative changes in phase-response curve and synchronization at the saddle-node loop bifurcation, pages 052203-25, Copyright 2017, with permission from Elsevier.

70. B. Hille. *Ion channels of excitable membranes*. Sinauer, Sunderland, Mass, 3. ed edition, 2001. ISBN 978-0-87893-321-1.

71. N. Hirokawa and R. Takemura. Molecular motors and mechanisms of directional transport in neurons. *Nature Reviews Neuroscience*, 6(3):201–214, March 2005.

72. B. Hochner and M. E. Spira. Preservation of motoneuron electrotonic characteristics during postembryonic growth. *The Journal of Neuroscience*, 7(1):261–270, January 1987.

73. A. L. Hodgkin and A. F. Huxley. A quantitative description of membrane current and its application to conduction and excitation in nerve. *The Journal of Physiology*, 117(4):500–544, August 1952.

74. A. L. Hodgkin. The local electric changes associated with repetitive action in a non-medullated axon. *The Journal of Physiology*, 107(2):165–181, March 1948.

75. A. J. Homburg and B. Sandstede. *Homoclinic and heteroclinic bifurcations in vector fields*. Elsevier, 2010.

76. S. Hong, Q. Robberechts, and E. D. Schutter. Efficient estimation of phase-response curves via compressive sensing. *Journal of Neurophysiology*, 108(7): 2069–2081, October 2012.

77. J. J. Hopfield. Pattern recognition computation using action potential timing for stimulus representation. *Nature*, 376(6535):33–36, July 1995.

78. F. C. Hoppensteadt and E. M. Izhikevich. *Weakly Connected Neural Networks*. Springer Science & Business Media, Berlin, July 1997. ISBN 978-0-387-94948-2.

79. E. M. Izhikevich. *Dynamical Systems in Neuroscience*. MIT Press, 2007. ISBN 978-0-262-09043-8.

80. J. J. B. Jack, D. Noble, and R. W. Tsien. *Electric current flow in excitable cells*. Clarendon Press, Oxford, 1975. ISBN 978-0-19-857365-4.

81. W. Jiang, T. M. Duong, and N. C. de Lanerolle. The neuropathology of hyperthermic seizures in the rat. *Epilepsia*, 40(1):5–19, January 1999.

82. C. Jozet-Alves, J. Modéran, and L. Dickel. Sex Differences in Spatial Cognition in an Invertebrate: The Cuttlefish. *Proceedings of the Royal Society B: Biological Sciences*, 275(1646):2049–2054, September 2008.

83. M. Kadekaro, A. M. Crane, and L. Sokoloff. Differential Effects of Electrical Stimulation of Sciatic Nerve on Metabolic Activity in Spinal Cord and Dorsal Root Ganglion in the Rat. *Proceedings of the National Academy of Sciences*, 82(17): 6010–6013, September 1985.

84. C. Kettner, P. Reimann, P. Hänggi, and F. Müller. Drift ratchet. *Physical Review E*, 61(1):312–323, January 2000.

85. Y.-T. Kim and C.-F. Wu. Distinctions in growth cone morphology and motility between monopolar and multipolar neurons in Drosophila CNS cultures. *Journal of Neurobiology*, 22(3):263–275, April 1991.

86. D. G. King. Organization of crustacean neuropil. II. Distribution of synaptic contacts on identified motor neurons in lobster stomatogastric ganglion. *Journal of Neurocytology*, 5(2):239–266, April 1976.

87. D. G. King. Organization of crustacean neuropil. I. Patterns of synaptic connections in lobster stomatogastric ganglion. *Journal of Neurocytology*, 5(2):207–237, April 1976.

88. B. Kirchhof and G. Bicker. Growth properties of larval and adult locust neurons in primary cell culture. *The Journal of Comparative Neurology*, 323(3):411–422, 1992.

89. C. Kirst, A. Herz, and M. Stemmler. From Integrator to Resonator: The Effect of Dendritic Geometry on Neuronal Excitability. event abstract, 4th Bernstein Symposium for Computational Neuroscience, 2008.

90. C. Kirst, J. Ammer, F. Felmy, A. Herz, and M. Stemmler. Fundamental Structure and Modulation of Neuronal Excitability: Synaptic Control of Coding, Resonance, and Network Synchronization. *bioRxiv*, page 022475, July 2015.

91. E. A. Kiyatkin, K. T. Wakabayashi, and M. Lenoir. Physiological Fluctuations in Brain Temperature as a Factor Affecting Electrochemical Evaluations of Extracellular Glutamate and Glucose in Behavioral Experiments. *ACS Chemical Neuroscience*, 4(5):652–665, May 2013.

92. B. J. Klauenberg and S. B. Sparber. A kindling-like effect induced by repeated exposure to heated water in rats. *Epilepsia*, 25(3):292–301, June 1984.

93. C. Koch and I. Segev. The role of single neurons in information processing. *Nature Neuroscience*, 3:1171–1177, November 2000.

94. S. Kreissl and G. Bicker. Dissociated neurons of the pupal honeybee brain in cell culture. *Journal of Neurocytology*, 21(8):545–556, August 1992.

95. H. Kuba, Y. Oichi, and H. Ohmori. Presynaptic activity regulates Na+ channel distribution at the axon initial segment. *Nature*, 465(7301):1075–1078, June 2010.

96. Y. Kuramoto. *Chemical Oscillations, Waves, and Turbulence*. Springer Science & Business Media, Berlin, December 1984. ISBN 978-3-642-69689-3.

97. Y. A. Kuznetsov. *Elements of Applied Bifurcation Theory*. Springer Science & Business Media, Berlin, March 2013. ISBN 978-1-4757-2421-9.

98. S. B. Laughlin and T. J. Sejnowski. Communication in Neuronal Networks. *Science*, 301(5641):1870–1874, September 2003.

99. T. Le, D. R. Verley, J.-M. Goaillard, D. I. Messinger, A. E. Christie, and J. T. Birmingham. Bistable behavior originating in the axon of a crustacean motor neuron. *Journal of Neurophysiology*, 95(3):1356–1368, March 2006.

100. E. M. Leise. Modular construction of nervous systems: a basic principle of design for invertebrates and vertebrates. *Brain Research. Brain Research Reviews*, 15(1):1–23, April 1990.

101. F. Libersat. Maturation of dendritic architecture: Lessons from insect identified neurons. *Journal of Neurobiology*, 64(1):11–23, July 2005.

102. C. Luscher, J. Streit, P. Lipp, and H. R. Luscher. Action potential propagation through embryonic dorsal root ganglion cells in culture. II. Decrease of conduction reliability during repetitive stimulation. *Journal of Neurophysiology*, 72(2): 634–643, August 1994.

103. Z. F. Mainen, J. Joerges, J. R. Huguenard, and T. J. Sejnowski. A model of spike initiation in neocortical pyramidal neurons. *Neuron*, 15(6):1427–1439, December 1995.

104. S. Marella and G. B. Ermentrout. Class-II neurons display a higher degree of stochastic synchronization than class-I neurons. *Physical Review E*, 77(4):041918, April 2008.

105. T. Mashimo, I. Ohmori, M. Ouchida, Y. Ohno, T. Tsurumi, T. Miki, M. Wakamori, S. Ishihara, T. Yoshida, A. Takizawa, M. Kato, M. Hirabayashi, M. Sasa, Y. Mori, and T. Serikawa. A Missense Mutation of the Gene Encoding Voltage-Dependent Sodium Channel (Nav1.1) Confers Susceptibility to Febrile Seizures in Rats. *Journal of Neuroscience*, 30(16):5744–5753, April 2010.

106. T. Matheson. Invertebrate Nervous Systems. In *eLS*. John Wiley & Sons, Ltd, 2001. ISBN 978-0-470-01590-2.

107. S. Matsuda, N. Kobayashi, T. Terashita, T. Shimokawa, K. Shigemoto, K. Mominoki, H. Wakisaka, S. Saito, K. Miyawaki, K. Saito, F. Kushihata, J. Chen, S.-Y. Gao, C.-Y. Li, M. Wang, and T. Fujiwara. Phylogenetic investigation of Dogiel's pericellular nests and Cajal's initial glomeruli in the dorsal root ganglion. *The Journal of Comparative Neurology*, 491(3):234–245, October 2005.

108. R. A. McDougal, T. M. Morse, T. Carnevale, L. Marenco, R. Wang, M. Migliore, P. L. Miller, G. M. Shepherd, and M. L. Hines. Twenty years of ModelDB and beyond: building essential modeling tools for the future of neuroscience. *Journal of Computational Neuroscience*, 42(1):1–10, February 2017.

109. R. Melinek and K. J. Muller. Action potential initiation site depends on neuronal excitation. *The Journal of Neuroscience*, 16(8):2585–2591, April 1996.

110. J. Milton and P. Jung. *Epilepsy as a Dynamic Disease*. Springer Science & Business Media, Berlin, 2003. ISBN 978-3-662-05048-4.

111. J. W. Mink, R. J. Blumenschine, and D. B. Adams. Ratio of central nervous system to body metabolism in vertebrates: its constancy and functional basis. *The American Journal of Physiology*, 241(3):R203–212, September 1981.

112. E. Moser, I. Mathiesen, and P. Andersen. Association between brain temperature and dentate field potentials in exploring and swimming rats. *Science*, 259(5099): 1324–1326, February 1993.

113. C. D. Moyes and P. M. Schulte. *Tierphysiologie*. Pearson Studium, München, 2008. ISBN 978-3-8273-7270-3. Principles of animal physiology, dt.

114. J. E. Niven and S. B. Laughlin. Energy limitation as a selective pressure on the evolution of sensory systems. *Journal of Experimental Biology*, 211(11):1792–1804, June 2008.

115. M. Nixon and J. Z. Young. *The brains and lives of cephalopods*. Oxford biology. Oxford Univ. Press, Oxford, 2003. ISBN 0-19-852761-6.

116. J. C. Oakley, F. Kalume, F. H. Yu, T. Scheuer, and W. A. Catterall. Temperature- and age-dependent seizures in a mouse model of severe myoclonic epilepsy in infancy. *Proceedings of the National Academy of Sciences*, 106(10):3994–3999, March 2009.

117. H. Ogawa, Y. Baba, and K. Oka. Direction of action potential propagation influences calcium increases in distal dendrites of the cricket giant interneurons. *Journal of Neurobiology*, 53(1):44–56, October 2002.

118. K. Ota, M. Nomura, and T. Aoyagi. Weighted Spike-Triggered Average of a Fluctuating Stimulus Yielding the Phase Response Curve. *Physical Review Letters*, 103(2):024101, July 2009.

119. E. Pannese. *Neurocytology: fine structure of neurons, nerve processes, and neuroglial cells*. Thieme, Stuttgart [u.a.], 1994. ISBN 3-13-781801-X.

120. M. K. Park, Y. M. Choi, Y. K. Kang, and O. H. Petersen. The Endoplasmic Reticulum as an Integrator of Multiple Dendritic Events. *The Neuroscientist*, 14 (1):68–77, February 2008.

121. E. Pena, M. T. Berciano, R. Fernandez, J. L. Ojeda, and M. Lafarga. Neuronal body size correlates with the number of nucleoli and Cajal bodies, and with the organization of the splicing machinery in rat trigeminal ganglion neurons. *The Journal of Comparative Neurology*, 430(2):250–263, 2001.

122. J. A. Perge, J. E. Niven, E. Mugnaini, V. Balasubramanian, and P. Sterling. Why Do Axons Differ in Caliber? *The Journal of Neuroscience*, 32(2):626–638, January 2012.

123. A. Peters and L. M. Kimerer. Bipolar neurons in rat visual cortex: A combined Golgi-electron microscope study. *Journal of Neurocytology*, 10(6):921–946, December 1981.

124. A. Pikovsky, M. Rosenblum, and J. Kurths. *Synchronization: A Universal Concept in Nonlinear Sciences*. Cambridge University Press, April 2003. ISBN 978-0-521-53352-2.

125. A. Pouget, P. Dayan, and R. Zemel. Information processing with population codes. *Nature Reviews Neuroscience*, 1(2):125–132, November 2000.

126. R. Pröpper and K. Obermayer. Spyke Viewer: a flexible and extensible platform for electrophysiological data analysis. *Frontiers in Neuroinformatics*, 7, 2013.

127. D. Purves, G. J. Augustine, W. C. Hall, A.-S. LaMantia, and L. E. White. *Neuroscience*. Sinauer, Sunderland, Mass., 5th ed. 2012 edition, 2012. ISBN 978-0-87893-967-1.

128. S. Ramón y Cajal, P. Pasik, and T. Pasik. *Texture of the Nervous System of Man and the Vertebrates*. Springer, 1999. ISBN 978-3-211-83057-4.

129. R. Reig, M. Mattia, A. Compte, C. Belmonte, and M. V. Sanchez-Vives. Temperature Modulation of Slow and Fast Cortical Rhythms. *Journal of Neurophysiology*, 103(3):1253–1261, March 2010.

130. M. J. E. Richardson, N. Brunel, and V. Hakim. From Subthreshold to Firing-Rate Resonance. *Journal of Neurophysiology*, 89(5):2538–2554, May 2003.

131. J. Rinzel and G. B. Ermentrout. *Analysis of neural excitability and oscillations*, pages 135–169. MIT Press, Cambridge, MA, USA, 1989. ISBN 978-0-262-11133-1.

132. M. Rivera-Alba, S. N. Vitaladevuni, Y. Mischenko, Z. Lu, S.-y. Takemura, L. Scheffer, I. A. Meinertzhagen, D. B. Chklovskii, and G. G. de Polavieja. Wiring economy and volume exclusion determine neuronal placement in the Drosophila brain. *Current Biology*, 21(23):2000–2005, December 2011.

133. M. Rivera-Alba, H. Peng, G. G. d. Polavieja, and D. B. Chklovskii. Wiring economy can account for cell body placement across species and brain areas. *Current Biology*, 24(3):R109–R110, February 2014.

134. F. A. Roemschied, M. J. Eberhard, J.-H. Schleimer, B. Ronacher, and S. Schreiber. Cell-intrinsic mechanisms of temperature compensation in a grasshopper sensory receptor neuron. *eLife*, 3:e02078, May 2014.

135. M. M. Rolls. Neuronal polarity in Drosophila: Sorting out axons and dendrites. *Developmental Neurobiology*, 71(6):419–429, June 2011.

136. M. M. Rolls, D. H. Hall, M. Victor, E. H. K. Stelzer, and T. A. Rapoport. Targeting of Rough Endoplasmic Reticulum Membrane Proteins and Ribosomes in Invertebrate Neurons. *Molecular Biology of the Cell*, 13(5):1778–1791, May 2002.

137. M. M. Rolls, D. Satoh, P. J. Clyne, A. L. Henner, T. Uemura, and C. Q. Doe. Polarity and intracellular compartmentalization of Drosophila neurons. *Neural Development*, 2:7, 2007.

138. D. H. Sanes, T. A. Reh, and W. A. Harris. *Development of the Nervous System*. Elsevier Academic Press, London, 2006. ISBN 978-0-12-618621-5.

139. H. B. Sarnat and M. G. Netsky. The brain of the planarian as the ancestor of the human brain. *The Canadian journal of neurological sciences. Le journal canadien des sciences neurologiques*, 12(4):296–302, November 1985.

140. H. B. Sarnat and M. G. Netsky. When does a ganglion become a brain? Evolutionary origin of the central nervous system. *Seminars in Pediatric Neurology*, 9 (4):240–253, December 2002.

141. S. Schecter. The Saddle-Node Separatrix-Loop Bifurcation. *SIAM Journal on Mathematical Analysis*, 18(4):1142–1156, July 1987.

142. J. H. Schleimer. *Spike statistics and coding properties of phase models*. PhD thesis, Humboldt-Universität zu Berlin, Mathematisch-Naturwissenschaftliche Fakultät I, July 2013.

143. J.-H. Schleimer and M. Stemmler. Coding of Information in Limit Cycle Oscillators. *Physical Review Letters*, 103(24):248105, December 2009.

144. S. Schreiber, I. Erchova, U. Heinemann, and A. V. M. Herz. Subthreshold Resonance Explains the Frequency-Dependent Integration of Periodic as well as Random Stimuli in the Entorhinal Cortex. *Journal of Neurophysiology*, 92(1): 408–415, July 2004.

145. S. Schreiber, I. Samengo, and A. V. M. Herz. Two Distinct Mechanisms Shape the Reliability of Neural Responses. *Journal of Neurophysiology*, 101(5):2239–2251, May 2009.

146. S. Schuchmann, D. Schmitz, C. Rivera, S. Vanhatalo, B. Salmen, K. Mackie, S. T. Sipilä, J. Voipio, and K. Kaila. Experimental febrile seizures are precipitated by a hyperthermia-induced respiratory alkalosis. *Nature Medicine*, 12(7):817–823, July 2006.

147. S. Schuchmann, S. Hauck, S. Henning, A. Grüters-Kieslich, S. Vanhatalo, D. Schmitz, and K. Kaila. Respiratory alkalosis in children with febrile seizures. *Epilepsia*, 52(11):1949–1955, November 2011.

148. B. Sengupta, M. Stemmler, S. B. Laughlin, and J. E. Niven. Action Potential Energy Efficiency Varies Among Neuron Types in Vertebrates and Invertebrates. *PLoS Comput Biol*, 6(7):e1000840, July 2010.

149. B. Sengupta, A. A. Faisal, S. B. Laughlin, and J. E. Niven. The effect of cell size and channel density on neuronal information encoding and energy efficiency. *Journal of Cerebral Blood Flow & Metabolism*, 33(9):1465–1473, September 2013.

150. B. Sengupta, M. B. Stemmler, and K. J. Friston. Information and Efficiency in the Nervous System—A Synthesis. *PLoS Comput Biol*, 9(7):e1003157, July 2013.

151. K. Shibasaki, M. Suzuki, A. Mizuno, and M. Tominaga. Effects of Body Temperature on Neural Activity in the Hippocampus: Regulation of Resting Membrane Potentials by Transient Receptor Potential Vanilloid 4. *The Journal of Neuroscience*, 27(7):1566–1575, February 2007.

152. J. Spampanato, I. Aradi, I. Soltesz, and A. L. Goldin. Increased Neuronal Firing in Computer Simulations of Sodium Channel Mutations That Cause Generalized Epilepsy With Febrile Seizures Plus. *Journal of Neurophysiology*, 91 (5):2040–2050, May 2004.

153. G. E. Spencer, N. I. Syed, E. van Kesteren, K. Lukowiak, W. P. M. Geraerts, and J. van Minnen. Synthesis and functional integration of a neurotransmitter receptor in isolated invertebrate axons. *Journal of Neurobiology*, 44(1):72–81, 2000.

154. L. Squire, F. E. Bloom, N. C. Spitzer, L. R. Squire, D. Berg, S. d. Lac, and A. Ghosh. *Fundamental Neuroscience*. Academic Press, London, April 2008. ISBN 978-0-08-056102-8.

155. D. C. Sterratt. Q10: the Effect of Temperature on Ion Channel Kinetics. In D. Jaeger and R. Jung, editors, *Encyclopedia of Computational Neuroscience*, pages 2551–2552. Springer New York, 2015. ISBN 978-1-4614-6674-1 978-1-4614-6675-8.

156. M. Stimberg, D. F. M. Goodman, V. Benichoux, and R. Brette. Equation-oriented specification of neural models for simulations. *Frontiers in Neuroinformatics*, 8, 2014.

157. N. Sánchez-Soriano, W. Bottenberg, A. Fiala, U. Haessler, A. Kerassoviti, E. Knust, R. Löhr, and A. Prokop. Are dendrites in Drosophila homologous to vertebrate dendrites? *Developmental Biology*, 288(1):126–138, December 2005.

158. V. Tancredi, G. D'Arcangelo, C. Zona, A. Siniscalchi, and M. Avoli. Induction of epileptiform activity by temperature elevation in hippocampal slices from young rats: an in vitro model for febrile seizures? *Epilepsia*, 33(2):228–234, April 1992.

159. L. Tauc and G. M. Hughes. Modes of Initiation and Propagation of Spikes in the Branching Axons of Molluscan Central Neurons. *The Journal of General Physiology*, 46(3):533–549, January 1963.

160. J.-n. Teramae and D. Tanaka. Robustness of the Noise-Induced Phase Synchronization in a General Class of Limit Cycle Oscillators. *Physical Review Letters*, 93 (20):204103, November 2004.

161. C. Thome, T. Kelly, A. Yanez, C. Schultz, M. Engelhardt, S. B. Cambridge, M. Both, A. Draguhn, H. Beck, and A. V. Egorov. Axon-Carrying Dendrites Convey Privileged Synaptic Input in Hippocampal Neurons. *Neuron*, 83(6):1418–1430, September 2014.

162. S. M. Thompson, L. M. Masukawa, and D. A. Prince. Temperature dependence of intrinsic membrane properties and synaptic potentials in hippocampal CA1 neurons in vitro. *The Journal of Neuroscience: The Official Journal of the Society for Neuroscience*, 5(3):817–824, March 1985.

163. G. C. Tombaugh and G. G. Somjen. Effects of extracellular pH on voltage-gated Na+, K+ and Ca2+ currents in isolated rat CA1 neurons. *The Journal of Physiology*, 493(3):719–732, June 1996.

164. B. Torben-Nielsen, M. Uusisaari, and K. M. Stiefel. A novel method for determining the phase-response curves of neurons based on minimizing spike-time prediction error. *arXiv:1001.0446 [q-bio]*, January 2010.

165. R. D. Traub, R. K. Wong, R. Miles, and H. Michelson. A model of a CA3 hippocampal pyramidal neuron incorporating voltage-clamp data on intrinsic conductances. *Journal of Neurophysiology*, 66(2):635–650, August 1991.

166. O. Trujillo-Cenóz. Some aspects of the structural organization of the arthropod ganglia. *Zeitschrift für Zellforschung und Mikroskopische Anatomie*, 56(5):649–682, 1962.

167. S. Trunova, B. Baek, and E. Giniger. Cdk5 regulates the size of an AIS-like compartment in Mushroom Body neurons of the Drosophila central brain. *The Journal of neuroscience : the official journal of the Society for Neuroscience*, 31(29): 10451–10462, July 2011.

168. P. J. Uhlhaas and W. Singer. Neural Synchrony in Brain Disorders: Relevance for Cognitive Dysfunctions and Pathophysiology. *Neuron*, 52(1):155–168, October 2006.

169. B. Ulfhake and S. Cullheim. Postnatal development of cat hind limb motoneurons. III: Changes in size of motoneurons supplying the triceps surae muscle. *The Journal of Comparative Neurology*, 278(1):103–120, 1988.

170. G. R. Ullal, P. Satishchandra, and S. K. Shankar. Effect of antiepileptic drugs and calcium channel blocker on hyperthermic seizures in rats: animal model for hot water epilepsy. *Indian Journal of Physiology and Pharmacology*, 40(4):303–308, October 1996.

171. H. Vanegas, M. Laufer, and J. Amat. The optic tectum of a perciform teleost I. General configuration and cytoarchitecture. *The Journal of Comparative Neurology*, 154(1):43–60, March 1974.

172. A. Verkhratsky. Physiology and Pathophysiology of the Calcium Store in the Endoplasmic Reticulum of Neurons. *Physiological Reviews*, 85(1):201–279, January 2005.

173. H. Walz, J. Grewe, and J. Benda. Static frequency tuning accounts for changes in neural synchrony evoked by transient communication signals. *Journal of Neurophysiology*, 112(4):752–765, August 2014.

174. H. Wang, B. Wang, K. P. Normoyle, K. Jackson, K. Spitler, M. F. Sharrock, C. M. Miller, C. Best, D. Llano, and R. Du. Brain temperature and its fundamental properties: a review for clinical neuroscientists. *Frontiers in Neuroscience*, 8, October 2014.

175. A. T. Winfree. *The geometry of biological time*, volume 12. Springer Science & Business Media, Berlin, 2001.

176. J. Zheng and M. C. Trudeau. *Handbook of Ion Channels*. CRC Press, London, February 2015. ISBN 978-1-4665-5142-8.

List of Figures

Acknowledgments

I would like to thank Susanne Schreiber for her inspiring guidance on my way to becoming a scientist. In all our scientific discussions, I have greatly appreciated Susanne's ideas, in particular her clear-sighted vision for our projects, and her genuine perception of logical fallacies. I am grateful for the opportunity to join her lab, and I feel truly privileged that my PhD could encompass so many facets, ranging from theory based on both simulations and mathematics, to experimental work including experimental design and data analysis.

I very much enjoyed working at the Institute for Theoretical Biology (ITB), the multidisciplinarity of its members, and in particular their open doors. Thank you all. In particular, I thank Jan-Hendrik Schleimer for our mathematical exploration of the SNL bifurcation. He and Grigory Bordyugov have helped me with the continuation software AUTO, and our seminar on homoclinic orbits was full of insights. Thanks also goes to my comrades with whom I joined forces in the struggle with the simulation environment NEURON, in particular Katharina Wilmes and Martina Michalikova. I thank Adam Wilkins for sharing both his expertise in writing scientific articles and his enthusiasm for biology. Besides the ITB, the graduate school of sensory computation and the Bernstein Center provided welcome distractions to the PhD project, and I thank my co-PhD-students, amongst others Achim Meyer and Robert Pröpper, for our support team, numerous seminars, barbecues and retreats, which have broadened my perspective on (neuro-)science. I would also like to thank our neighbors from the group of Behavioural Physiology. I thank Bernhard Ronacher for acting as my second supervisor, and for many details about insects relevant for the first project. Also Matthias Hennig and Sarah Wirtssohn were a source of knowledge on locust and crickets, and I especially thank Sarah for the opportunity to join her for a recording day on locusts.

An unexpected, great possibility to actually participate in experimental work arose from a phone call of Susanne in my fourth PhD year. Nikolaus Maier of the Schmitz lab (Charité) agreed to test our predictions in patch-clamp experiments. I greatly enjoyed the experience of working in an experimental lab, the ups and downs of a recording day, and the incredible amount of things that just can go wrong during experiments. I thank Dietmar Schmitz and his whole lab for their support, in particular those people who prepared the brain slices for us. And the experiments would have never been possible without Nikolaus endurance, his patience with stupid questions, and his never ending optimism. Thank you.

I thank the Mathematical Biosciences Institute (The Ohio State University, USA) and the organizers for inviting me to the workshop "Dynamical Systems and Data Analysis in Neuroscience: Bridging the Gap". It was a very interesting and lively meeting, and a great opportunity to present my work. I furthermore would like to acknowledge funding by the German Federal Ministry of Education and Research

(Grants No. 01GQ0901, No. 01GQ1001A, and No. 01GQ1403) and the Deutsche Forschungsgemeinschaft (SFB618, GK1589/1).

I would like to thank Elvira Lauterbach, Karin Winklhöfer, Vanessa Casagrande, Robert Martin, Camilla Groiß and Margret Franke for helpful assistance in all administrative concerns. I thank Rike-Benjamin Schuppner, Andreas Hantschmann and Willi Schiegel for constant support with computer and software related matters. A good program takes a lot of work, and I would like to acknowledge the open source projects brian2, AUTO, NEURON, spykeviewer, blender, inkscape, scribus, and git/gitlab, which I used during my PhD project.

Last but not least, I thank those friends from outside of the Humboldt University who continuously showed me the beauty of the world from their perspective, be it scientific or artistic. My curiosity keeps fresh thanks to you. And I thank Helge Aufderheide, for help with manuscripts and applications, and for a wonderful time, full of adventures and ever-lasting impressions from all over the world.

Selbständigkeitserklärung

Ich erkläre, dass ich die vorliegende Arbeit selbständig und nur unter Verwendung der angegebenen Literatur und Hilfsmittel angefertigt habe.

Berlin, den 11.05.2017 Janina Hesse